Theoretical study of electronic structure and spectroscopy of molecules containing metallic atoms

Shinsuke Hayashi

Université Paris-Est

Ecole Doctorale ICMS n^o 431

Thèse pour obtenir le grade de docteur

Chimie Théorique

Shinsuke HAYASHI

Theoretical study of electronic structure and spectroscopy of molecules containing metallic atoms

Thèse dirigée par Pr. Gilberte CHAMBAUD

Soutenue le 11 décembre 2008

Devant le jury composé de

Pr. Abdou BOUCEKKINE (Rapporteur: Université de Rennes I)

Pr. Jean-Pierre FLAMENT (Rapporteur: Université de Lille I)

Dr. Céline LEONARD (Examinateur: Université Paris-Est)

Dr. Annie SPIELFIEDEL (Examinateur: Observatoire de Paris)

Pr. Gilberte CHAMBAUD (Directeur: Université Paris-Est)

Acknowledgements

I wish to express my sincere gratitude to Professor Gilberte Chambaud for an opportunity to start my Ph.D. study and for her supervisions. My Ph.D. study of three years is a wonderful experience and now it is finishing with many nice souvenirs.

I am sincerely thankful to Professor Abdou Boucekkine and Professor Jean-Pierre Flament for being repoter, and to Dr. Annie Spielfiedel and Dr. Céline Leonard for being examiner for my Ph.D. defense.

I wish extremely to thank Dr. Céline Leonard and Dr. Marie Guitou for their helpful guidances, suggestions, and instructions. I have finally obtained the accurate descriptions of the HZnF system with the help by Dr. Céline Leonard and I could study many diatomic compounds concerned with piezoelectricity in collaboration with Dr. Marie Guitou. Two publications with them will remind me of the days in Marne-la-Vallée. I would like to remark also my appreciation for their helps to prepare le pot de thèse.

I am also grateful to Professor Pavel Rosmus and Dr. Isabelle Navizet for their supervisions during le stage du Master 2, and to Dr. Frédéric Le quéré for his corrections of my manuscript.

For a comfortable situation of laboratory and their supports, I wish to express my gratefulness to the current and ancient members of the theoretical chemistry group: Pr. Marius Lewerenz, Pr. Majdi Mochlaf, Dr. Alexander Mitrushchenkov, Dr. Mirjana Mladenović, Dr. Roberto, Dr. Claire, Dr. Matthieu, Dr. Jérôme, Dr. Ken, Dr. Géraldine, Dr. Hameth, Frédéric, Dr. Dalila, Dr.Hanka, Laurent, Mohamed, Vincent, Hossain, Christian, and Martine.

I consecrate the list line to express my gratitude to my familly, my friends, and Beatrice.

Abstract :
In this work we have investigated the electronic properties of several types of molecular systems involving a metallic element. Our motivation for such applications on metallic compounds was to obtain an accurate description of close lying electronic states, in which the relativistic effects of heavy atoms are known to be important. Thus various approaches and methods have been employed to treat these effects, including the multi-configurational method, with atomic pseudopotentials and large basis sets. In the first study, we have determined the properties of the low lying electronic states of the diatomic compounds MX, whose combinations in the solid phase produce ionic semi-conductor materials with piezoelectric properties. Based on highly correlated ab initio calculations, we have elucidated the common properties of the low lying electronic states of these diatomic compounds with eight valence electrons, which can be considered as precursors for piezoelectric effects in their solid phase. Based on our electronic structure calculations, we could identify among these diatomic compounds those who could lead to good candidates for piezoelectric effects. As the second application, we have determined the electronic structure and the spectroscopic constants for the ground state of the HZnF molecule and for the low lying electronic states of its diatomic fragments. This application was initiated and motivated by interesting and puzzling results on the close system HZnCl. Comforted by our experience with the previous studies, we used the pseudopotentials approach to obtain an accurate description of the low lying states of ZnH which could be satisfactorily compared with existing data. Next, the ZnF and ZnCl diatomic molecules have been studied with the same ansatz to reveal the properties of so far unknown electronic states. Finally, the potential energy surface of the ground state of HZnF has been determined, and several spectroscopic properties have been deduced.

Résumé :
Dans cette étude, nous avons déterminé les propriétés électroniques de plusieurs types de composés moléculaires possédant un élément métallique. Notre motivation pour l'étude de tels systèmes était de montrer qu'il était possible d'obtenir une description précise d'états électroniques très proches en énergie, pour lesquels il est connu que les effets relativistes jouent un rôle important. Pour traiter ces effets nous avons mis en œuvre différentes approches et méthodes, en particulier des méthodes multi-configurationnelles, des pseudopotentiels atomiques et de grandes bases de fonctions. Dans une première étude nous avons déterminé les propriétés des états électroniques de plus basse énergie de composés diatomiques MX dont l'association en phase solide conduit à des composés semi-conducteurs présentant des propriétés piézoélectrique importantes. A l'aide de calculs électroniques incluant une large part de la corrélation électronique nous avons mis en évidence les propriétés communes à une famille de composés diatomiques possédant huit électrons de valence et qui peuvent être considérés comme précurseurs des solides piézoélectriques. Il a ainsi été possible d'identifier les couples diatomiques qui constituaient les meilleurs candidats pour une production d'effet piézoélectrique en phase solide. Dans la deuxième application, nous avons calculé la structure électronique et les constantes spectroscopiques de l'état fondamental de la molécule HZnF ainsi que les états de plus basse énergie des fragments diatomiques associés. Cette étude était motivée par une analogie avec un système voisin HZnCl dont les premiers états électroniques présentent des caractéristiques non complètement résolues. Après avoir validé notre approche sur l'étude de ZnH et comparé nos résultats à ceux d'études antérieures, nous avons entrepris la détermination de la structure électronique des molécules ZnF et ZnCl pour lesquelles nous avons pu identifier des états électroniques encore mal connus. Utilisant les résultats obtenus sur ZnH et ZnF, nous avons déterminé la surface d'énergie potentielle de l'état fondamental de HZnF et nous en avons déduit plusieurs grandeurs spectroscopiques caractérisant cet état.

Contents

Second part: Applications

List of Figures

List of Tables

Introduction

This study focuses on the determination of the electronic structure and spectroscopy of diatomic and triatomic molecules containing metallic atoms. Even nowadays with efficient methods and powerful computers it remains challenging to achieve an accurate description of the close lying electronic states of such compounds, because of the complex interactions between them. Our interest in this study is to take into account the relativistic effects of heavy atoms, which are known to play an important role and to get a satisfactory description of the polarity of the metallic atoms in the different electronic states. For this purpose, multi-configurational approaches are required and atomic pseudopotentials are generally used to treat the relativistic effects without an explicit treatment of the core electrons.

We report in this study the electronic properties and the spectroscopy of the low lying electronic states of several families of diatomic compounds, MX, whose pairs [M,X] form ionic solids presenting piezoelectric effects. The second application concerns the description of the ground state of the zinc hydrofluoride HZnF with its related diatomic fragments.

The first part of this manuscript presents the theoretical methods employed for the electronic structure calculations and descriptions of the nuclear motions. Starting with the Schrödinger equation of the molecular system, we apply the Born-Oppenheimer approximation to treat separately the electronic and nuclear descriptions. For the electronic calculations, the Self-Consistent-Field Hartree-Fock method is the initial step for all the study and it is presented here briefly, then we mention several post Hartree-Fock methods accounting for the electronic correlation energies. Next is described the formalism of the atomic pseudopotentials used to include the relativistic effects and also to reduce the size of the computations. The basis set functions, whose linear combinations define the molecular orbitals in the electronic wavefunction are presented. Because the basis sets are always finite, which is a limitation in the accessible accuracy of the theoretical treatments, we present here an empirical extrapolation to the basis set limit. Following the methods for the electronic calculations, the methods used to describe the nuclear motions in the diatomic and triatomic molecules are explained. Numerical resolutions of the nuclear Hamiltonian allow accessing the spectroscopic constants, the rotational and vibrational energy levels, and various quantities characterizing the properties of molecular states, such approach is chosen for the diatomic molecules. For triatomic systems a variational method using a basis set representation is employed.

In the second part, we report the results of the calculations of the properties of the low lying electronic states of molecules containing metallic atoms. The first application is intended to characterize the electronic structure of the low lying electronic states of diatomic compounds related to piezoelectric effects in the solid phase. The piezoelectric effects were found at the end of the 19^{th} century and are now extensively applied to technology, which explains the interest for such systems. The ionic semiconductors presenting the piezoelectric effect are formed of pairs of atoms [M,X] having already at the diatomic level a set of common properties: they have close lying lowest electronic states with different by close geometry and the charge distribution in these electronic states is significantly different. In this study, based on highly correlated

electronic calculations of the low lying electronic states of the diatomic compounds (including a metal of Group IIa, IIb, or III and a non-metal of Group V, or VI), we show that strong correlations can be established between the properties of the solids and those of the parent molecules.

The second application is the theoretical investigation on the zinc hydrofluoride HZnF molecule with its associated diatomic fragments ZnH and ZnF. The zinc atom is an important metal in biology and its abundant natural isotopes make a specific and interesting signature in the vibrational spectra of its compounds. Our interest for this system started with the experimental results on the parent HZnCl molecule by P. Bernarth, exhibiting a complicated spectrum difficult to assign. Recent calculations on the HZnCl system confirm our exploratory study that it is very difficult to get a proper description of the electronic ground state. We have thus decided to investigate the low lying states of the HZnF and the concerned diatomic compounds at the Multi-Reference Configuration Interaction (MRCI) level including the Davidson correction, using the pseudopotentials to take relativistic effects into account. The calculated spectroscopic data of the low lying states of ZnH will be compared with the existing data to validate the method and the ZnH^+ cation will be treated using the same ansatz. Turning to the ZnF diatomic molecule, it is somehow surprising that there is no reliable information on the low lying states except for on its ground state. Thus we will perform the calculations to have an accurate description of the properties of the low lying states of ZnF. Additionally, the low lying electronic states of ZnCl will be also studied to discuss similarity to these of ZnF and to complete the subsequent comparison between the HZnF and HZnCl molecules. Using our results on the associated diatomic molecular fragments, the theoretical investigation on the HZnF molecule, focusing on its ground state will be reported. From the calculated potential energy surface, we will determine the equilibrium geometry and the harmonic wavenumbers of this system. The effects of substitutions of the isotopes of Zn will be compared with similar study for HZnCl. Finally the rovibrational energy levels of the ground state will be simulated.

First part: Theory

1 Born-Oppenheimer approximation

2 Calculations of the electronic structures

3 Basis sets and Pseudopotentials

4 Descriptions of the nuclear motions

1 Born-Oppenheimer approximation

1.1 Schrödinger equation

For a molecular system involving n electrons and N nuclei, the Schrödinger equation [1] is written as follows for stationary states situation where the Hamiltonian operator $\hat{H}$ is time-independent;

$$\hat{H}\Psi_\alpha(\mathbf{R};\mathbf{r}) = E_\alpha\Psi_\alpha(\mathbf{R};\mathbf{r}) \qquad (1.1)$$

where $\mathbf{R}$ and $\mathbf{r}$ represent respectively the coordinates of the nuclei and of the electrons and α labels the eigenstate. E_α is the eigenenergy of the α eigenstate under the non-relativistic Hamiltonian $\hat{H}$:

$$\hat{H} = \hat{T}_e + \hat{T}_N + \hat{V}_{ee} + \hat{V}_{eN} + \hat{V}_{NN} \qquad (1.2)$$

with the following terms:

$$\hat{T}_e = -\frac{1}{2m_e}\sum_{i=1}^{n}\Delta_i \qquad (1.3)$$

$$\hat{T}_N = -\sum_{a=1}^{N}\frac{\Delta_a}{2M_a} \qquad (1.4)$$

$$\hat{V}_{ee} = \frac{1}{2}\sum_{i,j=1}^{n}\frac{e^2}{|\mathbf{r}_i - \mathbf{r}_j|} \qquad (1.5)$$

$$\hat{V}_{eN} = -\sum_{i,a=1}^{n,N}\frac{Z_a e^2}{|\mathbf{R}_a - \mathbf{r}_i|} \qquad (1.6)$$

$$\hat{V}_{NN} = \frac{1}{2}\sum_{a,b=1}^{N}\frac{Z_a Z_b e^2}{|\mathbf{R}_a - \mathbf{R}_b|} \qquad (1.7)$$

where $\hat{T}_e$ and $\hat{T}_N$ are the kinetic energy operators of electrons and nuclei respectively. The electronic Coulomb repulsive potentials are expressed in the term $\hat{V}_{ee}$, as well as in the term $\hat{V}_{NN}$ for nuclear ones. $\hat{V}_{eN}$ represents the Coulomb attractive potential between an electron and a nucleus. Except for a few simple systems, it becomes difficult to obtain the exact solution of the Schrödinger equation (1.1). The following approximation developed by Born and Oppenheimer [2] will be applied.

1.2 Born-Oppenheimer approximation

The Born-Oppenheimer approximation [2] is a separation between the electronic motion and the nuclear one, based on the fact that the electrons move much more rapidly than the nuclei due to the huge difference between their masses. We can imagine a picture such that electrons move

around nuclei fixed at a given structure.

For the fixed nuclear coordinates $\mathbf{R}$, the electronic wavefunction $\psi(\mathbf{R};\,\mathbf{r})$ holds the following Schödinger equation with a parameter $\mathbf{R}$:

$$\left[\hat{T}_e + \hat{V}(\mathbf{R};\mathbf{r})\right]\psi_n(\mathbf{R};\mathbf{r}) = E_n(\mathbf{R})\psi_n(\mathbf{R};\mathbf{r}) \qquad (1.8)$$

where the potential is written as $\hat{V} = \hat{V}_{ee} + \hat{V}_{eN} + \hat{V}_{NN}$. n labels the electronic state and $\mathrm{E}_n(\mathbf{R})$ depends on the parameterized $\mathbf{R}$. The total wavefunction involving the nuclear part is expressed by superposition of the electronic states with coefficients $\chi_n(\mathbf{R})$:

$$\Psi(\mathbf{r};\mathbf{R}) = \sum_k \psi_k(\mathbf{R};\mathbf{r})\chi_k(\mathbf{R}) \qquad (1.9)$$

which should satisfy the equation (1.1). Thus we obtain the equation (1.10).

$$\left[-\frac{1}{2m_e}\sum_{i=1}^{n}\Delta_i - \sum_{a=1}^{N}\frac{\Delta_a}{2M_a} + \hat{V}\right]\sum_k \psi_k(\mathbf{R};\mathbf{r})\chi_k(\mathbf{R}) = E\sum_k \psi_k(\mathbf{R};\mathbf{r})\chi_k(\mathbf{R}) \qquad (1.10)$$

Manipulating the equation (1.10) with the help of the equation (1.8), we obtain the following expression (1.11):

$$\sum_k \chi_k(\mathbf{R})\left[-\frac{1}{2m_e}\sum_{i=1}^{n}\Delta_i + \hat{V}\right]\psi_k(\mathbf{r};\mathbf{R})$$

$$-\sum_k\sum_a \frac{1}{2M_a}\left[\Delta_a\psi_k(\mathbf{r};\mathbf{R})\chi_k(\mathbf{R}) + 2\nabla_a\psi_k(\mathbf{r};\mathbf{R})\cdot\nabla_a\chi_k(\mathbf{R}) + \psi_k(\mathbf{r};\mathbf{R})\Delta_a\chi_k(\mathbf{R})\right]$$

$$= E\sum_k \psi_k(\mathbf{R};\mathbf{r})\chi_k(\mathbf{R}) \qquad (1.11)$$

Operating $\psi^*_m(\mathbf{r};\,\mathbf{R})$ from the left on the equation (1.11) and integrating over $\mathbf{r}$, we obtain:

$$\left[-\sum_a \frac{\Delta_a}{2M_a} + E_m(\mathbf{R}) - E\right]\chi_m(\mathbf{R})$$

$$= \sum_k\sum_a \frac{1}{2M_a}\left[\langle\psi_m\,|\Delta_a|\,\psi_k\rangle\,\chi_k(\mathbf{R}) + 2\,\langle\psi_m\,|\nabla_a|\,\psi_k\rangle\cdot\nabla_a\chi_k(\mathbf{R})\right] \qquad (1.12)$$

where the orthonormality $\langle\psi_i|\psi_j\rangle = \delta_{ij}$ is used.

In the condition where the separation between electrons and nuclei holds, the right hand side of the equation (1.12) can be considered to be zero. Thus $\chi_m(\mathbf{R})$ will appear as the solution of the Schrödinger equation (1.13):

$$\left[-\sum_a \frac{\Delta_a}{2M_a} + E_m(\mathbf{R})\right]\chi_m(\mathbf{R}) = E\chi_m(\mathbf{R}) \qquad (1.13)$$

The equation (1.13) can be considered as the Schrödinger equation of the nuclear motion under the potential $E_m(\mathbf{R})$. The total wavefunction can be expressed as $\Psi(\mathbf{r};\mathbf{R}) = \psi_m(\mathbf{r};\mathbf{R})\chi_m(\mathbf{R})$ in the adiabatic approximation. Thus we can interpret the $\chi_m(\mathbf{R})$ as the nuclear wavefunction belonging to the electronic state described by $\psi_m(\mathbf{r};\mathbf{R})$. The $E_m(\mathbf{R})$ is called the adiabatic potential of the m^{th} electronic state and we will discuss in the next chapter the resolution of the electronic Schrödinger equation (1.8).

2 Calculations of the electronic structure

The equation (1.8), obtained in the last section, is the multi-electrons equation which determines the electronic state. First, we will describe the stream to the Hartree-Fock approximation and second various post Hartree-Fock methods.

2.1 Variation principle and Lagrange's method of undetermined multipliers

2.1.1 Variation principle

Supposing that E_0 and ϕ_0 are the eigenenergy and the eigenfunction of the Hamiltonian $\hat{H}$, the following relation holds for any arbitrary wavefunction ϕ;

$$E[\phi] = \frac{<\phi|\hat{H}|\phi>}{<\phi|\phi>} \geq E_0 \qquad (2.1)$$

This inequality is called the Variation principle. The minimum of the functional E[ϕ] gives the closest value to E_0. In the variation method, we can obtain an approximated energy, determining the parameters in the trial function which correspond to the stationary point of E[ϕ]. The quality of this approximation depends essentially on the choice of the trial functions.

2.1.2 Lagrange's method of undetermined multipliers

Based on the variation principle, we will seek the stationary points of E[ϕ] under the restrictions imposed on ϕ, using the Lagrange's method of undetermined multipliers. Introducing the undetermined multipliers λ_j, the new functional $F[\phi;\lambda]$ can be expressed as follows:

$$F[\phi;\lambda] = E[\phi] + \sum_j \lambda_j G_j[\phi], \quad G_j[\phi] = 0 \qquad (2.2)$$

where $G_j[\phi] = 0$ represents the restrictions imposed on ϕ. Then, the stationary point of E[ϕ] is given by the set of the trial functions $[\phi_1, ..., \phi_n]$ satisfying the following relations:

$$\frac{\partial F[\phi;\lambda]}{\partial \phi_i} = 0 \quad and \quad \frac{\partial F[\phi;\lambda]}{\partial \lambda_j} = 0 \qquad (2.3)$$

2.2 Slater determinant

The multi-electrons equation (1.8) can no longer be resolved exactly except for a few simple cases. The variational resolution of the equation (1.8) requires the initial wavefunction, written as $\Psi(\xi_1, \xi_2, ..., \xi_n)$ for the system including n electrons, where $\xi_i = (\mathbf{r}_i, \sigma_i)$ and $\mathbf{r}_i$ and σ_i are respectively the space and spin coordinates of the i^{th} electron. According to the Pauli principle that the wavefunction should be anti-symmetric for exchanges of two electrons, the following condition is imposed on the wavefunction:

$$\Psi(\xi_1, ..., \xi_i, ..., \xi_j, ..., \xi_n) = -\Psi(\xi_1, ..., \xi_j, ..., \xi_i, ..., \xi_n) \quad (i \neq j) \qquad (2.4)$$

We can describe the wavefunction of n electrons system by the Slater determinant which is automatically anti-symmetric under the exchanges of two electrons. Using the spin-orbital $\psi_k(\xi_i)$ defined as follows:

$$\psi_k(\xi_i) = \phi_k^S(\mathbf{r}_i)S(\sigma_i) \qquad (2.5)$$

where ϕ_k is the kth molecular orbital and S is the spin-function. The Slater determinant can be given as below for the configuration in which each of the n electrons fills one different spin-orbital.

$$\begin{aligned}\Psi(\xi_1, \xi_2, ..., \xi_n) &= ||\psi_{m_1}, \psi_{m_2}, ..., \psi_{m_n}|| \\ &= (n!)^{-1/2} \begin{vmatrix} \psi_{m_1}(\xi_1) & \psi_{m_1}(\xi_2) & .... & \psi_{m_1}(\xi_n) \\ \psi_{m_2}(\xi_1) & \psi_{m_2}(\xi_2) & .... & \psi_{m_2}(\xi_n) \\ .... & .... & .... & .... \\ \psi_{m_n}(\xi_1) & \psi_{m_n}(\xi_2) & .... & \psi_{m_n}(\xi_n) \end{vmatrix} \qquad (2.6)\end{aligned}$$

The Slater determinant is mono-configurational, thus the total wavefunction of n electrons with m spin-orbitals can be expressed by superposition of these determinants for specified configurations:

$$\begin{aligned}&\Psi^{el}(\xi_1, \xi_2, ..., \xi_n) \\ &= \sum_{1 \le m_1 < m_2 < ... < m_n \le m} C(m_1, m_2, ..., m_n)||\psi_{m_1}, \psi_{m_2}, ..., \psi_{m_n}|| \qquad (2.7)\end{aligned}$$

2.3 Hartree-Fock equation

For the wavefunction of n electrons expressed by the Slater determinant $\Psi(\xi_1, \xi_2, ..., \xi_n)$, Hartree-Fock approximaton [3–5] gives a set of spin-orbitals $(\psi_1, \psi_2, ..., \psi_n)$ corresponding to the minimum of the expectation value $<\Psi|\hat{H}|\Psi>$, using a variation method. We first simplify the Hamiltonian of n electrons, using atomic units ($\hbar = m_e = e = 1$):

$$\hat{H} = \sum_{\mu=1}^{n} \hat{h}(\mathbf{r}_\mu) + \frac{1}{2}\sum_{\mu\nu} \frac{1}{r_{\mu\nu}} \qquad (2.8)$$

$$\hat{h}(\mathbf{r}_\mu) = -\frac{1}{2}\Delta_\mu + v(\mathbf{r}_\mu) \qquad (2.9)$$

$$r_{\mu\nu} = |\mathbf{r}_\mu - \mathbf{r}_\nu| \qquad (2.10)$$

where $v(\mathbf{r}_\mu)$ represents a sum of the Coulomb potentials between the μ^{th} electron and all nuclei in a molecule.

The first term of the equation (2.8) is a one-body operator and the second a two-body operator. Supposing the orthonormality of spin-orbitals $\langle\psi_i|\psi_j\rangle = \delta_{ij}$, we can reduce $<\Psi|\hat{H}|\Psi>$ as follows:

$$< \Psi|\hat{H}|\Psi >= \sum_{i=1}^{n} < \psi_i|\hat{h}|\psi_i > + \frac{1}{2}\sum_{i=1}^{n}\sum_{j=1}^{n}\left(\left\langle \psi_i\psi_j \left| \frac{1}{r_{12}} \right| \psi_i\psi_j \right\rangle - \left\langle \psi_i\psi_j \left| \frac{1}{r_{12}} \right| \psi_j\psi_i \right\rangle\right) \qquad (2.11)$$

$$\left\langle \psi_i\psi_j \left| \frac{1}{r_{12}} \right| \psi_i\psi_j \right\rangle = \int d\xi_1 \int d\xi_2 \psi_i^*(\xi_1)\psi_j^*(\xi_2)\frac{1}{|\mathbf{r_1}-\mathbf{r_2}|}\psi_i(\xi_1)\psi_j(\xi_2) \qquad (2.12)$$

$$\left\langle \psi_i\psi_j \left| \frac{1}{r_{12}} \right| \psi_j\psi_i \right\rangle = \int d\xi_1 \int d\xi_2 \psi_i^*(\xi_1)\psi_j^*(\xi_2)\frac{1}{|\mathbf{r_1}-\mathbf{r_2}|}\psi_j(\xi_1)\psi_i(\xi_2) \qquad (2.13)$$

we search for a set of the spin-orbitals $(\psi_1, \psi_2, ..., \psi_n)$ corresponding to the minimum of $<\Psi|\hat{H}|\Psi>$ under the restriction $\langle\psi_i|\psi_j\rangle = \delta_{ij}$. Based on the Lagrange's method of undetermined multipliers ϵ_{ji}, we seek the conditions to satisfy the following equation:

$$\delta\left[< \Psi|\hat{H}|\Psi > - \sum_{i=1}^{n}\sum_{j=1}^{n}\left(\epsilon_{ji}\left\langle\psi_i|\psi_j\right\rangle - \delta_{ij}\right)\right] = 0 \qquad (2.14)$$

with respect to the variations $\delta\psi_i(\xi)$ and $\delta\psi_i^*(\xi)$. In consequence, the equations (2.15) and (2.16) yield,

$$\left[\hat{h} + \sum_{j=1}^{n}\left(\hat{J}_j - \hat{K}_j\right)\right]\psi_i(\xi) = \sum_{j=1}^{n}\psi_j(\xi)\epsilon_{ji} \qquad (2.15)$$

$$\psi_i^*(\xi)\left[\hat{h} + \sum_{j=1}^{n}\left(\hat{J}_j^* - \hat{K}_j^*\right)\right] = \sum_{j=1}^{n}\psi_j^*(\xi)\epsilon_{ij} \qquad (2.16)$$

where the operators $\hat{J}_j$ and $\hat{K}_j$ are defined as follows:

$$\hat{J}_j\psi_i(\xi) = \int d\xi_2 \psi_j^*(\xi_2)\frac{1}{|\mathbf{r_1}-\mathbf{r_2}|}\psi_i(\xi_1)\psi_j(\xi_2) \qquad (2.17)$$

$$\hat{K}_j\psi_i(\xi) = \int d\xi_2 \psi_j^*(\xi_2)\frac{1}{|\mathbf{r_1}-\mathbf{r_2}|}\psi_j(\xi_1)\psi_i(\xi_2) \qquad (2.18)$$

Comparing the complex conjugate of (2.16) with (2.15), an additional condition on ϵ_{ji} is found:

$$\epsilon_{ij}^* = \epsilon_{ji} \qquad (2.19)$$

2.4 Canonical Hartree-Fock equation

Introducing the ikth element of an unitary matrix as u_{ik}, the set of unitary transformed spin-orbitals $\psi_i^{'}$ can be expressed:

$$\psi_i^{'} = \sum_{k=1}^{n} u_{ik}\psi_k \quad (i = 1, 2, ..., n) \qquad (2.20)$$

The set of transformed spin-orbitals $(\psi_1^{'}, \psi_2^{'}, ..., \psi_n^{'})$, can satisfy the Hartree-Fock equation (2.15). This character arises from an unitary invariance of the Slater determinant. We can derive the following relation between two Slater determinants $\Psi^{'} = ||\psi_1^{'}, \psi_2^{'}, ..., \psi_n^{'}||$ and $\Psi = ||\psi_1, \psi_2, ..., \psi_n||$:

$$\Psi' = \begin{vmatrix} u_{11} & u_{12} & ... & u_{1n} \\ u_{21} & u_{22} & ... & u_{2n} \\ ... & ... & ... & ... \\ u_{n1} & u_{n2} & ... & u_{nn} \end{vmatrix} \Psi = \pm\Psi \qquad (2.21)$$

The relation (2.21) leads to an equality $<\Psi'|\hat{H}|\Psi'> = <\Psi|\hat{H}|\Psi>$, which confirms that both the initial and the unitary transformed set are solutions of the Hartree-Fock equation (2.15). As shown in the relation (2.19), ϵ_{ij} is an element of a Hermitian matrix. Thus the matrix defined as $(\mathbf{E})_{ij} = \epsilon_{ij}$ can be diagonalized as $\epsilon^c_{ij} = \epsilon_i \delta_{ij}$, by an appropriate unitary matrix $(\mathbf{U})_{ij} = u^c_{ij}$. Using the unitary matrix $\mathbf{U}$ which diagonalizes the matrix $\mathbf{E}$, a set of the canonical orbitals $(\psi^c_1, \psi^c_2, ..., \psi^c_n)$ can be expressed as follows:

$$\psi^c_i = \sum_{k=1}^{n} u^c_{ik} \psi_k \quad (i = 1, 2, ..., n) \qquad (2.22)$$

$$\epsilon^c_{ij} = \sum_{l=1}^{n} \sum_{m=1}^{n} u^c_{il} \epsilon_{lm} u^c_{mj} = \epsilon_i \delta_{ij} \qquad (2.23)$$

With the help of (2.22) and (2.23), the Hartree-Fock equation (2.15) is transformed for the canonical orbital ψ^c_i and the diagonal energy ϵ_i.

$$\left[\hat{h} + \sum_{i \neq j}^{n} \left(\hat{J}_j - \hat{K}_j \right) \right] \psi^c_i = \epsilon_i \psi^c_i \quad (i = 1, 2, ..., n) \qquad (2.24)$$

The equation (2.24) is likely to take the same form as the Schrödinger equation for the canonical orbital ψ^c_i, and ϵ_i (namely the orbital energy) seems to be the eigenenergy for ψ^c_i. This picture gives the concept of the n independent electrons, however the interactions between electrons are included in the operators $\hat{J}_j$ and $\hat{K}_j$. Indeed the total energy $<\Psi|\hat{H}|\Psi>$ is not equal to a sum of the orbital energies $\sum_i \epsilon_i$.

The term $\hat{J}_j$ is called the Coulomb operator and the term $\sum_{i \neq j} \hat{J}_j$ in the equation (2.24) can be interpreted as the sum of the electronic Coulomb potentials except for the ith electron. The exchange operator $\hat{K}_j$ arises from the Pauli principle. Because the term $\sum_{i \neq j}(\hat{J}_j - \hat{K}_j)$ has a sense of the mean potential over all electrons without the ith one, the Hartree-Fock method is considered as a mean field approximation. According to the equation (2.24), ψ^c_1 is determined under the mean field over ψ^c_2, ..., ψ^c_n, in turn, ψ^c_i under that over ψ^c_1, ..., ψ^c_{i-1}, ψ^c_{i+1}, ..., ψ^c_n. It is necessary to determine iterativelly the best set of $(\psi^c_1, \psi^c, ..., \psi^c_n)$. Thus in this sense, the Hartree-Fock method is self-consistent.

2.5 Unrestricted and Restricted Hartree-Fock methods

With respect to the orbital $\phi_k(\mathbf{r})$ in the spin orbital $\psi_k(\xi)$, there are two approaches for the Hartree-Fock method. In the first one, namely the Unrestricted Hartree-Fock (UHF) method, we express $\psi_k(\xi)$, fixing the spin-functions as $\alpha(\sigma)$ or $\beta(\sigma)$.

$$\psi_k(\xi) = \phi_k^{\alpha}(\mathbf{r})\alpha(\sigma) \quad or \quad \phi_k^{\beta}(\mathbf{r})\beta(\sigma) \qquad (2.25)$$

In the other one, the Restricted Hartree-Fock (RHF) method, the spin orbital is constructed using the same orbital $\phi_k(\mathbf{r})$ for the $\alpha(\sigma)$ and $\beta(\sigma)$ spin functions.

$$\psi_k(\xi) = \phi_k(\mathbf{r})\alpha(\sigma) \quad or \quad \phi_k(\mathbf{r})\beta(\sigma) \qquad (2.26)$$

In the RHF method, the orbital $\phi_k(\mathbf{r})$ is filled by one electron with the $\alpha(\sigma)$ spin function and the other with the $\beta(\sigma)$. According to the fact that the less restricted trial function gives variationally in general the lower energy, the UHF method is better than the RHF for optimization of energy. However, the wavefunction of a molecule for stationary states should be the eigenfunction of the total electronic spin $\hat{\mathbf{S}^2}$ and its projection $\hat{S}_z$. This character holds in the RHF method, but if the wavefunction determined by the UHF method can satisfy the eigenfunction of $\hat{S}_z$, it is not the case for $\hat{\mathbf{S}^2}$. This point is an advantage of the RHF method, which is performed in most cases.

2.6 Roothaan-Hall equation

The Hartree-Fock equation mentioned above is a differential equation. In practice, instead of solving this HF equation, we expand the spin orbital using a basis set χ_p, which is similar to the atomic orbital. Thus this expansion is called the Linear Combination of Atomic Orbitals -Molecular Orbitals (LCAO-MO).

$$\psi_i = \sum_{p=1}^{m} \chi_p C_{pi} \quad (p = 1, 2, ..., m > n) \qquad (2.27)$$

The expansion coefficients C_{pi} are included in the Slater determinant and determined to give the stationary points of $<\Psi|\hat{H}|\Psi>$. Substituting $\psi_i(\xi)$ written as (2.27) into the equation (2.24), we obtain:

$$\hat{h}\psi_i(\xi) + \sum_{j=1}^{n}(\hat{J}_j - \hat{K}_j)\psi_i(\xi) = \sum_{k=1}^{m} \hat{h} C_{ki}\chi_k(\xi)$$

$$+ \sum_{k,l,p=1}^{m} C_{ki} \sum_{j=1}^{n} C_{pj}^{*} C_{lj} \left[\int d\xi_2 \chi_p^{*}(\xi_2) \frac{1}{r_{12}} \chi_l(\xi_2)\chi_k(\xi_1) - \int d\xi_2 \chi_p^{*}(\xi_2) \frac{1}{r_{12}} \chi_k(\xi_2)\chi_l(\xi_1) \right]$$

$$= \epsilon_i \sum_{k=1}^{m} C_{ki}\chi_k(\xi) \qquad (2.28)$$

Multiplying the equation (2.28) by $\chi_q^{*}(\xi)$ from the left and integrating over ξ, the following equation is obtained,

$$\sum_{k=1}^{m} C_{ki} \left[< \chi_q|\hat{h}|\chi_k > + \sum_{l,p=1}^{m} \sum_{j=1}^{n} C_{pj}^{*} C_{lj} \left([qk|pl] - [ql|pk] \right) \right] = \epsilon_i \sum_{k=1}^{m} C_{ki} \left\langle \chi_q|\chi_k \right\rangle \qquad (2.29)$$

$$[qk|pl] = \int d\xi_1 \int d\xi_2 \chi_q^*(\xi_1)\chi_p^*(\xi_2)\frac{1}{r_{12}}\chi_l(\xi_2)\chi_k(\xi_1) \qquad (2.30)$$

Defining the matrices $\mathbf{F}$ and $\mathbf{S}$ and the vector $\mathbf{C}_i$ as follows:

$$(\mathbf{F})_{qk} =< \chi_q|\hat{h}|\chi_k > + \sum_{l,p=1}^{m}\sum_{j=1}^{n} C_{pj}^* C_{lj} \left([qk|pl] - [ql|pk]\right) \quad (2.31)$$

$$(\mathbf{S})_{qk} = \langle \chi_q|\chi_k \rangle \qquad (2.32)$$

$$(\mathbf{C}_i)_k = C_{ki} \qquad (2.33)$$

Finally the Roothaan-Hall equation [6, 7] is written as below:

$$\mathbf{F}\mathbf{C}_i = \epsilon_i \mathbf{S}\mathbf{C}_i \quad (i = 1, 2, ..., n) \qquad (2.34)$$

Here, instead of resolving the differential equations, we solve the eigenvalue problem of the Roothaan-Hall equation (2.34). In this method, the spin-orbital is expanded as a linear combination of the m atomic orbital-like basis set. The expectation energy of $<\Psi|\hat{H}|\Psi>$ is rewritten under the orthonormality $<\psi_i|\psi_j> =\delta_{ij}$:

$$E = \sum_{i=1}^{n} \epsilon_i - \frac{1}{2}\sum_{i,j=1}^{n}\sum_{k,l,p,q=1}^{m} C_{qi}^* C_{ki} C_{pj}^* C_{lj} \left([qk|pl] - [ql|pk]\right) \qquad (2.35)$$

The Roothaan-Hall equation is also a self-consistent-field method, because of inclusion of C_{pi} in the $\mathbf{F}$ matrix and should be treated iteratively. The n spin-orbitals ψ_i (i=1,2,...,n) are constructed with the optimized coefficients C_{pi} (p=1,2,...,m). As m > n, we can additionally obtain the extra (m - n) spin-orbitals, called "virtual orbitals" which are used for the post Hartree-Fock methods.

2.7 Limit of the Hartree-Fock method

The Hartree-Fock method mentioned above can account for 99% of the total exact energy, however, the remaining 1% of the total energy is important to describe chemical pictures. This residual arises from the electronic correlation, separated into the two following types: the first one is the static correlation related to degenerated or quasi-degenerated states, which cannot be correctly described by a mono-configurational wavefunction. This correlation depends also on the size of the system and becomes important at dissociation asymptotes. The second one is called the dynamical correlation related to collisions of electrons leading to the two-, three-, or multi-electron excitation configurations. This type is independent of the size of the system, but depends on the number of electrons in the system. We will next discuss the post Hartree-Fock methods to recover the remaining 1% of the total exact energy.

2.8 Configuration Interaction method

The first post Hartree-Fock method is the Configuration Interaction (CI) method, in which the wavefunction of n electrons Ψ_{CI} is expressed by a linear combination of the Slater determinants Ψ_I and the corresponding coefficients C_I:

$$\Psi_{CI} = \sum_{I=0} C_I \Psi_I \qquad (2.36)$$

where Ψ_I is constructed with a set of spin-orbitals $\psi_1, \psi_2, ..., \psi_m$ (m>n). Ideally we can obtain, using the CI method with an infinite set of spin-orbitals, the exact solution of the Schrödinger equation under the Born-Oppenheimer approximation. In the case where the CI wavefunction is expended on the maximum number of Slater determinants constructed with the finite set of spin-orbitals, the maximum electronic correlation can be accounted within this limited spin-orbitals number and the method is then called the Full CI method. The number of Slater determinants of n electrons with m spin-orbitals N^{FCI}, at the Full CI level, is counted as follows:

$$N^{FCI} = \frac{m!}{n!(m-n)!} \qquad (2.37)$$

Thus feasibility of the Full CI method depends on the size of the system and of the spin-orbital set. In practice, we can rewrite the combination (2.36) as follows:

$$\Psi_{CI} = C_0 \Psi_{HF} + \sum_S C_S \Psi_S + \sum_D C_D \Psi_D + \sum_T C_T \Psi_T + ... \qquad (2.38)$$

where Ψ_S, Ψ_D, and Ψ_T correspond respectively to the single-, double-, and triple-electron excitations from the spin-orbitals included in the HF Slater determinant Ψ_{HF} to the virtual orbitals obtained by the Hartree-Fock method. For the facility of actual computations, the above expansion is cut off after the doublet-excitation (CISD) or the triple-excitation (CISDT). In the CISD and CISDT levels, the total number of Slater determinants is decreased to feasible size for computations, however, these methods are no longer size-extensive. The term "size-extensive" means that, for the system including two molecules, the energy of the combined AB system is equal to the sum of the energies of the separated A and B molecules in a size-consistent method.

In the CI method, we determine variationally only the coefficients C_I to obtain the minimum energy under the restriction of normalization imposed on the CI wavefunction. Using the Lagrange's undetermined multipliers λ, we find the coefficients which give the stationary points of the following functional F:

$$F = < \Psi_{CI} | \hat{H} | \Psi_{CI} > -\lambda(< \Psi_{CI} | \Psi_{CI} > -1)$$
$$= \sum_{I,J} C_I^* C_J < \Psi_I | \hat{H} | \Psi_J > -\lambda \sum_{I,J} C_I^* C_J < \Psi_I | \Psi_J > +\lambda \qquad (2.39)$$

Thus we obtain the equation (2.40).

$$\frac{\partial F}{\partial C_I^*} = \sum_J (< \Psi_I | \hat{H} | \Psi_J > -\lambda < \Psi_I | \Psi_J >) C_J = 0 \qquad (2.40)$$

The definition $H_{IJ} = <\Psi_I|\hat{H}|\Psi_J>$ and $S_{IJ} = <\Psi_I|\Psi_J> = \delta_{IJ}$ leads to the following secular equation:

$$\begin{pmatrix} H_{00}-\lambda & H_{01} & ... & H_{0J} & ... \\ H_{10} & H_{11}-\lambda & ... & H_{1J} & ... \\ ... & ... & ... & ... & ... \\ H_{J0} & H_{J1} & ... & H_{JJ}-\lambda & ... \\ ... & ... & ... & ... & ... \end{pmatrix} \begin{pmatrix} C_0 \\ C_1 \\ ... \\ C_J \\ ... \end{pmatrix} = \begin{pmatrix} 0 \\ 0 \\ ... \\ 0 \\ ... \end{pmatrix} \qquad (2.41)$$

The diagonalization of this matrix allows us to obtain the eigenvalues which correspond to a series of energies from the ground state to higher excited states.

2.9 Multi-Configuration Self-Consistent-Field (MCSCF) method

This method is a CI method, in which the coefficients of the Slater determinants in a linear combination are variationally optimized, as well as the molecular orbitals included in these determinants. This variational optimization is performed iteratively as in the SCF method. In the MCSCF method, the spaces of the molecular orbitals are divided into three sub-spaces (inactive, active, and external) according to the occupation numbers of electrons in the molecular orbitals. The orbitals in the inactive space are doubly occupied in all the configurations and correspond to the core orbitals. The active space consists of the orbitals which can take the occupation number among 0, 1, and 2. The definition of the active space is essential in the MCSCF method. The orbitals in the external space are empty in the MCSCF wavefunction. The multi-configurational character of the wavefunction due to these partially occupied molecular orbitals allows us to recover a large part of the electronic correlation. The static correlation can be accounted by inclusion of the quasi-degenerated configurations in the MCSCF wavefunction.

In the MCSCF method, the wavefunction can be expressed by a linear combination of the Configuration State Functions (CSFs) Ψ_I with the associated coefficients C_I:

$$\Psi_{MCSCF} = \sum_I C_I \Psi_I, \quad \sum_I C_I^2 = 1 \qquad (2.42)$$

The CSFs Ψ_I is again constructed as a linear combination of the Slater determinants which are built with a set of the canonical molecular orbitals ψ_k. The ψ_k is expressed by the unitary transformation of the basis set functions χ_μ, with the orthonormal restriction $<\psi_k|\psi_l> = \delta_{kl}$:

$$\psi_k = \sum_\mu c_{k\mu} \chi_\mu \qquad (2.43)$$

The simultaneous optimization of the coefficients C_I and the canonical molecular orbitals ψ_k via $c_{k\mu}$ is required in the MCSCF method. Introducing the Lagrange's undetermined multipliers, the following secular equation can give optimization of the coefficients C_I:

$$\sum_J (H_{IJ} - E\delta_{IJ}) C_J = 0 \qquad (2.44)$$

The determination of ψ_k and the corresponding minimum energy are given using the Newton-Raphson method [8].

The most popular approach of the MCSCF method is the Complete Active Space Self-Consistent Field (CASSCF) method, which takes the valence space as the active space. In the inactive space, the molecular orbitals are doubly occupied or virtual. These doubly occupied orbitals can be treated as "frozen" (not optimized and their electrons are not correlated) or as "closed" (optimized). The configurations involved in the CASSCF method are all the configurations constructed by filling the molecular orbitals in the active space with the valence electrons as much as possible and keeping the inactive space orbitals doubly occupied. In this sense, the CASSCF method is one kind of Full CI method in a limited active space. The active space should be appropriately selected to correctly treat modifications of the orbitals with the geometry distortions of the system.

The MCSCF method can recover about 40% of the electronic correlation and can describe correctly the wavefunction. However, for the case where we need more accurate descriptions, it is necessary to perform beyond the MCSCF method, the subsequent MRCI method, which can account for almost completely the electronic correlation.

2.10 Multi-Reference Configuration Interaction (MRCI) method

The Multi-Reference Configuration Interaction (MRCI) method is also a CI method, which uses the multi-configurational function as reference. In general, the optimized MCSCF wavefunction is taken as reference. The MRCI method can account for the interactions between the determinants corresponding to the single and double excitations from the reference determinants.

As the previous CI methods, we write the MRCI wavefunction as a linear combination of the CSFs Ψ_I.

$$\Psi_{MRCI} = \sum_I C_I \Psi_I + \sum_S \sum_a C_S^a \Psi_S^a + \sum_P \sum_{a,b} C_P^{a,b} \Psi_P^{a,b} \qquad (2.45)$$

taking the MCSCF function as reference:

$$\Phi_0 = \sum_R C_R \Psi_R \qquad (2.46)$$

where I indicates the sum over the CSFs, in contrast, R runs over the configurations of reference. We call "internal space" the set of orbitals which construct the configuration in reference and "external space" the set of orbitals occupied by the single or double excitations. The orbitals in the external space are symbolized by a and b. The S and P correspond to the single and double excitations from the configurations of reference, respectively. Practically, as the division of orbitals in the CASSCF method, we can define the "closed-shells" which are correlated in the internal space, in contrast, the "core" orbitals are always doubly occupied and non-correlated.

This technique can significantly reduce the size of calculations.

The coefficients C_I are variational parameters to be optimized via the secular equation. The problem of the MRCI method is the huge number of included configurations. One of the procedures to reduce the dimension of configurations is "internal contraction" developed by Werner and Reinsch [9]: contraction of all the configurations owning the same external space but different internal space. The following formula of the internal contraction have been developed by Werner and Knowles [10, 11] for the configurations resulting from the double excitation to the external space.

$$\Psi_{ijp}^{ab} = \frac{1}{2}\left(\hat{E}_{ai,bj} + p\hat{E}_{aj,bi}\right)\Phi_0$$

$$= \sum_R C_R \left(\hat{E}_{ai,bj} + p\hat{E}_{aj,bi}\right)\Psi_R = \sum_R C_R \Psi_{ijp,R}^{ab} \qquad (2.47)$$

p is the spin factor taking 1 for the singlet coupling and -1 for the triplet coupling. $\hat{E}_{ai,bj}$ is an operator corresponding to the double excitations from the i and j internal orbitals to the a and b external orbitals respectively. Internally contracted MRCI wavefunctions can be rewritten as follows:

$$\Psi_{MRCI} = \sum_I C_I \Psi_I + \sum_S \sum_a C_S^a \Psi_S^a + \sum_D \sum_{a,b} \sum_p C_{Dp}^{ab} \Psi_{Dp}^{ab} \qquad (2.48)$$

The configurations of the single excitations to the external space are not contracted. If these configurations of the single excitations were also internally contracted, the number of variational parameters would not depend on the size of the reference space.

The expansion of the MRCI wavefunction is limited to the double excitations. Thus this method is not size-consistent as the previous CISD and CISDT methods. The Davidson correction [12] can estimate the energy with contributions up to quadruple excitations, based on the MRCI energy up to double excitations. It uses the following formula:

$$\Delta E_Q = \Delta E_{SD}\left(1 - \sum_R C_R^2\right) \qquad (2.49)$$

where ΔE_{SD} represents the contribution to the correlation energy, of the single and double excitations accounted within the MCSCF reference wavefunction Φ_0, and C_R is the same coefficient as in the expansion (2.46).

3 Basis sets and Pseudopotentials

3.1 Basis sets

As mentioned in the last paragraph, the molecular orbitals are written as a linear combination of the atomic basis functions χ_i. There are two types of basis function: Slater Type functions (STO) [17] and Gaussian Type functions (GTO) [18]. In the spherical coordinates (r, θ, ϕ), the STO takes the following form, derived directly from the hydrogenous function:

$$\chi_{\zeta,n,l,m}(r,\theta,\phi) = NY_{l,m}(\theta,\phi)r^{n-1}exp(-\zeta r) \qquad (3.1)$$

where ζ is a parameter to denote the radial extension. This type of function can provide a good description from the short to the long distances from nucleus, however, it is not convenient to perform bi-electronic integrations. The other one (GTO) is written as follows:

$$\chi_{\zeta,n,l,m}(r,\theta,\phi) = NY_{l,m}(\theta,\phi)r^{2n-2-l}exp(-\zeta r^2) \qquad (3.2)$$

The GTO can facilitate multi-centric integrations. In contrast to the STO, the description of the GTO is incorrect at the short and the long distances, because of its zero slope due to r^2 dependency in exponential and of the decay of $e^{-\zeta r^2}$ faster than $e^{-\zeta r}$. In practice, we combine linearly several GTO functions to express the atomic orbital. With a large ζ, the GTO function is localized close to the nucleus and describes the core region. A medium coefficient ζ is used to reproduce the chemical bonds and for properties as polarization and dipole moments. The GTO functions are diffused with the small values of ζ.

In a linear combination, the GTO functions are partially contracted, i.e. the coefficients of several GTO functions are frozen, to reduce the number of parameters in calculations. We use n for the number of contractions to represent the valence orbitals, in general, n = 2, 3, 4, 5. Adding more primitive Gaussian functions, the "correlation-consistent polarized n-zeta basis set (cc-pVnZ)" is designed to account for the correlation energy. The basis set augmented with diffuse functions is denoted by aug-cc-pVnZ, which we use mainly in this work. The more correlation energy is accounted for the larger cardinal number n. This fact leads to the idea of extrapolation to the Complete Basis Set (CBS), i.e. the convergence of energy E_{CBS} at n = ∞. E_{CBS} can be estimated, using the parameters determined in the following relations:

$$E(n) = E_{CBS} + Be^{-(n-1)} + Ce^{-(n-1)^2} \qquad (3.3)$$

$$E(n) = E_{CBS} + B/n^3 \qquad (3.4)$$

For the three cardinal numbers n = 3, 4, 5, we use the equation (3.3) and note CBS(1) [19,20]. In contrast, the extrapolation can be performed with the second one (3.4) for n = 4, 5 and this method is denoted by CBS(2) [21, 22].

3.2 Pseudopotentials

Pseudopotentials (or synonymously effective core potentials) are used as standard tools nowadays in valence *ab initio* quantum chemical calculations. The essential idea of pseudopotentials relies on the fact that inactive core electrons in atoms do not participate to the chemical bonds, contrary to the active electrons in the valence shells. Thus it is reasonable to replace the core electrons by effective potentials including all informations about them and to treat explicitly the valence electrons. This procedure has two advantages specially for atoms owning the large atomic numbers. The size of calculations is proportional to n^4 (n is the number of electrons included in the system), thus inclusion of the inactive core electrons in pseudopotentials allows us to reduce the actual cost of calculations without loss of the physical and chemical informations. It has been recognized that the relativistic effects are important for heavy atoms, principally in the inner orbitals. The second advantage of pseudopotentials is the automatical inclusion of relativistic effects of heavy atoms, in the non-relativistic calculations of valence electrons.

In this method of pseudopotentials, the electrons in the inner shells are represented by the energy-consistent pseudopotentials $V_{PP}(i)$ and the Hamiltonian of the electrons in valence is given in atomic units by:

$$\hat{H}_{val} = -\sum_i \frac{\Delta_i}{2} + \frac{1}{2}\sum_{i,i'} \frac{1}{r_{ii'}} + \sum_i V_{PP}(i) \qquad (3.5)$$

where the indices i and i$'$ denote the valence electrons.

In this study, we employ the pseudopotentials (ECP10MDF) for Zn, recently reported by Figgen *et al.* [13]. The term "MDF" means the simultaneously adjusted two-component relativistic pseudopotentials (i.e., scalar-relativistic and spin-orbit), based on the numerical all-electron four-component multi-configuration Dirac-Hartree-Fock (MCDHF) calculation. The ECP2MWB and ECP10MWB pseudopotentials, developed by Bergner *et al.* [14] are used respectively for F and Cl atom. The MWB type of pseudopotential is a one-component quasi-relativistic pseudopotentials (i.e., spin-orbit averaged), determined from the numerical all-electron Wood-Boring calculations.

$V_{PP}(i)$ of the MDF type is written in a semi-local ansatz as follows:

$$V_{PP}(i) = -\frac{Q}{r_i} + \sum_{l,j}\sum_k A_{lj,k} exp(-\alpha_{lj,k} r_i^2)\hat{P}_{l,j} \qquad (3.6)$$

and for the MWB type:

$$V_{PP}(i) = -\frac{Q}{r_i} + \sum_{l}\sum_k B_{l,k} exp(-\beta_{l,k} r_i^2)\hat{P}_{l} \qquad (3.7)$$

where Q denotes the core charge of the atom. $\hat{P}_{l,j}$ or $\hat{P}_l$ represents the projection operator with respect to the angular momentum quantum number l and j = l $\pm$ 1/2 or l. k indicates the number of parameters for each l. Using the valence wavefunction $\phi_{l(j)}(r)$ from the all-electron calculations, the following transformation leads to the nodeless pseudo-orbital $\tilde{\phi}_{l(j)}(r)$:

$$\tilde{\phi}_{l(j)}(r) = \phi_{l(j)}(r) \quad (r \geq r_c), \quad = f_{l(j)}(r) \quad (r < r_c) \qquad (3.8)$$

The parameters in $V_{PP}(i)$ are determined to provide as far as possible the energies obtained from all-electron calculations, using the Hamiltonian for the valence electrons (3.5) and the pseudo-orbitals (3.8). For the ECP10MDF of Zn, the reference data to adjust the parameters is the valence energy E_i^{val} of the i^{th} state in the neutral atom and near-neutral ions, obtained from the all-electron calculation at the four-component numerical MCDHF level, based on the Dirac-Coulomb Hamiltonian with the two-electron Breit interaction treated to first-order perturbation theory. While, for the MWB type, E_i^{val} corresponds to the valence energy of the lowest LS states of a multitude of low lying configurations of the neutral atoms and the LS ground state of the singly charged anions. Then the reference data to determine the parameters of the MWB effective core potentials are provided by the numerical Wood-Boring all-electron calculations, which add a mass-velocity and a Darwin terms to the non-relativistic Hamiltonian [15, 16]. Denoting the corresponding valence energy E_i^{PP} calculated by the non-relativistic valence Hamiltonian (3.5), the adjustment of the parameters are performed by a least-squares fit to minimize the following functional:

$$\sum_i (E_i^{val} - E_i^{PP})^2 \qquad (3.9)$$

For Zn, using the ECP10MDF, the 1s, 2s, and 2p orbitals are replaced by pseudopotentials and the outer core 3spd shells, in addition to 4sp shells are treated explicitly for the valence. The ECP2MWB of F and the ECP10MWB of Cl replace respectively 2 and 10 core electrons by pseudopotentials and 7 outer electrons in both atoms are treated explicitly in the all-electron valence calculations.

4 Description of the nuclear motions

4.1 Generality of the nuclear motions

Having resolved the electronic Schrödinger equation within the Born-Oppenheimer approximation, using the methods mentioned above, the question is then to obtain descriptions of the nuclear motions under the adiabatic potential $E_m(\mathbf{R})$ included in the equation (1.13). For the N atoms in a molecule, the degree of freedom of the nuclear motions is 3N, among which 3 degrees of freedom are attributed to the three directions of translation. 3 degrees (or 2 degrees for linear molecules) result from the rotations. The remaining (3N - 6) (or (3N - 5) for the linear molecules) are related to the vibrations. Because of the invariance of the potential energy function under the translation of nuclear coordinates, 3 degrees attributed to translation can be removed into the motion of the center of mass. In this chapter, we will explain the descriptions of the nuclear vibrations and rotations and the actual approaches to obtain the spectroscopic constants characterizing these motions under the potential energy function $E_m(\mathbf{R})$, for the diatomic and the triatomic molecules.

4.2 Diatomic molecule and NUMEROV program

4.2.1 Rotational and vibrational energy levels

The Hamiltonian of the nuclear motions in diatomic molecules under the potential V can be written as:

$$\hat{H}_N = -\frac{\hbar^2}{2m_1}\Delta_1 - \frac{\hbar^2}{2m_2}\Delta_2 + V(|\mathbf{R}_1 - \mathbf{R}_2|) \qquad (4.1)$$

where m_1 and m_2 are the mass of the nuclei 1 and 2 respectively. The potential V depends only on the interatomic distance between the two atoms and equals to the adiabatic potential $E_m(\mathbf{R})$.

Defining $\mathbf{R} = \mathbf{R}_1$ - $\mathbf{R}_2$, neglecting the translation of the center of mass, and introducing the spherical coordinates (R, θ, ϕ), we can rewrite the Hamiltonian (4.1) as follows:

$$\hat{H}_N = -\frac{\hbar^2}{2\mu}\Delta + V(R) = -\frac{\hbar^2}{2\mu}\frac{1}{R^2}\frac{\partial}{\partial R}\left(R^2\frac{\partial}{\partial R}\right) + \frac{\hat{N}^2}{2\mu R^2} + V(R) \qquad (4.2)$$

where μ represents the reduced mass. The angular momentum operator $\hat{N}^2$ and its eigen spherical harmonic functions $Y_{Nm}(\theta, \phi)$ are defined as follows:

$$\hat{N}^2 = -\frac{1}{sin\theta}\frac{\partial}{\partial\theta}\left(sin\theta\frac{\partial}{\partial\theta}\right) - \frac{1}{sin^2\theta}\frac{\partial^2}{\partial\phi^2} \qquad (4.3)$$

$$\hat{N}^2 Y_{Nm}(\theta, \phi) = \hbar^2 N(N+1) Y_{Nm}(\theta, \phi) \qquad (4.4)$$

Thus we express the nuclear wavufunction $\Phi(R, \theta, \phi)$, using the $Y_{Nm}(\theta, \phi)$ and the radial function R(R). Substituting $\Phi(R, \theta, \phi)$ into the stationary Schrödinger equation for the Hamiltonian (4.2), we obtain the following equation for the radial function R(R):

$$\Phi(R,\theta,\phi) = \frac{R(R)}{R} Y_{Nm}(\theta,\phi) \qquad (4.5)$$

$$\left[-\frac{\hbar^2}{2\mu} \left(\frac{d}{dR} \right)^2 + V(R) + \frac{\hbar^2 N(N+1)}{2\mu R^2} - E \right] R(R) = 0 \qquad (4.6)$$

with the bound conditions imposed on R(R):

$$R(R=0) = 0 \quad and \quad R(R \to \infty) \to 0 \qquad (4.7)$$

The third term in the equation (4.6) represents the centrifugal distortion effects and indicates that the molecule can no longer be treated as a rigid body. After the Taylor expansion around the equilibrium distance R_e of the potential V(R) up to the 4^{th} order of R, we can separate the Hamiltonian $\hat{H}_N$ into the harmonic oscillator and the rigid body rotation part $\hat{H}_0$ and the perturbative parts $\hat{H}_1$ and $\hat{H}_2$:

$$\hat{H}_N = \hat{H}_0 + \hat{H}_1 + \hat{H}_2 \qquad (4.8)$$

$$\hat{H}_0 = -\frac{\hbar^2}{2\mu} \frac{d^2}{d\zeta^2} + V(R_e) + \frac{1}{2} k\zeta^2 + \frac{\hbar^2 N(N+1)}{2\mu R_e^2} \qquad (4.9)$$

$$\hat{H}_1 = -a\zeta^3 - \frac{\hbar^2 N(N+1)}{\mu R_e^3} \zeta \qquad (4.10)$$

$$\hat{H}_2 = b\zeta^4 + \frac{3\hbar^2 N(N+1)}{2\mu R_e^4} \zeta^2 \qquad (4.11)$$

where $\zeta = R - R_e$. The term $\frac{1}{2}k\zeta^2$ denotes the harmonic potential and the third and fourth anharmonicities are included by the terms $-a\zeta^3$ and $b\zeta^4$ respectively. Taking the perturbation corrections by $\hat{H}_1$ and $\hat{H}_2$, we can express the vibrational and rotational energy levels in power series expansion of (v+1/2) and N(N+1). Including contributions from the higher order perturbations, the energy levels E(v,N) for nuclear motions in diatomic molecules are obtaind as follows:

$$E(v,N) = G(v) + F(N) \qquad (4.12)$$

$$G(v) = \omega_e (v + \frac{1}{2}) - \omega_e x_e (v + \frac{1}{2})^2 + ... \qquad (4.13)$$

$$F(N) = B(v)N(N+1) - D[N(N+1)]^2 + ... \qquad (4.14)$$

$$B(v) = B_e - \alpha_e (v + \frac{1}{2}) + ... \qquad (4.15)$$

where G(v) represents the vibrational energy levels and F(N) the rotational levels including the centrifugal distortion constant D and the rotation-vibration interaction constant α_e via B(v). B_e is the equilibrium rotation constant given as $B_e = \frac{1}{2\mu R_e^2}$. This type of energy levels is called the Dunham expansion [23].

4.2.2 Vibronic transition

Within the dipole approximation of the interaction between photons and molecules, electronic transitions are allowed between two electronic states satisfying the following conditions.

$$\Delta\Lambda = 0, \quad or \quad \Delta\Lambda = \pm 1 \qquad (4.16)$$

where Λ is the eigen value of the projection on the z axis of the electronic orbital angular momentum. $\Delta\Lambda = 0$ is applied for the parallel transitions and $\Delta\Lambda = \pm 1$ for the perpendicular transitions. In addition, electronic transition is allowed between two Σ^+ states or two Σ^- states and forbidden between the Σ^+ and Σ^- states.

For the vibrationally resolved absorption, we can use the oscillator strength to characterize the intensities of transitions. This quantity $I_{vv'}$ has no dimension and is defined as below for the vibronic transition from the v' vibrational level of the initial electronic state to the v vibrational state of the final electronic state.

$$I_{vv'} = 2\nu_{vv'} B_{vv'} c^2 \qquad (4.17)$$

$$B_{vv'} = \frac{1}{2\pi\epsilon_0 3} |\mathbf{R}_{vv'}|^2 \qquad (4.18)$$

$$\mathbf{R}_{vv'} = \int dr \psi_v^* \mu_{ee'} \psi_{v'} \qquad (4.19)$$

where $B_{vv'}$ is the Einstein's B coefficient and $\nu_{vv'}$ is the wavenumber of the corresponding spectrum line. $\mathbf{R}_{vv'}$ represents the transition matrix and is defined by the equation (4.19), using the dipole moment function $\mu_{ee'}(R)$ and $\psi_v(R) = R_v(R)/R$.

4.2.3 NUMEROV program

Using the NUMEROV program [24], which can give a numerical resolution of the nuclear Schrödinger equation in diatomic molecules (4.6), we obtain the spectroscopic constants and the quantities to describe the vibrationally resolved absorption. In the first step of this program, the adiabatic potential E(R) obtained by the electronic calculations is fitted by the following Morse type potential V(R) and the difference between E(R) and V(R) is adjusted by cubic splines:

$$V(R) = v_a + e^{-v_b(R-v_c)} + cubic \quad splines \qquad (4.20)$$

The NUMEROV program is able to calculate the spectroscopic constants ω_e and $\omega_e x_e$ from vibrational energy levels G(v). The equilibrium distance r_e and B_e are deduced at the minimum of the V(R) potential. Since the vibrational wavefunctions can be calculated simultaneously for the two different electronic states, we can also obtain the quantities to characterize the vibronic transition such as the oscillator strength.

This program resolves numerically the equation (4.6), using the Numerov's method. Defining d as the difference between two consecutive discrete distances:

$$d = R_{i+1} - R_i \qquad (4.21)$$

we rewrite the functions in the equation (4.6) as follows:

$$V_i = V(R_i) \quad G_i = R(R_i) \qquad (4.22)$$

And then F_i is introduced by:

$$F_i = \frac{2\mu}{\hbar^2}(E - V_i) - \frac{N(N+1)}{R_i^2} \qquad (4.23)$$

Thus the equation (4.6) leads to the following equation, which is resolved iteratively.

$$G_{i+1} = \frac{(2 - \frac{5}{6}d^2F_i)G_i - (1 + \frac{d^2}{12}F_{i-1})G_{i-1}}{1 + \frac{d^2}{12}F_{i+1}} \qquad (4.24)$$

4.3 Nuclear motions in triatomic molecule

4.3.1 Nuclear Hamiltonian in triatomic molecule

The nuclear Hamiltonian for rotations and vibrations can be constructed using the normal coordinates Q_s, following the procedure described below. For the jth nucleus in molecule, we write its space-fixed coordinate $\mathbf{R}_j$ in terms of the center of mass fixed at space $\mathbf{R}_G$ and the molecule-fixed coordinate of the jth nucleus $\mathbf{r}_j$ with the origin fixed at the center of mass:

$$\mathbf{R}_j = \mathbf{R}_G +^t \mathbf{D}(\alpha\beta\gamma)\mathbf{r}_j \quad (j = 1, 2, 3) \qquad (4.25)$$

where α, β, and γ denote the Euler angles, and the corresponding 3×3 matrix $\mathbf{D}(\alpha\beta\gamma)$ relates the space-fixed coordinates to the ones fixed at molecule. Taking the displacement d$\mathbf{R}_j$ and ignoring the displacement of center of mass d$\mathbf{R}_G$, we obtain the following relation between two coordinates;

$$d\mathbf{R}_j = d\mathbf{\Omega} \times ({}^t\mathbf{D}\mathbf{r}_j) +^t \mathbf{D}d\mathbf{r}_j \qquad (4.26)$$

where d$\mathbf{\Omega}$ represents the infinitesimal rotation angles around the axes of the space-fixed coordinate. From (4.26) the term of d$\mathbf{R}_j$·d$\mathbf{R}_j$ is expressed as the following relation:

$$d\mathbf{R}_j \cdot d\mathbf{R}_j = (d\mathbf{\Omega} \times^t \mathbf{D}\mathbf{r}_j) \cdot (d\mathbf{\Omega} \times^t \mathbf{D}\mathbf{r}_j) + 2(d\mathbf{\Omega} \times^t \mathbf{D}\mathbf{r}_j) \cdot^t \mathbf{D}d\mathbf{r}_j + ({}^t\mathbf{D}d\mathbf{r}_j) \cdot ({}^t\mathbf{D}d\mathbf{r}_j) \qquad (4.27)$$

In the right hand side the second term can be deduced as follows, using the $d\mathbf{\Omega}' = \mathbf{D}d\mathbf{\Omega}$ and the relation $(\mathbf{A} \times \mathbf{B}) \cdot \mathbf{C} = \mathbf{A} \cdot (\mathbf{B} \times \mathbf{C})$.

$$2(d\mathbf{\Omega} \times^t \mathbf{D}\mathbf{r}_j) \cdot^t \mathbf{D}d\mathbf{r}_j = 2(d\mathbf{\Omega}' \times \mathbf{r}_j) \cdot d\mathbf{r}_j = 2d\mathbf{\Omega}' \cdot (\mathbf{r}_j \times^t \mathbf{D}d\mathbf{r}_j) \qquad (4.28)$$

With the help of (4.28) and the definition of the inertia tensor $\mathbf{I} = \sum_j m_j(|\mathbf{r}_j|^2 - \mathbf{r}_j^t\mathbf{r}_j)$, we can write the sum of $\frac{1}{2}m_j d\mathbf{R}_j \cdot d\mathbf{R}_j$ from the equation (4.27).

$$\frac{1}{2}\sum_j m_j d\mathbf{R}_j \cdot d\mathbf{R}_j = \frac{1}{2} d\mathbf{\Omega}' \cdot \mathbf{I} d\mathbf{\Omega}' + d\mathbf{\Omega}' \cdot \sum_j m_j (\mathbf{r}_j \times d\mathbf{r}_j) + \frac{1}{2}\sum_j m_j d\mathbf{r}_j \cdot d\mathbf{r}_j \qquad (4.29)$$

We denote the equilibrium geometry of the jth nucleus as $\mathbf{r}_j^e$ and the displacement from it as $\Delta\mathbf{r}_j = \mathbf{r}_j - \mathbf{r}_j^e$. Then the transformation between $\Delta\mathbf{r}_j$ and the normal coordinates Q_s is given by:

$$(m_j)^{1/2}\Delta\mathbf{r}_j = \sum_s \mathbf{l}_{js} Q_s \qquad (4.30)$$

Using the $\mathbf{l}_{js}$ in the transformation (4.30), the Coriolis constant $\zeta_{ss'}$ can be defined as (4.31) and then the matrix $\mathbf{Z}$ is defined as (4.32):

$$\zeta_{ss'} = \sum_j \mathbf{l}_{js} \times \mathbf{l}_{js'} \qquad (4.31)$$

$$\mathbf{Z}_{\alpha s'} = \sum_s \zeta_{ss'}^{\alpha} Q_s \qquad (4.32)$$

The equation (4.29) can be rewritten in the following matrix formula:

$$\frac{1}{2}\sum_j m_j d\mathbf{R}_j \cdot d\mathbf{R}_j = \begin{pmatrix} {}^t d\mathbf{\Omega}' & {}^t d\mathbf{Q} \end{pmatrix} \begin{pmatrix} \mathbf{I} & \mathbf{Z} \\ {}^t\mathbf{Z} & \mathbf{1} \end{pmatrix} \begin{pmatrix} d\mathbf{\Omega}' \\ d\mathbf{Q} \end{pmatrix} \qquad (4.33)$$

From the relation (4.33) of the coordinate transformation, we can write the kinetic energy operator $\hat{T}$ in terms of $\mathbf{\Omega}'$ and $\mathbf{Q}$:

$$\hat{T} = -\frac{\hbar^2}{2}(det\mathbf{g})^{-1/2} \begin{pmatrix} {}^t\frac{\partial}{\partial\mathbf{\Omega}'} & {}^t\frac{\partial}{\partial\mathbf{Q}} \end{pmatrix} \mathbf{g}^{-1} (det\mathbf{g})^{1/2} \begin{pmatrix} \frac{\partial}{\partial\mathbf{\Omega}'} \\ \frac{\partial}{\partial\mathbf{Q}} \end{pmatrix} \qquad (4.34)$$

$$\mathbf{g} = \begin{pmatrix} \mathbf{I} & \mathbf{Z} \\ {}^t\mathbf{Z} & \mathbf{1} \end{pmatrix} \qquad (4.35)$$

For the matrix $\mathbf{g}$, $\mathbf{g}^{-1}$ and det($\mathbf{g}$) can be deduced after the manipulation.

$$\mathbf{g}^{-1} = \begin{pmatrix} \mathbf{1} & \mathbf{0} \\ -{}^t\mathbf{Z} & \mathbf{1} \end{pmatrix} \begin{pmatrix} (\mathbf{I} - \mathbf{Z}{}^t\mathbf{Z})^{-1} & \mathbf{0} \\ \mathbf{0} & \mathbf{1} \end{pmatrix} \qquad (4.36)$$

$$det(\mathbf{g}) = det(\mathbf{I} - \mathbf{Z}{}^t\mathbf{Z}) \qquad (4.37)$$

Introducing the total angular momentum $\hat{\mathbf{J}}$, the vibrational angular momentum $\hat{\pi}$, and the μ tensor, the kinetic energy operator $\hat{T}$ takes the following form:

$$\hat{T} = \frac{1}{2}{}^t(\hat{\mathbf{J}} - \hat{\pi})\mu(\hat{\mathbf{J}} - \hat{\pi}) - \frac{\hbar^2}{2}\frac{\partial}{\partial\mathbf{Q}} \cdot \frac{\partial}{\partial\mathbf{Q}} \qquad (4.38)$$

$$\hat{\mathbf{J}} = \frac{\hbar}{i}\frac{\partial}{\partial\mathbf{\Omega}'} \qquad (4.39)$$

$$\hat{\pi} = \frac{\hbar}{i}\mathbf{Z}\frac{\partial}{\partial\mathbf{Q}} \qquad (4.40)$$

$$\mu = \mathbf{I}'^{-1} \quad \mathbf{I}' = \mathbf{I} - \mathbf{Z}^t\mathbf{Z} \qquad (4.41)$$

In consequence, the Hamiltonian for the rotational and vibrational nuclear motions around the equilibrium configuration in polyatomic molecule can be expressed as the following formula in terms of $\hat{\mathbf{J}}$, $\hat{\pi}$, μ, and the potential $\mathrm{V}(\mathrm{Q}_s)$:

$$\hat{H}_N = \frac{1}{2}\sum_{\alpha,\beta}\mu_{\alpha\beta}(\hat{J}_\alpha - \hat{\pi}_\alpha)(\hat{J}_\beta - \hat{\pi}_\beta) + \frac{1}{2}\sum_s \hat{P}_s^2 + V(Q_s) \qquad (4.42)$$

where $\hat{P}_s$ denotes the conjugate momentum of the normal coordinate Q_s.

4.3.2 Perturbative resolution: SURFIT program

The SURFIT program can give by perturbative treatment the rovibrational energy levels for the nuclear motions in triatomic molecule, based on the nuclear Hamiltonian (4.42) [25]. In the first step, the potential energy surface obtained by the electronic calculations are rewritten in polynomial expression in term of the molecular internal coordinates d_i:

$$V(d_1, d_2, d_3) = \sum_{i,j,k} C_{ijk} f_1(d_1)^i f_2(d_2)^j f_3(d_3)^k \qquad (4.43)$$

where the order of polynomials can range from 4 to 8, according to the case. The polynomial expression (4.43) should satisfy the following conditions: The symetry of the system must be adopted in the polymonials. The energies obtained by the electronic calculations have to be accurately reproduced in the polynomial expression within the error less than 1 cm^{-1}. The polynomials should provide the potential energy surface obtained from the electronic calculations, up to the suitable energy value (about 1 eV) from the minimum point. This energy value is a criterion of validity, such that the rovibrational levels are correct up to this energy value. In the SURFIT program, the function $\mathrm{f}_i(\mathrm{d}_i)$ can take several types. In this study, we use the displacements of the internal coordinates and limit the order of polynomials up to 4. Then $\mathrm{f}_i(\mathrm{d}_i)$ can be expressed by:

$$f_i(d_i) = d_i - d_i^e \qquad (4.45)$$

where d_i^e denotes the internal coordinate d_i at the equilibrium geometry. The coefficients C_{ijk} of the polynomial expression are determined by a least-squares method to give the minimum of the following sum Γ:

$$\Gamma = \sum_n^P [V_n(d_1, d_2, d_3) - E_n(d_1, d_2, d_3)]^2 \qquad (4.46)$$

where E_n is the energy value obtained by the electronic calculation at the n^{th} nuclear geometry.

For the perturbative resolution of the nuclear Schrödinger equation, it is necessary to express the potential in term of dimensionless normal coordinates q_k. Then we write the $\mu_{\alpha\beta}$ tensor and the potential by the Taylor expansion in term of q_k around the equilibrium geometry. First, q_k and its conjugate momentum p_k are introduced by:

$$q_k = \lambda_k^{1/4} Q_k \quad p_k = \lambda_k^{-1/4} Q_k \qquad (4.47)$$

where $\lambda = (2\pi c\omega_k)^2$ and ω_k is the harmonic wavenumber of the kth normal mode. Second, we can write the Taylor expansion as follows:

$$\mu_{\alpha\beta} = \mu^0_{\alpha\beta} + \sum_k hcB^k_{\alpha\beta} q_k + ... \quad B^\alpha_e = \frac{1}{2hc}\mu^0_{\alpha\alpha} = \frac{1}{2hcI^e_\alpha} \qquad (4.48)$$

$$\frac{V}{hc} = \frac{1}{2}\sum_k \omega_k q_k^2 + \frac{1}{6}\sum_{l,m,n} \Phi_{lmn} q_l q_m q_n + \frac{1}{24}\sum_{l,m,n,p} \Phi_{l,m,n,p} q_l q_m q_n q_p + ... \qquad (4.49)$$

where the coefficients Φ_{lmn} and Φ_{lmnp} represent the cubic and quartic constants of the potential, which are respectively determined by the third and fourth derivatives of the potential with respect to the dimensionless normal coordinate q_k. Finally, we can deduce $\hat{H}_N/hc$ as the sum of the perturbative terms up to the fourth order (4.50):

$$\hat{H}_{02} = \sum_\alpha B^\alpha_e J^2_\alpha$$

$$\hat{H}_{12} = \sum_{\alpha\beta}\sum_k B^k_{\alpha\beta} q_k J_\alpha J_\beta$$

$$\hat{H}_{22} = \frac{3}{8}\sum_{\alpha\beta\gamma}\sum_{kl} (B^\gamma_e)^{-1}(B^k_{\alpha\gamma}B^l_{\gamma\beta} + B^l_{\alpha\gamma}B^k_{\gamma\beta}) q_k q_l J_\alpha J_\beta$$

$$\hat{H}_{21} = -2\sum_{kl}\left(\frac{\omega_l}{\omega_k}\right)^{1/2} q_k p_l \sum_\alpha B^\alpha_e \zeta^\alpha_{kl} J_\alpha$$

$$\hat{H}_{20} = \frac{1}{2}\sum_k \omega_k (p_k^2 + q_k^2)$$

$$\hat{H}_{30} = \frac{1}{6}\sum_{klm} \Phi'_{klm} q_k q_l q_m$$

$$\hat{H}_{40} = \frac{1}{24}\sum_{klmn} \Phi'_{klmn} q_k q_l q_m q_n + \sum_{klmn}\sum_\alpha B^\alpha_e \zeta^\alpha_{kl}\zeta^\alpha_{mn}\left(\frac{\omega_l\omega_n}{\omega_k\omega_m}\right)^{1/2} q_k p_l p_m p_n$$

We can attribute the following interpretations to the terms in the equations (4.50): $\hat{H}_{02}$ rigid rotator, $\hat{H}_{12}$ and $\hat{H}_{22}$ centrifugal distortion, $\hat{H}_{21}$ Coriolis interaction, $\hat{H}_{20}$ harmonic oscillator, $\hat{H}_{30}$ vibrational anharmonicity, and $\hat{H}_{40}$ vibrational anharmonicity and l-doubling.

The perturbative method of the rotation and vibration Hamiltonian of the polyatomic molecule was developed by Shaffer, Nielsen, and Thomas [26]. The essential idea is the successive block diagonalizations of the perturbative part of the Hamiltonian, using the Van Vleck transformation which will be explained below.

The concerned Hamiltonian $\hat{H}$ can be separated into the non-perturbative $\hat{H}_0$ and the perturbative $\hat{H}_1$ parts such that $\hat{H}_0 \gg \hat{H}_1$:

$$\hat{H} = \hat{H}_0 + \hat{H}_1 \qquad (4.51)$$

where the non-perturbative part $\hat{H}_0$ is initially diagonal. To diagonalize this Hamiltonian, we need to find the transformation that decomposes $\hat{H}_1$ into the small terms $\hat{D}^{(i)}$ commuting with $\hat{H}_0$.

$$\hat{H}_D = \hat{U}^\dagger \hat{H} \hat{U} = \hat{H}_0 + \hat{D}^{(1)} + \hat{D}^{(2)} + \hat{D}^{(3)} + ... \qquad (4.52)$$

For the complete diagonalization, these terms are required to be mutually commuting. The unitary transformation $\hat{U}$ responsible for the diagonalization of Hamiltonian can be expressed as a product of operators $\hat{W}_j$, which transforms the small terms to commute with all the larger terms:

$$\hat{U} = \prod_{j=1} \hat{W}_j \qquad (4.53)$$

and then,

$$\hat{H}_{D1} = \hat{W}_1^\dagger \hat{H} \hat{W}_1 = \hat{H}_0 + \hat{D}_1^{(1)} + \hat{D}_1^{(2)} + \hat{D}_1^{(3)} + ... \qquad (4.53)$$

where $[\hat{H}_0, \hat{D}_1^{(i)}] = 0$, but the $\hat{D}_1^{(i)}$ are not required to commute with each other. In the first step, the Hamiltonian becomes to be block diagonal with respect to $\hat{H}_0$, denoted as $\hat{H}_{D1}$. The second operator $\hat{W}_2$ can be then applied to the terms $\hat{D}_1^{(i)}$ with i≥2, transforming into the terms $\hat{D}_2^{(i)}$ with i≥2:

$$\hat{H}_{D2} = \hat{W}_2^\dagger \hat{H}_{D1} \hat{W}_2 = \hat{H}_0 + \hat{D}_1^{(1)} + \hat{D}_2^{(2)} + \hat{D}_2^{(3)} + ... \qquad (4.54)$$

where $[\hat{H}_0 + \hat{D}_1^{(1)}, \hat{D}_2^{(i)}] = 0$ for i≥2, but the terms $\hat{D}_2^{(i)}$ are not required to commute among themselves. The resulting Hamiltonian $\hat{H}_{D2}$ is block diagonalized with respect to $\hat{H}_0$ and $\hat{D}_1^{(1)}$. This procedure continues up to the desired order of the block diagonalization. Once the terms $\hat{D}_j^{(i)}$ for $i \geq j$ after the jth transformation with the operator $\hat{W}_j$ commute with themselves, the progressive diagonalization is completed. The operator $\hat{W}_j$ can be written in terms of the generators $\hat{G}_j^k$ for the unitary transformations:

$$\hat{W}_j = exp\left(i \sum_{k=1} \hat{G}_j^k\right) \qquad (4.55)$$

where $\hat{G}_j^k$ is an Hermitian operator and then the operator $\hat{U}$ is denoted as follows:

$$\hat{U} = \prod_{j=1} exp\left(i \sum_{k=1} \hat{G}_j^k\right) \qquad (4.56)$$

In general, the harmonic oscillator term $\hat{H}_{20}$ is taken as the non-perturbative part, for which the eigenenergy is well known:

$$\frac{E_0(v)}{hc} = \sum_k \omega_k (v_k + \frac{d_k}{2}) \qquad (4.57)$$

where d_k denotes the degeneracy of the kth vibration mode. The corresponding wavefunction of the non-degenerated mode and of the doubly degenerated mode are also known as follows:

$$\Psi_k(Q_k) = N_k e^{-1/2\gamma_k Q_k^2} H_{v_k}(\gamma_k^{1/2} Q_k) \qquad (4.58)$$

for the non-degenerated mode

$$\Psi_{v,k}(\rho,\phi) = N_{v,|l|} e^{-\rho^2/2} \rho^{|l|} L^{|l|}_{(v-|l|)/2}(\rho^2) e^{-il\phi} \qquad (4.59)$$

for the doubly degenerated mode, where H_{v_k} and $L^{|l|}_{(v-|l|)}$ denote respectively the Hermite polynomial and the associated Legendre polynomial. γ_k is equal to ω_k/h. The doubly degenerated normal coordinates Q_a and Q_b are transformed as $Q_a = rcos\phi$ and $Q_b = rsin\phi$ and the $\rho = (h/\omega_k)^{1/2} r$. The number l is associated to the vibrational angular momentum.

In turn, we obtain the Hamiltonian for the pure vibrations:

$$\hat{H}_v = \hat{H}_{20} + \hat{H}_{40} \qquad (4.60)$$

Within this representation, the energy levels for the harmonic oscillators with the contributions from the anharmonic vibrations up to the fourth order:

$$G(v_1, v_2, ...) = \sum_{i}^{3N-6(3N-5)} \omega_i (v_i + \frac{d_i}{2}) + \sum_i \sum_{k \geq i} x_{ik} (v_i + \frac{d_i}{2})(v_k + \frac{d_k}{2}) + \sum_i \sum_{k \geq i} g_{ik} l_i l_k \qquad (4.61)$$

where x_{ik} and g_{ik} are the anharmonic constants.

For the pure rotation, the Hamiltonian of rigid rotator can be given by:

$$\hat{H}_{02} = A_e J_x^2 + B_e J_y^2 + C_e J_z^2 \qquad (4.62)$$

with the eigenvalues in the |J,K> representation, which is the eigenfunction of $\hat{J}^2$ and $\hat{J}_z$.

$$< J,K|\hat{H}_{02}|J,K >= \frac{1}{2}\left[(A_e + B_e)[J(J+1) - K^2] + 2C_e K^2\right] \qquad (4.63)$$

$$< J,K|\hat{H}_{02}|J,K\pm 2 >= \frac{1}{4}(A_e - B_e)[J(J+1) - K(K\pm 1)]^{1/2}[J(J+1) - (K\pm 1)(K\pm 2)]^{1/2} \qquad (4.64)$$

Using the expressions described above, the SURFIT program can give the rotation and vibration energy levels up to the fourth order without the centrifugal distortion and the Coriolis coupling:

$$\frac{E(v,J)}{hc} = G(v) + F(v,J) \qquad (4.65)$$

The first term G(v) has already been given in (4.61) and the secod term F(v,J) denotes the eigenvalues of the Hamiltonian of rigid rotator $\hat{H}_{02}$ and of the most important part of the rotation-vibration coupling terms in $\hat{H}_{22}$. F(v,J) takes different forms according to the types of the concerned molecule. In this study, we will treat the linear molecule and then F(v,J) can be rewritten as follows:

$$F(v,l,J) = B_v[J(J+1) - l^2], \quad B_v = B_e + \sum_k \alpha_k^b (v_k + \frac{d_k}{2}) \qquad (4.66)$$

For the linear molecule, there is no rotation around the molecular axes, thus K=l. The constant α_k^b included in the second equation denotes the vibrational dependency of the rotational constant.

4.3.3 Variational resolution: RVIB3 program

The RVIB3 program, developed by Carter and Handy [27], gives a variational resolution for the rotational and vibrational nuclear Hamiltonian expressed as follows. Diagonalizing the matrix elements of the Hamiltonian with the initially constructed basis function, this method can reveal the rovibronic or rovibrational energy levels and the corresponding wavefunctions.

In the case of a triatomic molecule, the nuclear kinetic operator can be expressed by the terms $\hat{T}_v$ and $\hat{T}_{vr}$, with the internal coordinates (R_1,R_2,θ).

$$\begin{aligned}\hat{T}_v(R_1,R_2,\theta) = &-\frac{1}{4}\left(\frac{1}{\mu_1 R_1^2} + \frac{1}{\mu_2 R_2^2} - \frac{2cos\theta}{m_B R_1 R_2}\right)\left(\frac{\partial^2}{\partial\theta^2} + cot\theta\frac{\partial}{\partial\theta}\right) \\ &-\frac{1}{2\mu_1}\frac{\partial^2}{\partial R_1^2} - \frac{1}{2\mu_2}\frac{\partial^2}{\partial R_2^2} - \frac{cos\theta}{m_B}\frac{\partial^2}{\partial R_1 \partial R_2} \\ &+\frac{1}{m_B}\left(\frac{1}{R_1}\frac{\partial}{\partial R_2} + \frac{1}{R_2}\frac{\partial}{\partial R_1}\right)\left(sin\theta\frac{\partial}{\partial\theta} + cos\theta\right) \qquad (4.62)\end{aligned}$$

$$\begin{aligned}\hat{T}_{vr}(R_1,R_2,\theta,\hat{\mathbf{J}},\hat{\mathbf{L}},\hat{\mathbf{S}}) = &\frac{1}{8cos^2\theta/2}\left(\frac{1}{\mu_1 R_1^2} + \frac{1}{\mu_2 R_2^2} + \frac{2}{m_B R_1 R_2}\right)(\hat{\mathbf{J}}_z + \hat{\mathbf{L}}_z + \hat{\mathbf{S}}_z)^2 \\ &+\frac{1}{8sin^2\theta/2}\left(\frac{1}{\mu_1 R_1^2} + \frac{1}{\mu_2 R_2^2} - \frac{2}{m_B R_1 R_2}\right)(\hat{\mathbf{J}}_x + \hat{\mathbf{L}}_x + \hat{\mathbf{S}}_x)^2 \\ &\frac{1}{8}\left(\frac{1}{\mu_1 R_1^2} + \frac{1}{\mu_2 R_2^2} + \frac{2}{m_B R_1 R_2}\right)(\hat{\mathbf{J}}_y + \hat{\mathbf{L}}_y + \hat{\mathbf{S}}_y)^2 \\ &-\frac{1}{4sin\theta}\left(\frac{1}{\mu_1 R_1^2} - \frac{1}{\mu_2 R_2^2}\right)[\hat{\mathbf{J}}_z + \hat{\mathbf{L}}_z + \hat{\mathbf{S}}_z, \hat{\mathbf{J}}_x + \hat{\mathbf{L}}_x + \hat{\mathbf{S}}_x]_+ \\ &+\frac{i}{2}\left(\frac{1}{\mu_1 R_1^2} - \frac{1}{\mu_2 R_2^2}\right)\left(\frac{cot\theta}{2} + \frac{\partial}{\partial\theta}\right)(\hat{\mathbf{J}}_y + \hat{\mathbf{L}}_y + \hat{\mathbf{S}}_y) \\ &+\frac{i}{2}\frac{sin\theta}{m_B}\left(\frac{1}{R_2}\frac{\partial}{\partial R_1} - \frac{1}{R_1}\frac{\partial}{\partial R_2}\right)(\hat{\mathbf{J}}_y + \hat{\mathbf{L}}_y + \hat{\mathbf{S}}_y) + A_{SO}\hat{\mathbf{L}}\cdot\hat{\mathbf{S}} \qquad (6.63)\end{aligned}$$

where all the included variables are defined, for the ABC triatomic molecule with the centered B atom, as follows:

R_1: interatomic distance between the A and B atoms.
R_2: interatomic distance between the B and C atoms.

θ: bending angle $\widehat{ABC}$.
μ_1: reduced mass of the A atom mass m_A and that of the B atom m_B, $1/\mu_1 = 1/m_A + 1/m_B$.
μ_2: reduced mass of the B atom mass and that of the C atom m_C, $1/\mu_2 = 1/m_B + 1/m_C$.
$A_{SO}\hat{\mathbf{L}} \cdot \hat{\mathbf{S}}$: inclusion of the spin-orbit coupling by the semi-empirical term.

Thus the Hamiltonian of issue can be given by:

$$\hat{H} = \hat{T}_v + \hat{T}_{vr} + \hat{V} \qquad (4.64)$$

where $\hat{V}$ denotes the potential energy surface obtained by the electronic calculations and is actually taken from the polynomial expansion in term of the internal coordinates performed precedently by the SURFIT program. For the degenerated electronic state, $\hat{V}$ can be written by the corresponding two components V_X and V_Y, with the projection operators $\hat{P}_X$ and $\hat{P}_Y$ on the X and Y two components of the degenerated state, respectively.

$$\hat{V} = V_X \hat{P}_X + V_Y \hat{P}_Y \qquad (4.65)$$

In this study, however, the RVIB3 program will be employed to treat a $^1\Sigma^+$ state, being non-degenerated.

The next issue is how to establish the initial basis set, with which the size of the matrix elements is limited at best. In general, the wavefunctions of the electronic states and the eigenfunctions of the electronic spins are introduced as initial basis set. For the singlet non-degenerated electronic state, however, the construction of the basis functions is simple, because the eigen values of the $\hat{L}_z$ and $\hat{S}_z$ operators equal to zero. Thus the corresponding functions are not included.

For the stretching vibrations with the R_1 and R_2 internal coordinates, the wavefunctions of harmonic oscillator are employed, owning the following form:

$$F_n(R_i) = C_n e^{-\frac{(R_i - R_i^e)^2}{2\beta^2}} H_n(\frac{R_i - R_i^e}{\beta}), \quad \beta = \left(\frac{1}{\mu_i f_i}\right)^{1/4} \qquad (4.67)$$

where R_i^e denotes the equilibrium distance of R_i, μ_i the reduced mass of the two corresponding atoms, and f_i the force constant. H_n represents the Hermite polynomial. For the case that the stretching vibration has the large anharmonicity, the wavefunction of the Morse oscillator can be applied.

For the bending vibration, the function is required to cancel all singularities arising in the kinetic energy operator in linear geometry. To satisfy this claim, Carter and Handy use the associated Legendre polynomial $P_n^{|l|}(cos\theta)$ with the bending coordinate θ. Because $P_n^{|l|}(cos\theta)$ can be expressed for any $|l|$ using the terms $P_n^0(cos\theta)$ and $P_n^1(cos\theta)$, it is sufficient to employ $P_n^0(cos\theta)$ for even K and even Λ or odd K and odd Λ, or $P_n^1(cos\theta)$ for even K and odd Λ or odd K and even Λ, where K denotes the quantum number of the operator $\hat{J}_z$ and Λ that of the operator $\hat{L}_z$. The z axis of the molecule-fixed coordinate becomes the linear axis as the angle θ tends to 180°.

The inclusion of the rotation part in the initial basis set is simplified for the $^1\Sigma^+$ state of our interest, because there is no contribution from the electronic orbital and the electronic spin angular momenta. In general case, the eigenfunctions of the $\hat{\mathbf{L}}_z^2$ and the electronic spin function should be included. For the singlet non-degenerated state, the rotation part in the basis function consists of the Wang combinations of the rotation-matrix eigenfunctions:

$$D^J_{m,K^\pm}(\alpha,\beta,\gamma) = \frac{1}{\sqrt{2}}[D^J_{m,K}(\alpha,\beta,\gamma) \pm D^J_{m,-K}(\alpha,\beta,\gamma)] \qquad (4.68)$$

$$D^J_{m,K}(\alpha,\beta,\gamma) = e^{im\alpha} d^J_{m,K}(\beta) e^{i\gamma K} \qquad (4.69)$$

where α, β, and γ denote the Euler angles in the molecule-fixed coordinates (x, y, z) related to the space-fixed coordinates (X, Y, Z). $\mathrm{d}^J_{m,K}(\beta)$ is the rotation matrix. m and K are respectively the quantum numbers of the operator $\hat{\mathbf{J}}_Z$ and $\hat{\mathbf{J}}_z$. Taking 0 for m, $D^J_{m,K^\pm}(\alpha,\beta,\gamma)$ becomes as follows:

$$D^J_{0,K^\pm}(\alpha,\beta,\gamma) = \frac{1}{\sqrt{2}}[d^J_{0,K}(\beta) e^{i\gamma K} \pm d^J_{0,-K}(\beta) e^{-i\gamma K}] \qquad (4.70)$$

In this method, to reduce the dimension of the Hamiltonian matrix elements, diagonalization are performed successively, starting with the smallest effective Hamiltonian where several coordinates are fixed at equilibrium. The proper vectors obtained by the preceding diagonalization are used as the basis functions for the next diagonalization of the larger Hamiltonian with more variables. This procedure, developed by Carter and Handy, is quite effective to diagonalize the rovibrational matrix.

References

[1] E. Schrödinger, *Ann. Phys.*, **79**, 361 (1926).

[2] M. Born and R. Oppenheimer, *Ann. Phys.*, **84**, 457 (1927).

[3] D. R. Hartree, *Proc. Camb. Phil. Soc.*, **24**, 329 (1928).

[4] V. A. Fock, *Z. Phys.*, **15**, 126 (1930).

[5] C. J. Slater, *Phys. Rev.*, **35**, 210 (1930).

[6] C. Roothaan, *Rev. Mod. Phys.*, **23**, 69 (1951).

[7] G. Hall, *Proc. R. Soc. London A*, **205**, 541 (1951).

[8] P. Jensen and P. R. Bunker, *Introduction to Computational Molecular Spectroscopy*, John Wiley & Sons 2000.

[9] H.-J. Werner and E.-A. Reinsch, *J. Chem. Phys.*, **76**, 3144 (1982).

[10] H.-J. Werner and P. J. Knowles, *J. Chem. Phys.*, **89**, 5853 (1988).

[11] P. J. Knowles and H.-J. Werner, *Chem. Phys. Lett.*, **145**, 514 (1988).

[12] S. R. Langhoff and E. R. Davidson, *Int. J. Quantum Chem.*, **8**, 61 (1974).

[13] D. Figgen, G. Rauhut, M. Dolg, and H. Stoll, *Chem. Phys.*, **311**, 227 (2005).

[14] A. Bergner, M. Dolg, W. Kuechle, H. Stoll, and H. Preuss, *Mol. Phys.*, **80**, 1431 (1993).

[15] R. D. Cowan and D. C. Griffin, *J. Opt. Soc. Am.*, **66**, 1010 (1976).

[16] J. H. Wood and A. M. Boring, *Phys. Rev. B*, **18**, 2701 (1978).

[17] J. Slater, *Phys. Rev.*, **36**, 57 (1930).

[18] S. F. Boys, *Proc. Roy. Soc.*, **A 200**, 542 (1950).

[19] G. Jansen and B. A. Hess, *Phys. Rev.*, **39**, 6016 (1989).

[20] K. A. Peterson, D. E. Woon, and T. H. Dunning Jr., *J. Chem. Phys.*, **100**, 7410 (1994).

[21] T. Helgaker, W. Klopper, H. Koch, and J. Noga, *J. Chem. Phys.*, **106**, 9639 (1997).

[22] A. Halkier, T. Helgaker, P. Jørgensen, W. Klopper, H. Koch, J. Olsen, and A. K. Wilson, *Chem. Phys. Lett.*, **286**, 243 (1998).

[23] J. L. Dunham, *Phys. Rev.*, **41**, 721 (1932).

[24] The NUMEROV program written by J. Senekowitsch *et al.*, Johan Wolfgang Goethe Universität, Frankfort, 1989.

[25] The SURFIT program written by J. Senekowitsch *et al.*, Johan Wolfgang Goethe Universität, Frankfort, 1989.

[26] W. H. Shaffer, H. H. Nielsen, and L. H. Thomas, *Phys. Rev.*, **56**, 895 (1939).

[27] S. Carter, N. C. Handy, C. Puzzarini, R. Tarroni, and P. Palmieri, *Mol. Phys.*, **98**, 1697 (2000).

Second part: Applications

5 Electronic properties of the diatomic compounds concerned with piezoelectric effects

6 Theoretical investigation of the HZnF molecule

5 Electronic properties of the diatomic compounds concerned with piezoelectric effects

5.1 Introduction

Piezoelectric effect is related to the electric polarization in solid and to its modification under an applied strain, as is pyroelectric effect resulting from a change of temperature. The first demonstration of the direct piezoelectric effect was achieved in 1880 by Pierre and Jacques Curie, using crystals of tourmaline, quartz, topaz, cane sugar, and Rochelle salt (sodium potassium tartrate tetrahydrate), among which, quartz and Rochelle salt exhibited the largest piezoelectricity. The converse piezoelectric effect, which is the induced strain under an applied electric field, was found by Gabriel Lippemann in 1881.

Piezoelectric effects are generally observed in ionic semiconductor materials, involving a metal of Group IIa, IIb, or III, and a non-metal of Group V or VI. Typical examples are ZnO and AlN. Many theoretical studies have been performed during the last decades to obtain a reliable representation of piezoelectric effects in solid of ZnO, ZnS, BeO, AlN, and AlP, leading to the determination of their piezoelectric constants. Even at the molecular level, those diatomic molecules, consisting of the same pair of elements which present the piezoelectric effects in solid phase, have the following common feature; two low lying, very close electronic states, a $^1\Sigma^+$ and a $^3\Pi$ states or a $^3\Pi$ and a $^3\Sigma^-$ states, with different electric properties and slightly different equilibrium geometries. Consequently, the ground state of the molecule changes abruptly with a small modification of the geometry, resulting in a large change of the charge distribution.

The purpose of this study is to elucidate these properties of the low lying states of the concerned diatomic compounds, and to examine whether these pairs of elements are good candidates for piezoelectric effects in solid phase. First, we will present the theoretical developments achieved during the last decades to obtain a reliable representation of the electric polarization in solid under an applied strain and summarize the existing piezoelectric tensors reported theoretically and experimentally. Secondly will be discussed the electronic structures of the low lying states of the ZnO and AlN diatomic molecules, which are already well known for piezoelectric effects in solid phase, and of the ZnS and BN diatomic molecules for comparison in the same families. The properties of the low lying states of Alkaline earth chalcogenides diatomic molecules will also be investigated, based on highly correlated *ab initio* electronic calculations.

5.2 Piezoelectric effects in solid phase

Piezoelectric effect is characterized by the induced piezoelectric polarization $\mathbf{P}$, which is related to an applied strain ϵ and to the piezoelectric tensor e_{ij}. In the linear regime, these parameters are connected as follows:

$$P_i = \sum_j e_{ij}\epsilon_j \qquad (5.1)$$

Then the piezoelectric tensor e_{ij} is obtained

$$e_{ij} = \frac{\partial P_i}{\partial \epsilon_j} \qquad (5.2)$$

In the wurtzite structure (hexagonal Bravais lattice, C_{6v} point group), the unit cell contains four atoms and is fully defined by the length of the hexagonal edge a_0, the height of the prism c_0, and the fractional z coordinate u_0 of the sublattice. In this structure, the piezoelectric tensor e_{ij} has just three independent components [1]. Two of them are related to the polarization induced along the c axis (e_{33}) or in the basal plane (e_{31}). The third component e_{15} describes the polarization induced perpendicularly to the c axis by a shear strain. We focus on the components e_{33} and e_{31} in this study and the polarization along the z axis P_3 can be written as follows:

$$P_3 = e_{33}\epsilon_3 + e_{31}(\epsilon_1 + \epsilon_2) \qquad (5.3)$$

where $\epsilon_3 = (c - c_0)/c_0$ and $\epsilon_1 = \epsilon_2 = (a - a_0)/a_0$.

In the last decades, many theoretical studies have been performed to calculate the induced piezoelectric polarization $\mathbf{P}$ and to estimate the piezoelectric tensor. In the very early study, Martin [2] revealed that the piezoelectric tensor is a bulk quantity and independent of sample termination. The method was developed by King-Smith and Vanderbilt [3, 4], which uses the Berry phase to calculate the piezoelectric polarization in function of the strain ϵ. Their method has been applied and further developed in many other studies.

The Berry phase ϕ_h (h = 1,2,3) along the h^{th} crystallographic axis under the strain ϵ is given by the following formula:

$$\phi_h = \frac{2\pi V}{|e|}\mathbf{P} \cdot \mathbf{a}_h^* = \frac{V}{4\pi^2}\sum_n \int d\mathbf{k} < u_n(\mathbf{k})| - i\mathbf{a}_h^* \cdot \nabla_k |u_n(\mathbf{k}) > \qquad (5.4)$$

where V denotes the unit-cell volume, |e| the electron charge, $\mathbf{a}_h^*$ the h^{th} reciprocal lattice vector, n the electron band index, $\mathbf{k}$ the wave vector in the first Brillouin zone, and $u_n(\mathbf{x}, k) = \psi_n(\mathbf{x}, \mathbf{k}) exp(i\mathbf{k} \cdot \mathbf{x})$ where $\psi_n(\mathbf{x}, \mathbf{k})$ is the n^{th} crystalline orbital as the eigenfunction of the one-electron Hamiltonian. $\mathbf{P}$, $\mathbf{a}_h$, and $u_n(\mathbf{x}, \mathbf{k})$ quantities depend on the ϵ parameter. ϵ can be expressed by six components ϵ_k (k = 1,...,6). For the wurtzite structure, the strain can be written as follows in the Voigt notation; [0,0,ϵ,0,0,0] for e_{33} and [ϵ,ϵ,0,0,0,0] for e_{31}. Using the j^{th} direct lattice basis vector $\mathbf{a}_j$ and its i^{th} Cartesian component, we can express the piezoelectric tensor e_{ik} by the following formula:

$$e_{ik} = \frac{|e|}{2\pi V}\sum_j a_{ji}\frac{\partial \phi_j}{\partial \epsilon_k} \qquad (5.5)$$

where we use the orthonormality between the direct and reciprocal lattice vectors.

Table 1: Theoretical and experimental piezoelectric tensors e_{33} and e_{31} in solid with the wurtzite structure.

Molecule	e_{33} /C.m^{-2}	e_{31} /C.m^{-2}	Method	Ref. and Year
ZnO	1.34	-0.57	LDA-DFT	Gopal06$^{(a)}$
	0.89	-0.51	GGA-DFT	Bernardini97$^{(b)}$
	1.19	-0.55	DFT	Catti03$^{(c)}$
	0.92	-0.39	LDA-DFT	Dal Corso94$^{(d)}$
	1.19	-0.53	CRYSTAL	Noel01$^{(e)}$
	1.06-1.31	-0.54 to -0.69	CRYSTAL	Noel02$^{(f)}$
	1.29		HF/DFT	Wu05$^{(g)}$
	1.30	-0.66	DFT	Hill00$^{(h)}$
	1-1.55	-0.36 to -0.62	Exp.	Madelung87$^{(i)}$
	0.96	-0.62	Exp.	Madelung93$^{(j)}$
ZnS	0.18	-0.13	DFT	Catti03$^{(c)}$
	0.24	-0.51	LDA-DFT	DalCorso94$^{(d)}$
	0.34	-0.10	Exp.	Madelung93$^{(k)}$
CdO	1.67	-0.48	LDA-DFT	Gopal06$^{(a)}$
BeO	0.02	-0.02	GGA-DFT	Bernardini97$^{(b)}$
	0.04	-0.07	CRYSTAL	Noel01$^{(e)}$
	0.07		CRYSTAL	Noel02$^{(f)}$
	0.10		DFT	Hill00$^{(h)}$
	0.09		Exp.	Madelung87$^{(i)}$
MgO	1.64	-0.58	LDA-DFT	Gopal06$^{(a)}$
AlN	1.46	-0.60	GGA-DFT	Bernardini97$^{(b)}$
	1.55	-0.58	Exp.	Gualtieri94$^{(l)}$
AlP	0.04	-0.02	LDA-DFT	Gironcoli90$^{(m)}$
GaN	0.73	-0.49	GGA-DFT	Bernardini97$^{(b)}$
InN	0.97	-0.57	GGA-DFT	Bernardini97$^{(b)}$

(a): Taken from ref. [14]: DFT calculations, standard LDA, pseudopotentials.
(b): Taken from ref. [13]: Plane wave, pseudopotential GGA DFT.
(c): Taken from ref. [10]: B3LYP and LDA DFT.
(d): Taken from ref. [8]: LDA-DFT Polarization calculations.
(e): Taken from ref. [5]: HF calculations.
(f): Taken from ref. [6]: HF, LDA-DFT, PBE-DFT, and B3LYP-DFT calculations.
(g): Taken from ref. [11]: HF, DFT.
(h): Taken from ref. [9]: Plane waves, pseudopotentials DFT.
(i): Taken from ref. [15, 16]: Experimental values.
(j): Taken from ref. [17, 18]: Experimental values.
(k): Taken from ref. [17, 19]: Experimental values.
(l): Taken from ref. [20]: Experimental value.
(m): Taken from ref. [21]: DFT, LDA approximation, pseudopotentials, Plane waves.

In the other types of study, as an alternative to the delocalized crystalline orbitals introduced in the Berry phase formalism, well-localized Wannier functions were successfully employed to calculate the polarization properties [5] and several types of Hamiltonian have been checked within the DFT methods [6]. New approaches as molecular dynamics simulations have been used recently to evaluate the piezoelectric tensor in quartz crystal [7]. Among the previous studies, the most investigated systems are ZnO [5, 6, 8–12], ZnS [8, 10], BeO [5, 6, 8], GaAs [3], and (AlN, AlP, GaN, GaP, InN, InP) [13]. Finally we list in Table 1 the piezoelectric tensor e_{31} and e_{33} from the previous theoretical and experimental works.

5.3 General properties of the molecular structure

We will examine the characteristics of the low lying electronic states, which should be considered as precursors of piezoelectric effects, in diatomic compounds with total eight valence electrons, involving a di- or tri-valent metal. This type of diatomic compounds yields from a combination either between a metal of Group IIa(Be, Mg, Ca) or IIb(Zn, Cd, Hg) with a valence electronic configuration ns^2 and a chalcogen (O, S, Se, Te) with a valence electronic configuration $n's^2n'p^4$ or between an element of Group IIIa (B, Al) and an element of Group V (N, P) with a valence electronic configuration ns^2np^1 and $n's^2n'p^3$ respectively. The former compounds are named as the II-VI compounds and the latter named as the III-V compounds.

5.3.1 Nature of the electronic states in the molecular region

The characteristics of the low lying electronic states of the concerned diatomic compounds can be discussed using a simplified molecular orbitals (MOs) diagram constructed with the valence ns and np atomic orbitals of both atoms and without the participative role of the (n-1)d shell, as presented in Figure 1 for ZnO. In this diagram, the label of the MOs runs only from 1σ to 4σ and from 1π to 2π for simplification, with increasing energy as follows; 1σ, 2σ, 1π, 3σ, 2π, and 4σ. Because of the difference of electronegativity between the two atoms, the three lowest MOs, which are principally bonding orbitals, have the dominant character of the more electronegative atom. The 3σ orbital, being the first anti-bonding molecular orbital and preferentially localized on the metal atom, has a key role in these compounds and its energy relative to that of the 1π orbital depends on the difference of electronegativity between the two concerned atoms. If the difference of electronegativity is large, the 3σ is higher in energy than the 1π orbital. Such situation occurs generally for the II-VI compounds, in contrast, for a small difference of electronegativity, the 3σ can be lower in energy than the 1π orbital. The values of electronegativity for concerned atoms are listed in Table 2.

With eight valence electrons, the two lowest 1σ and 2σ orbitals are fully occupied and the four remaining electrons are contained in the 3σ and 1π orbitals. When the four electrons fill completely the 1π orbital, the resulting configuration $1\sigma^2 2\sigma^2 1\pi^4$ leads the molecular system to be ionic and strongly bound with a short bond length. The molecular state is a $^1\Sigma^+$ state, which is the ground state in many cases of the II-VI compounds. The first type of excited configuration

is $1\sigma^2 2\sigma^2 1\pi^3 3\sigma^1$, leading to a $^3\Pi$ and a $^1\Pi$ states whose energies are close to that of the $^1\Sigma^+$ state. These states are less ionic than the $^1\Sigma^+$ state due to an electron transferred back to the metal and are less bound because one electron fills an anti-bonding orbital instead of a bonding one. The $^3\Pi$ state is lying energetically very close to the $^1\Sigma^+$ state and can become alternatively the ground state. The $^1\Pi$ state is higher than these two states but generally within 1.0 eV (8065 cm^{-1}). The second excited configuration is written as $1\sigma^2 2\sigma^2 1\pi^2 3\sigma^2$. The lowest resulting state is a $^3\Sigma^-$ state, being even less ionic and less bound than the $^3\Pi$ and $^1\Pi$ states. This state can be the ground state in the III-V compounds as AlP [24–26].

Table 2: Spectroscopic data of the atoms concerned with this study.

Element	$\chi^{(a)}$	Term	Energy$^{(b)}$/cm^{-1}	Element	$\chi^{(a)}$	Term	Energy$^{(b)}$/cm^{-1}
Be	1.57	^1S_g	0	O	3.44	^3P_g	0
		^3P_u	21980			^1D_g	15709
Be^+		^2S_g	75262				
Mg	1.31	^1S_g	0	S	2.58	^3P_g	0
		^3P_u	21877			^1D_g	8843
Mg^+		^2S_g	61731				
Zn	1.65	^1S_g	0				
		^3P_u	32567				
Zn^+		^2S_g	75847				
Cd	1.69	^1S_g	0				
		^3P_u	30865				
Cd^+		^2S_g	72601				
Hg	2.00	^1S_g	0				
		^3P_u	40366				
Hg^+		^2S_g	84266				
B	2.04	^2P_u	0	N	3.04	^4S_u	0
		^4P_g	28810			^2D_u	19227
B^+		^1S_g	66994				
Al	1.61	^2P_u	0	P	2.19	^4S_u	0
		^2S_g	25347			^2D_u	11368
Al^+		^1S_g	48317				

(a): Taken from ref. [22]. (b): Taken from ref. [23], averaged over the fine structure levels.

Figure 1: Simplified molecular orbitals diagram for the concerned diatomic compounds (presented for ZnO).

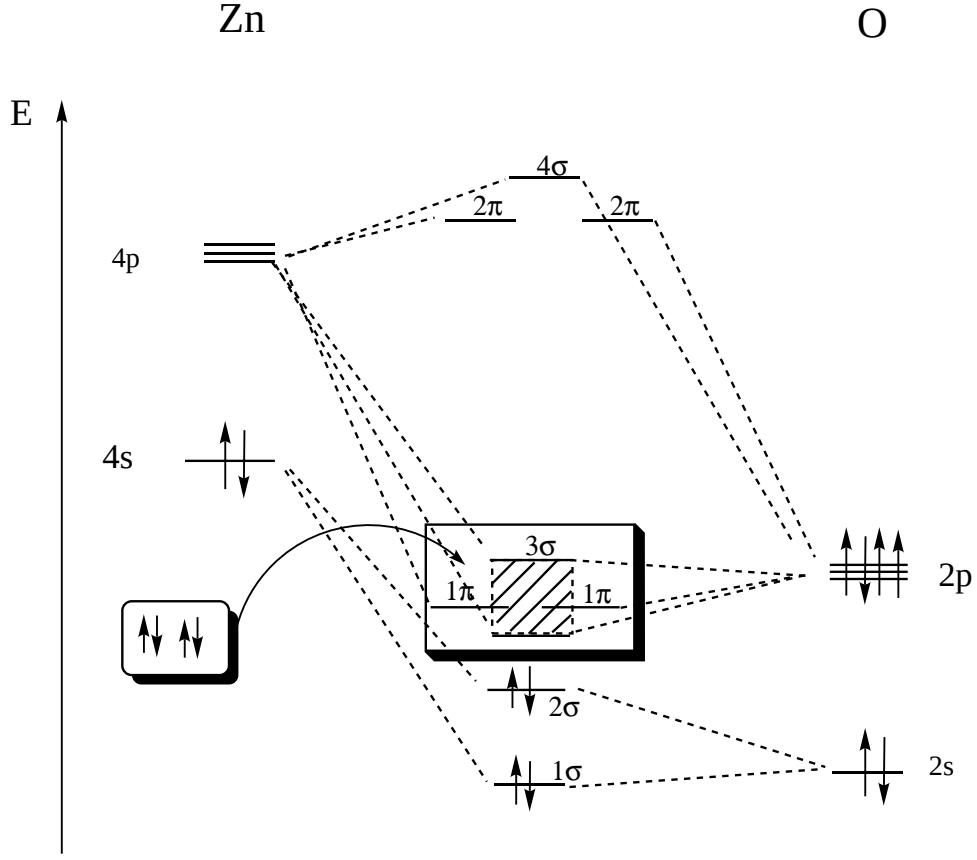

5.3.2 Nature of the electronic states in the asymptotic region

For the II-VI compounds, as presented in Table 2, the energy difference between the two lowest dissociation asymptotes corresponds to the excitation energy from the ^3P_g ground state to the ^1D_g first excited state in the chalcogen atoms (O, S). The first dissociation asymptote results from a combination between the ^1S_g ground state of the metal atom and the ^3P_g ground state of the chalcogen atom, correlating with one $^3\Pi$ and one $^3\Sigma^-$ molecular states. One $^1\Sigma^+$, one $^1\Pi$, and one $^1\Delta$ molecular states result from the second one, corresponding to the ^1S_g ground state of the metal atom and the ^1D_g first excited state of the chalcogen atom. All of the four molecular states $^1\Sigma^+$, $^3\Pi$, $^1\Pi$, and $^3\Sigma^-$ discussed in the last paragraph are adiabatically correlated with these two lowest dissociation asymptotes. The $^1\Delta$ state correlated with the second one lies generally higher in energy than the four others in the molecular region. The first ionic asymptote lies above these two lowest neutral asymptotes, depending on the ionization energy of the metal and on the electronic affinity of the chalcogen. The energy position of this ionic asymptote and the size of atoms determine a zone of crossing between the ionic states and those

correlated with the two lowest covalent asymptotes, which makes the main differences in the II-VI compounds.

For the III-V compounds, the two lowest dissociation asymptotes differ by an excitation in the N or P atom. The first one resulting from the ^2P_u ground state of B or Al and the ^4S_u ground state of N or P, correlates adiabatically with one $^{3,5}\Pi$ and one $^{3,5}\Sigma^-$ molecular states. One $^{1,3}\Sigma^+$, one $^{1,3}\Sigma^-$, one $^{1,3}\Pi$, one $^{1,3}\Delta$, and one $^{1,3}\Phi$ molecular states result from the second one involving the ^2D_u excited state of N or P. All of the four states mentioned above are involved in these two lowest dissociation asymptotes.

5.4 Molecular structure of the diatomic compounds concerned with piezoelectric effects

Using a simplified molecular orbitals diagram as described in the last section, we have revealed roughly the principal electronic properties of the low lying states of the diatomic compounds concerned with piezoelectric effects. However for an accurate picture of these states, it is necessary to perform highly correlated *ab initio* calculations by multi-configurational approaches. In this study, for the first step, state averaged Multi Configuration Self Consistent Field (MCSCF) calculations [27, 28] have been carried out with valence active molecular orbitals to represent the wavefunction of the outer electrons. Taking the MCSCF wavefunctions as reference, subsequently the internally contracted Multi Reference Configuration Interaction (MRCI) calculations [29, 30] have been performed including the Davidson correction which approximates contributions of higher excitation terms [31,32]. All these electronic structure calculations have been realized with the MOLPRO program package [33].

Spin-orbit effects and zero-point energy of vibration are not taken into account in this study. Because the main configurations of the $^1\Sigma^+$ and the $^3\Pi$ states (or between the $^3\Pi$ and the $^3\Sigma^-$ states) differ only by one spin-orbital (namely $1\pi/3\sigma$), the spin-orbit coupling between two states in each family could be considered to be of the same order of magnitude. As a consequence, it is not a factor which can differentiate the charge transfer effect in the diatomic compound and the resulting piezoelectric effects in solid phase.

5.4.1 Group IIb chalcogenides

The equilibrium distance r_e, the harmonic wavenumber ω_e, the dipole moment μ_e, and the relative energy T_e, for the lowest electronic states of the IIb-VI compounds MX (M = Zn, Cd, and Hg, X = O and S) are compared and compiled with the available existing data to illustrate the electronic characteristics as precursors for piezoelectric effects.

To take relativistic effects of heavy atoms into account, atomic pseudopotentials have been employed for the metallic atoms [34] with the associated correlation consistent cc-pwCV5Z-PP basis sets reported by Peterson *et al.* [35,36]. For the oxygen the aug-cc-pVnZ (n = 3, 4, 5)basis sets [37,38] and for the sulfur the aug-cc-pV(n+d)Z (n = 3, 4, 5) basis sets [39,40] have been used

respectively. Due to the multi-configurational character of these low lying states, it is required to include more states in the calculations for an accurate description. In the MCSCF step, for example, the included electronic states for both ZnO and ZnS are as follows; two $^1\Sigma^+$, two $^1\Pi$, one $^1\Sigma^-$, one $^1\Delta$, two $^3\Pi$, two $^3\Sigma^-$, and one $^3\Delta$ states. Taking the MCSCF wavefunction as reference, the potential curves at the MRCI+Q level and the dipole moments at the MRCI level have been calculated for the $^1\Sigma^+$, $^1\Pi$, $^3\Pi$, and $^3\Sigma^-$ states, separately in each space and spin symmetries. The (n-1)s, (n-1)p, (n-1)d, ns, and np orbitals of the metals were optimized in the MCSCF calculations but neither the (n-1)s orbital nor (n-1)p orbital were correlated at both the MCSCF and the MRCI steps. The MCSCF calculations have optimized the core orbitals of the chalcogens, but the corresponding electrons have not been correlated in the MCSCF and the MRCI steps.

Table 3: Spectroscopic constants of the low lying electronic states of ZnO and ZnS.

State	Method	r_e /bohr	ω_e /cm^{-1}	T_e /cm^{-1}	μ_e /a.u.
ZnO					
$^1\Sigma^+$					
This work[a]	MRCI+Q	3.22	753.6	0	1.69
Peterson07[b]	MRCI+Q/CBS	3.23	721.7	0	
Peterson07[b]	CCSD(T)	3.223	731.2	0	2.10
Jensen07[c]	DFT	3.33			1.90
Boldyrev97[d]	QCISD	3.27	690	0	2.11
Kullie06[e]	DFT	3.18	750		
Dolg86[f]	MRCI	3.27	643		2.49
Bauschlicher98[g]	CCSD(T)	3.25	727	0	
Bakalbassis96[h]	ASED	3.19	813		1.76
Fancher98[i]	Exp.		805	0	
Kim01[j]	Exp.		770	0	
$^3\Pi$					
This work[a]	MRCI+Q	3.47	571.4	1969	1.07
Peterson07[b]	MRCI+Q/CBS	3.468	581.8	1920	
Boldyrev97[d]	QCISD	3.54	525	1734	1.03
Bauschlicher98[g]	CCSD(T)	3.51	567	2097	
Fancher98[i]	Exp.			2016	
Kim01[j]	Exp.	3.50	540	2460	
$^1\Pi$					
This work[a]	MRCI+Q	3.44	742.4	3967	1.15
Kim01[j]	Exp.	3.47	600	4960	

State	Method	r_e /bohr	ω_e /cm^{-1}	T_e /cm^{-1}	μ_e /a.u.
ZnS					
$^1\Sigma^+$					
This work$^{(a)}$	MRCI+Q	3.87	472.7	0	2.01
Peterson07$^{(b)}$	MRCI+Q/CBS	3.867	459.4	0	
Peterson07$^{(b)}$	CCSD(T)	3.886	453.5	0	2.00
Raptis99$^{(k)}$	CCSD(T)	3.91			1.99
Jensen07$^{(c)}$	DFT	4.01			1.90
Boldyrev97$^{(d)}$	QCISD	3.92	447	0	2.06
$^3\Pi$					
This work$^{(a)}$	MRCI+Q	4.22	347.0	3980	0.81
Peterson07$^{(b)}$	MRCI+Q/CBS	4.197	343.8	3840	
Boldyrev97$^{(d)}$	QCISD	4.27	329	2258	0.71
$^1\Pi$					
This work$^{(a)}$	MRCI+Q	4.21	363.8	6888	0.86

(a): AV5Z basis set.
(b): Taken from ref. [42] : MRCI+Q and Complete basis set CBS extrapolation; dipole moment calculated at the CCSD(T)/AVTZ level of theory; T_0 values.
(c): Taken from ref. [45] : BLYP calculations.
(d): Taken from ref. [46] : QCISD(T) calculations, QCISD for dipole moment and ω_e values.
(e): Taken from ref. [47] : Relativistic DFT calculations.
(f): Taken from ref. [48] : MRCI+Q calculations.
(g): Taken from ref. [49] : CCSD(T) calculations.
(h): Taken from ref. [50] : ASED-MO approach.
(i): Taken from ref. [51] : from photoelectron spectroscopy : T_0 value.
(j): Taken from ref. [43] : from photoelectron spectroscopy : T_0 value.
(k): Taken from ref. [52] : equilibrium geometry and dipole moment calculated at the CCSD(T) level with relativistic correction.

The potentials curves of the low lying states of ZnO and ZnS calculated at the MRCI+Q level, are presented in Figures 2 and 3. The electronic structures of these two compounds show similar properties in the bonding region. It is clearly found that the $^1\Sigma^+$ state is the lowest one followed by the $^3\Pi$ and the $^1\Pi$ states in turn. These three states are lying quite close to each other. The repulsive $^3\Sigma^-$ state has not been depicted in Figures 2 and 3. The dipole moments of these four states of ZnO and ZnS, calculated at the MRCI level, are presented in Figures 4 and 5, showing the common characteristics in both compounds. The dipole value of the $^1\Sigma^+$ state is much higher than that of the two Π states, which lie somehow above that of the $^3\Sigma^-$ state. Except for the dipole moment of the $^1\Pi$ state, these values vary little with the interatomic distance.

The spectroscopic constants for the $^1\Sigma^+$, $^3\Pi$, and $^1\Pi$ states of ZnO and ZnS have been

Figure 2: Potential energy curves of the low lying states of ZnO at the MRCI+Q level of theory.

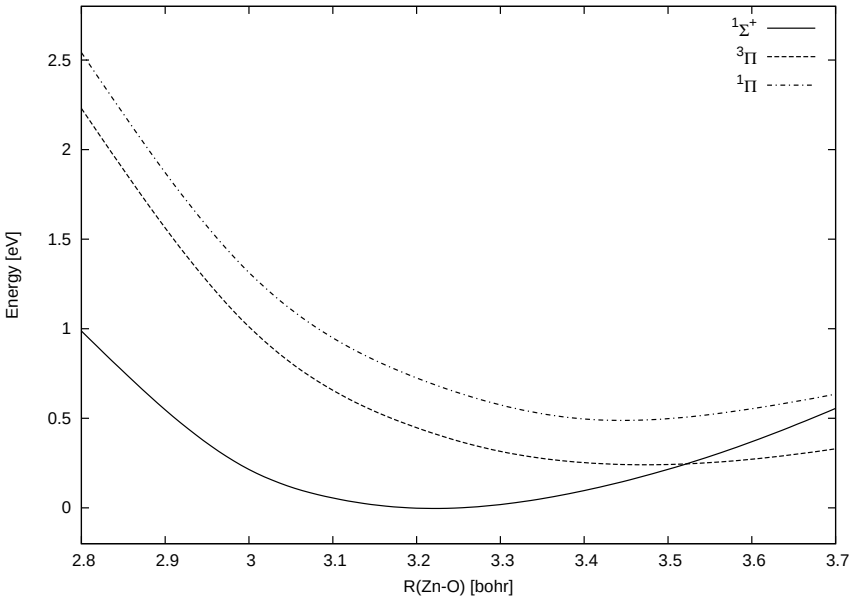

Figure 3: Potential energy curves of the low lying states of ZnS at the MRCI+Q level of theory.

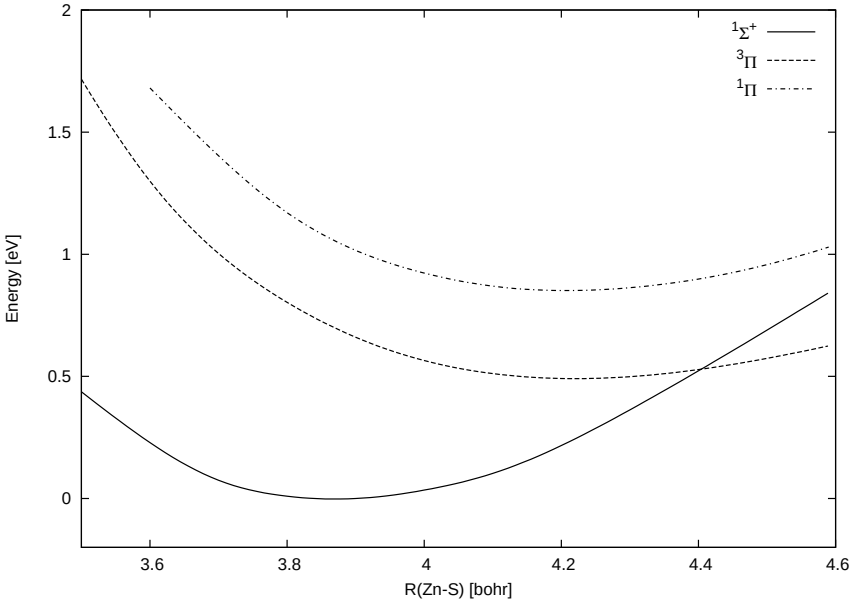

Figure 4: Dipole moments of the low lying states of ZnO at the MRCI level of theory.

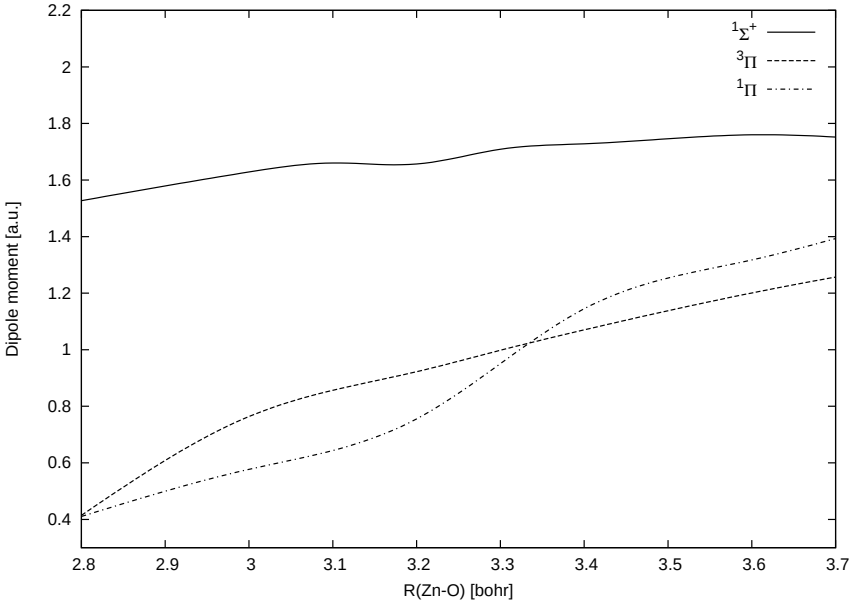

Figure 5: Dipole moments of the low lying states of ZnS at the MRCI level of theory.

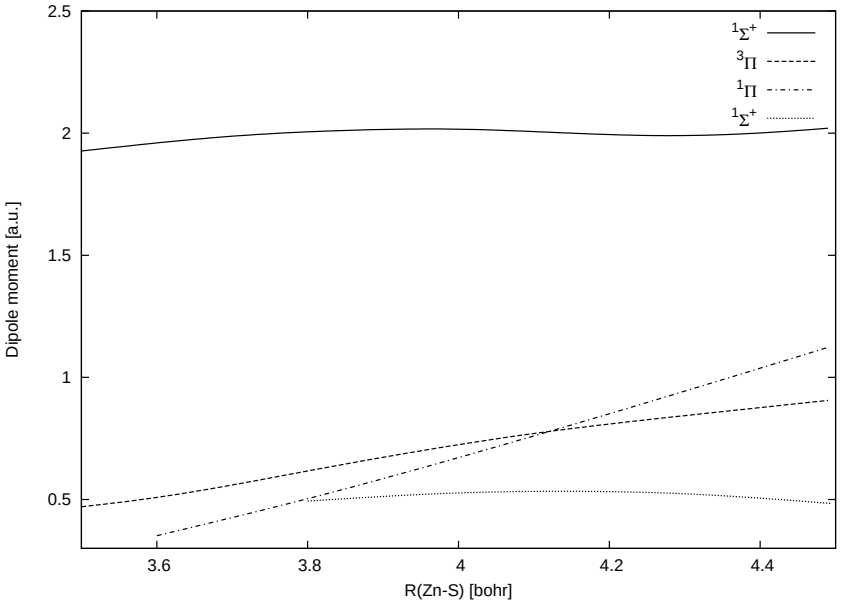

obtained using the NUMEROV algorithm [41] and are listed in Table 3. The previous values are compiled together in Table 3 and the experimental and theoretical methods are mentioned in the footnotes. Our calculated equilibrium distances of the $^1\Sigma^+$ and $^3\Pi$ states show good agreement with those calculated by Peterson *et al.* [42] at the MRCI+Q level with the CBS extrapolation method. The equilibrium distances of the $^3\Pi$ state are longer by 0.25 and 0.35 bohr than those of the $^1\Sigma^+$ state for ZnO and ZnS respectively. The energy differences of the $^3\Pi$ state relative to the $^1\Sigma^+$ ground state are found to be 1969 cm^{-1} for ZnO and 3980 cm^{-1} for ZnS in this study, which compare well with the values reported by Peterson *et al.* [42]. In the case of ZnO, our calculated value is somehow smaller than the experimental values [43, 44]. In both compounds, the second $^1\Pi$ excited state is well separated in energy from the $^3\Pi$ first excited state, by about 2000 cm^{-1} for ZnO and about 3000 cm^{-1} for ZnS. Except for a slightly too small value for the $^1\Sigma^+$ ground state of ZnO, our calculated dipole moments show good agreement with the previous values. The ratio of the dipole moments between the $^1\Sigma^+$ state and the $^3\Pi$ state is found to be 1.6 for ZnO and 2.5 for ZnS.

For the low lying states of CdO and CdS compounds, we show in Figures 6 and 7 the potentials curves at the MRCI+Q level and in Figures 8 and 9 their dipole moments at the MRCI level, using the AV5Z basis set. The calculated spectroscopic constants of the cadmium compounds are presented in Table 4 and these for mercury compounds are listed in Table 5. In these four compounds, the $^1\Sigma^+$ and $^3\Pi$ states are the two lowest states and the former is the ground state except for HgO. There is no existing experimental data, however our results are in good agreement with the spectroscopic values of the previous calculations. Our calculated excitation energies T_e of the $^3\Pi$ states of CdO and HgO show the difference from these of Perterson *et al.*. These discrepancies can be due to different number of states included in the state averaged MCSCF calculations and inclusion of extrapolation to the Complete Basis Set. Based on our calculation, the energy difference between these two lowest states ranges from 322 (HgO) to 2453 cm^{-1} (CdS). In all compounds, for the concerned two states, the ratio of the dipole moments is equal to 2 or more and the difference of the equilibrium distances is about 0.4 bohr.

Table 4: Calculated spectroscopic constants of the low lying electronic states of CdO and CdS.

State	Method	r_e /bohr	ω_e /cm^{-1}	T_e /cm^{-1}	μ_e /a.u.
CdO					
$^1\Sigma^+$					
This work[a]	MRCI+Q	3.61	622.3	0	2.21
Peterson07[b]	MRCI+Q/CBS	3.619	604.3	0	
Peterson07[b]	CCSD(T)	3.627	597.1	0	2.22
Kullie06[c]	DFT	3.56	628		
$^3\Pi$					
This work[a]	MRCI+Q	3.89	474	1225	1.32
Peterson07[b]	MRCI+Q/CBS	3.891	482.9	626	
CdS					
$^1\Sigma^+$					
This work [a]	MRCI+Q	4.25	419.4	0	2.22
Peterson07[b]	MRCI+Q/CBS	4.252	382.6	0	
Peterson07[b]	CCSD(T)	4.267	376.7	0	2.25
Raptis99[d]	CCSD(T)	4.31			2.26
$^3\Pi$					
This work[a]	MRCI+Q	4.61	294.4	2453	0.99
Peterson07[b]	MRCI+Q/CBS	4.594	289.7	2413	

(a): AV5Z basis set.
(b): Taken from ref. [42] : The energy values are calculated at the MRCI+Q level with the Complete basis set CBS extrapolation. The dipole moments are calculated at the CCSD(T)/AVTZ level of theory. T_0 values.
(c): Taken from ref. [47] : Relativistic DFT calculations.
(d): Taken from ref. [52] : Equilibrium geometry and dipole moment calculated at the CCSD(T) level with relativistic correction.

Table 5: Calculated spectroscopic constants of the low lying electronic states of HgO and HgS.

State	Method	r_e /bohr	ω_e /cm^{-1}	T_e /cm^{-1}	μ_e /a.u.
HgO					
$^1\Sigma^+$					
This work[a]	MRCI+Q	3.62	610.0	0	1.85
Peterson07[b]	MRCI+Q/CBS	3.602	612.6	0	
Peterson07[b]	CCSD(T)	3.627	594.5	0	1.83
Kullie06[c]	DFT	3.55	648		
$^3\Pi$					
This work[a]	MRCI+Q	4.06	337.1	-322	0.96
Peterson07[b]	MRCI+Q/CBS	4.075	302.2	-70	
HgS					
$^1\Sigma^+$					
This work[a]	MRCI+Q	4.23	383.4	0	1.88
Peterson07[b]	MRCI+Q/CBS	4.256	357.7	0	
Peterson07[b]	CCSD(T)	4.282	349.3	0	1.73
Raptis99[d]	CCSD(T)	4.33			1.74
Guitou07[e]	MRCI+Q/CBS	4.24	363	0	1.89
$^3\Pi$					
This work[a]	MRCI+Q	4.76	190.3	859	0.53
Peterson07[b]	MRCI+Q/CBS	4.751	188.1	1486	
Guitou07[e]	MRCI+Q/CBS	4.82	150	1557	0.72
$^1\Pi$					
Guitou07[e]	MRCI+Q/CBS	4.54	298	5823	0.87

(a): AV5Z basis set.
(b): Taken from ref. [42] : The energy values are calculated at the MRCI+Q level with the Complete basis set CBS extrapolation. The dipole moments are calculated at the CCSD(T)/AVTZ level of theory. T_0 values.
(c): Taken from ref. [47] : Relativistic Dirac-Fock-Slater DFT calculations.
(d): Taken from ref. [52] : Equilibrium geometry and dipole moment calculated at the CCSD(T) level with relativistic correction.
(e): Taken from ref. [53] : MRCI+Q calculations with Complete Basis Set CBS extrapolation.

We can summarize the characteristics of the two lowest states at the diatomic level as precursors for piezoelectric effects: (1) the small difference between the equilibrium distances (2) the large difference between the dipole moments in the molecular region (3) the small energy difference between the two lowest states. For the zinc compounds, according to these criteria, it

Figure 6: Potential energy curves of the low lying states of CdO at the MRCI+Q level of theory.

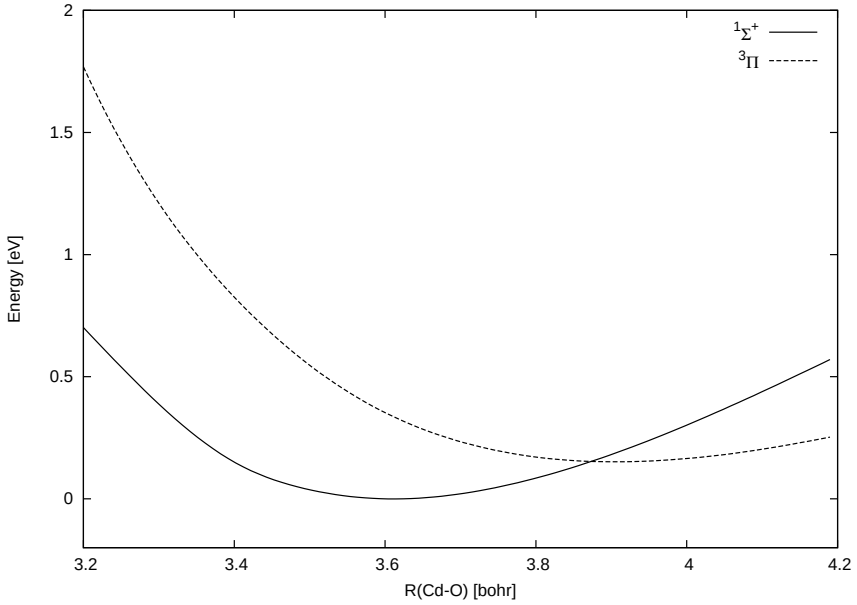

Figure 7: Potential energy curves of the low lying states of CdS at the MRCI+Q level of theory.

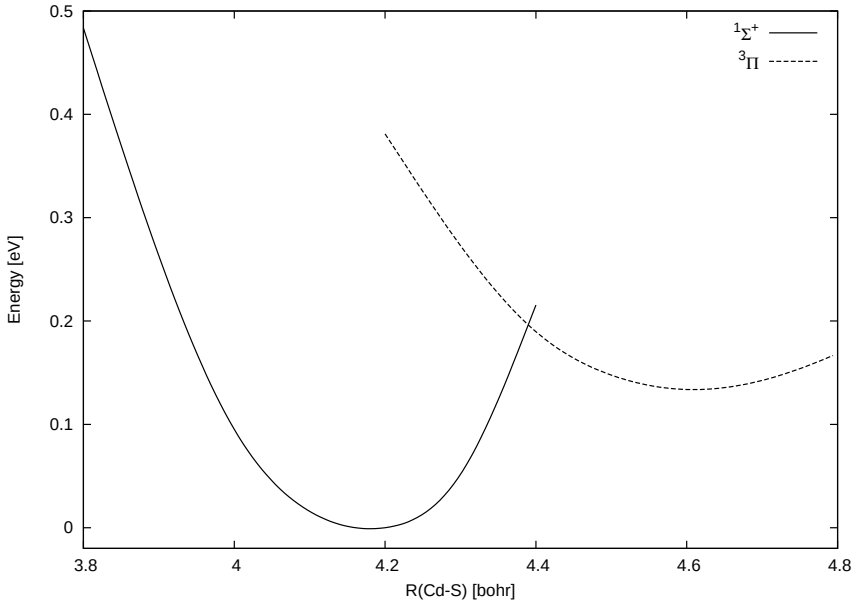

Figure 8: Dipole moments of the low lying states of CdO at the MRCI level of theory.

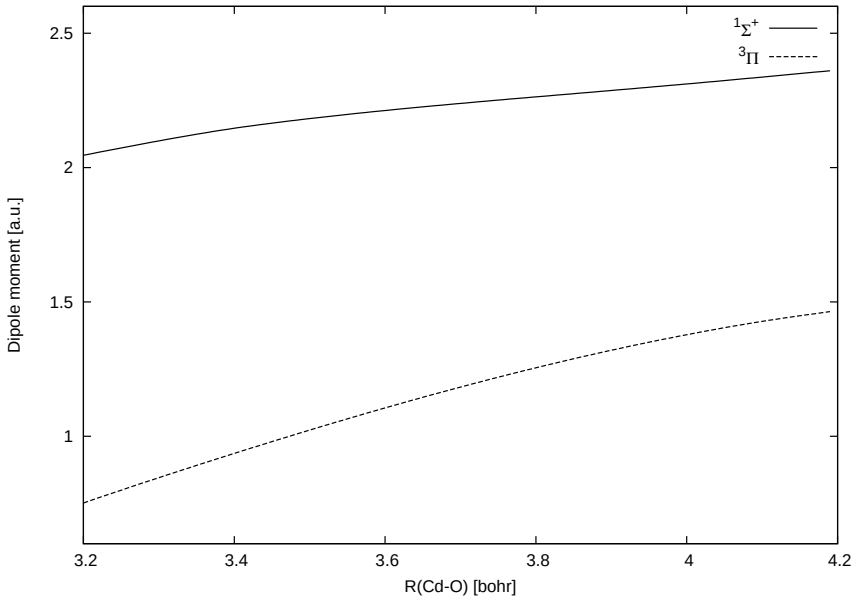

Figure 9: Dipole moments of the low lying states of CdS at the MRCI level of theory.

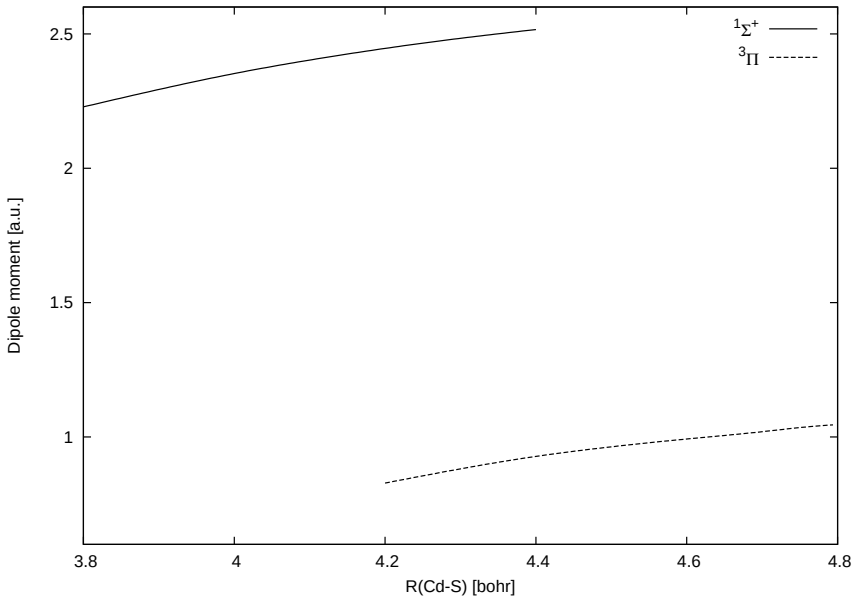

Figure 10: Potential energy curves of the low lying states of HgO at the MRCI+Q level of theory.

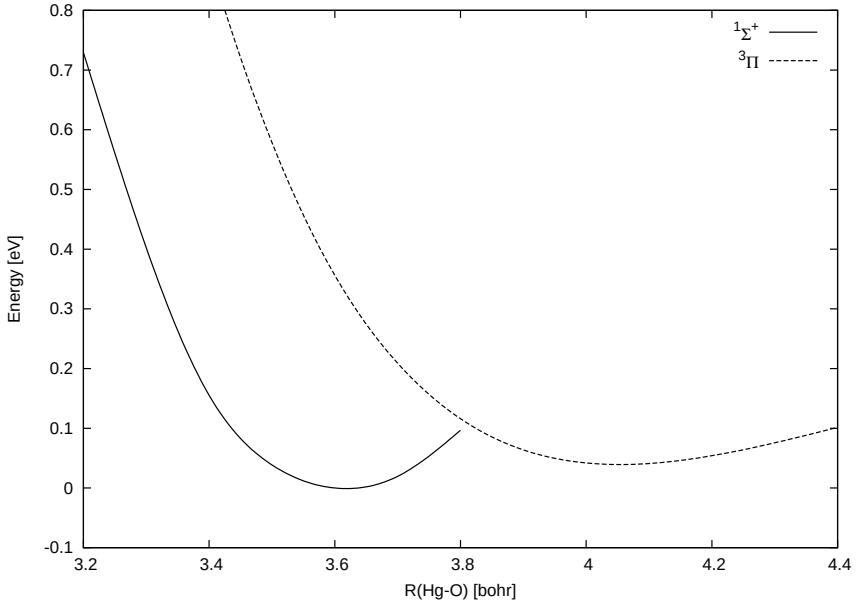

Figure 11: Potential energy curves of the low lying states of HgS at the MRCI+Q level of theory.

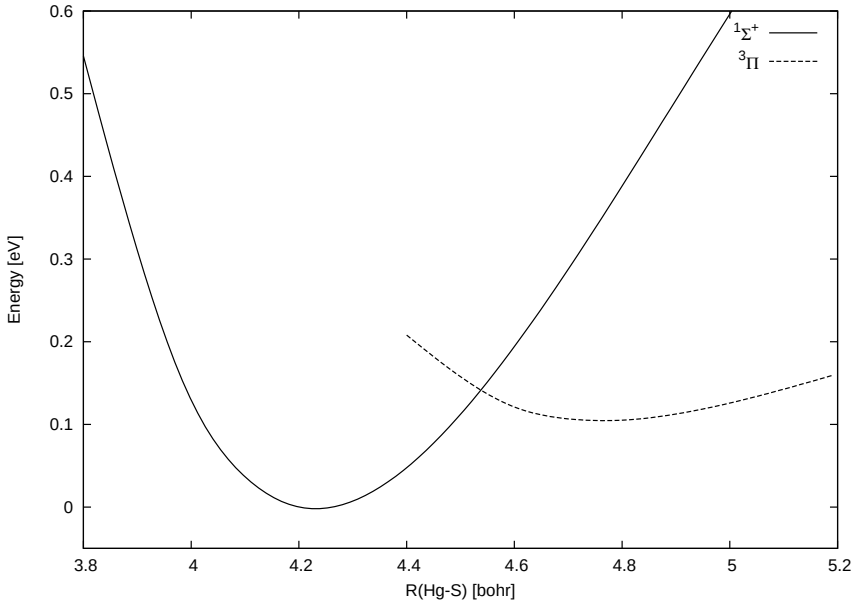

Figure 12: Dipole moments of the low lying states of HgO at the MRCI level of theory.

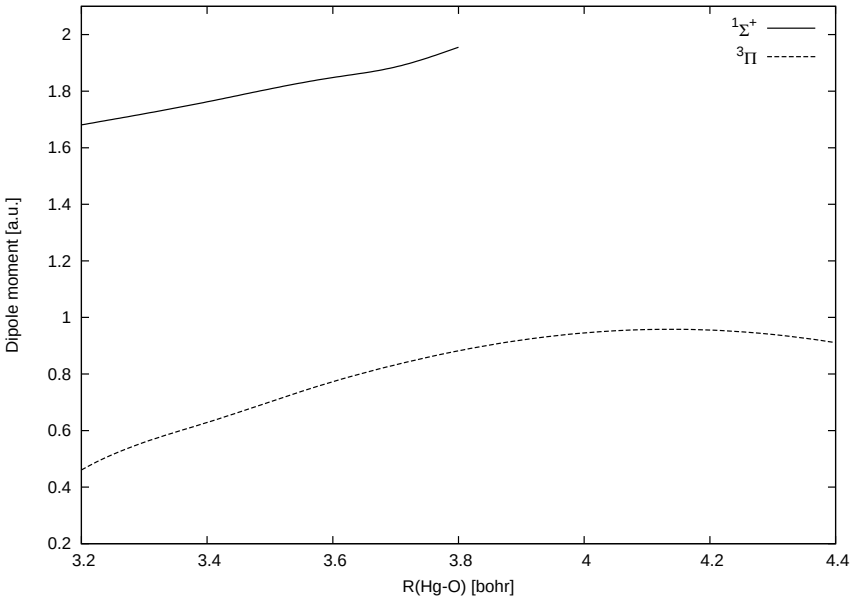

Figure 13: Dipole moments of the low lying states of HgS at the MRCI level of theory.

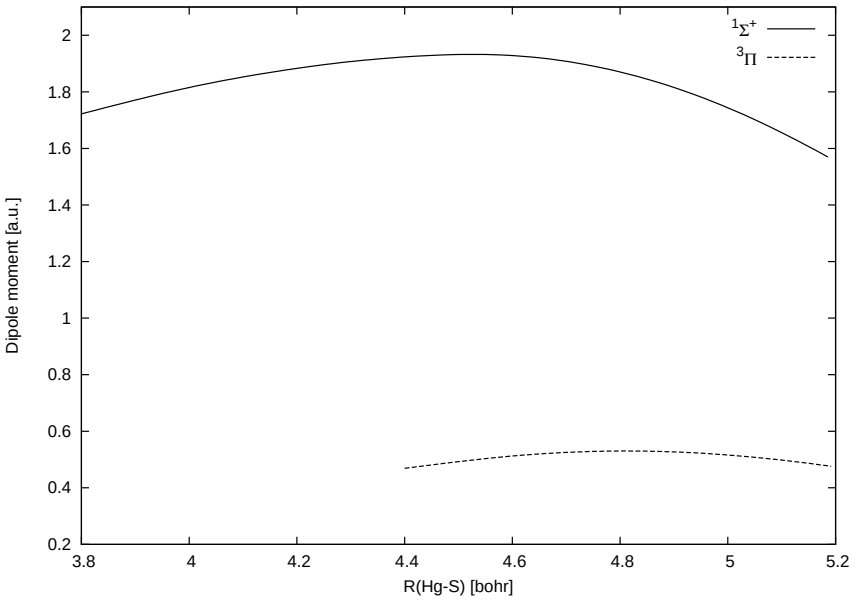

can be concluded that ZnO is a better candidate for piezoelectric effects than ZnS, in consistency with the piezoelectric coefficients presented in Table 1. The Cadmium and mercury compounds satisfy well these conditions and are expected to be important for piezoelectric effects. For CdO, the calculated piezoelectric tensors 1.64 (e_{33}) and -0.48 Cm^{-2} (e_{31}) confirm our analysis.

5.4.2 III-V molecular compounds

In this paragraph we report the properties of the lowest states of BN, BP, AlN, and AlP as examples of the III-V compounds, from all electron electronic structure calculations at the MRCI level including the Davidson correction. Using the correlation consistent aug-cc-pVnZ (n = 3, 4, 5) basis sets of Dunning and coworkers [37–40] for the B, P, N, and Al atoms, the MCSCF calculations have been performed in the first step, from which the wavefunctions have been taken as reference in the subsequent MRCI calculations. The active space has been defined as the valence space and all valence electrons have been correlated in both the MCSCF and MRCI steps. The Complete Basis Set extrapolation approach for the n = 4, 5 basis sets has been applied, determining the parameters in the following equation [54, 55].

$$E(n) = E_{CBS} + B/n^3 \qquad (5.6)$$

We show the potential curves of the eight lowest electronic states of BN in Figure 14 and their dipole moments in Figure 15. Table 6 lists the spectroscopic constants for the three lowest states of BN, which compare quite well with the previous values. As seen in Figure 14, the lowest state is the $^3\Pi$ state, followed closely by the $^1\Sigma^+$ state with the T_e value of 242 cm^{-1}. The next one is the $^1\Pi$ state lying parallel to the potential curve of the $^3\Pi$ state, with an energy difference of more than 3700 cm^{-1}. Our calculated equilibrium distances at the CBS limit are 2.419, 2.517, and 2.521 bohr for the $^1\Sigma^+$ state, the $^3\Pi$ state, and the $^1\Pi$ state respectively. This trend is consistent with our discussions, based on a simplified molecular orbitals picture. The dipole moments of these three states are almost constant in the concerned region. The spectroscopic data for BP have been recently provided by Linguerri *et al.* [56] and are listed in Table 7 with the values of the previous calculations. Based on these spectroscopic values, it appears that the $^3\Pi$ state and the $^1\Sigma^+$ state are the two lowest ones with a small difference of the dipole moments and a large energy difference. According to the quite small difference of their dipole moments, neither BN nor BP can induce an electric change under an applied strain in solid. Thus the BN and BP compounds are found to have little capability for piezoelectric effects.

Table 6: Spectroscopic constants of the low lying electronic states of BN.

State	Method	r_e /bohr	ω_e /cm^{-1}	T_e /cm^{-1}	μ_e /a.u.
$^3\Pi$					
This work[a]	MRCI+Q	2.517	1525.2	0	0.78
	MRCI+Q/CBS	2.513	1531.6	0	
Denis04[b]	CCSD(T)	2.513			
Martin92[c]	MRCI	2.527	1494.9	0	
Bauschlicher96[d]	MRCI+Q	2.515	1506	0	
Peterson95[e]	MRCI+Q	2.510	1508.2	0	0.780
Gan06[f]	FCI	2.524		0	
Lu05[g]	DQMC	2.516	1529	0	
Lorenz96[h]	Exp.		1519.2	0	
$^1\Sigma^+$					
This work[a]	MRCI+Q	2.419	1725.1	304.2	0.76
	MRCI+Q/CBS	2.419	1725.1	242.0	
Denis04[b]	CCSD(T)	2.402			
Martin92[c]	MRCI	2.400	1733.7	160	
Bauschlicher96[d]	MRCI+Q	2.417	1694	180	
Peterson95[e]	MRCI+Q	2.413	1697.5	305	0.766
Gan06[f]	FCI	2.408		328.8	
Lu05[g]	DQMC	2.410	1709	178	
Karton06[i]	CCSDTQ			158	
Lorenz96[h]	Exp.		1700.9	15-182	
Asmis98[j]	Exp.	2.408		153	
$^1\Pi$					
This work[a]	MRCI+Q	2.521	1541.2	3735.0	0.88
	MRCI+Q/CBS	2.518	1547.0	3700.2	
Bauschlicher96[d]	MRCI+Q	2.534	1476.7	3633	
Lorenz96[h]	Exp.		1532.5	3646	
Asmis98[j]	Exp.	2.513		3767	

(a): MRCI+Q calculation and AV5Z basis set. The Complete Basis set CBS extrapolation has also been applied. Absolute energy value calculated at the minimum of the $^1\Sigma^+$ state of BN : -79.29307098 a.u.
(b): Taken from ref. [57] CCSD(T) calculations.
(c): Taken from ref. [58] MRCI calculations.
(d): Taken from ref. [59] MRCI+Q calculations.
(e): Taken from ref. [60] MRCI calculations.
(f): Taken from ref. [61] Full CI calculations.
(g): Taken from ref. [62] Diffusion Quantum Monte Carlo calculations.
(h): Taken from ref. [63] Fourier transform absorption and laser-induced fluorescence.

(i): Taken from ref. [64] CCSDTQ calculations.
(j): Taken from ref. [65] Anion photoelectron spectroscopy.

Table 7: Calculated spectroscopic constants of the low lying electronic states of BP.

State	Method	r_e /bohr	ω_e /cm^{-1}	T_e /cm^{-1}	μ_e /a.u.
BP					
$^3\Pi$					
Boldyrev93$^{(a)}$	QCISD	3.322	1148	0	
Boldyrev94$^{(b)}$	MRCISD	3.335	897	0	
Linguerri08$^{(c)}$	MRCI+Q	3.303	941	0	0.06
$^1\Sigma^+$					
Boldyrev93$^{(a)}$	QCISD	3.182	1072	2378	
Boldyrev94$^{(b)}$	MRCISD	3.188	1026	3113	
Linguerri08$^{(c)}$	MRCI+Q	3.176	1040	2548	0.27
$^1\Pi$					
Linguerri08$^{(c)}$	MRCI+Q	3.329	934	3145	1.05
$^3\Sigma^-$					
Boldyrev93$^{(a)}$	QCISD	3.672	585	6890	
Linguerri08$^{(c)}$	MRCI+Q	3.721	634	7412	0.21

(a): Taken from ref. [25] QCISD calculations (MP2 results for the ω_e values).
(b): Taken from ref. [66] MRCISD+Q calculations.
(c): Taken from ref. [56] MRCI+Q calculations, aug-cc-pV6Z.

Figure 14: Potential energy curves of the low lying states of BN at the MRCI+Q level of theory.

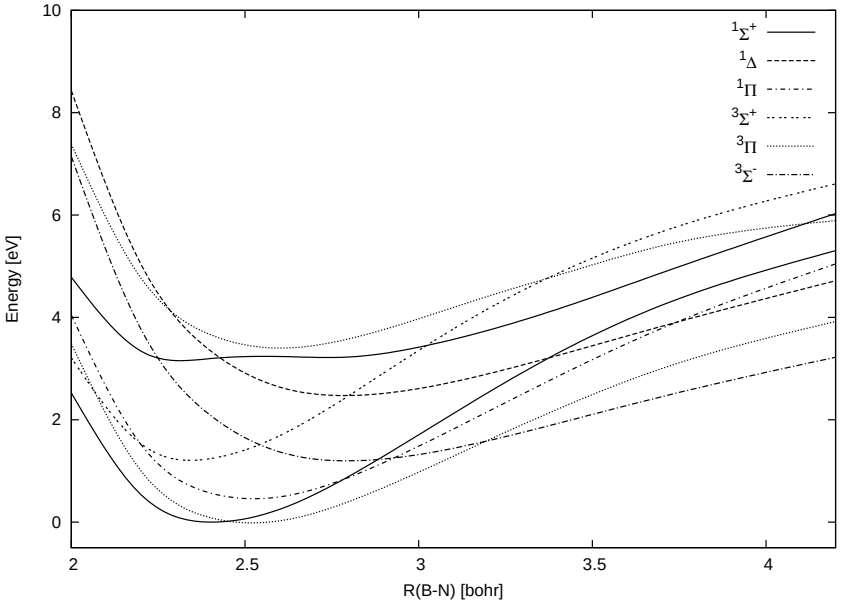

Figure 15: Dipole moments of the low lying states of BN at the MRCI level of theory.

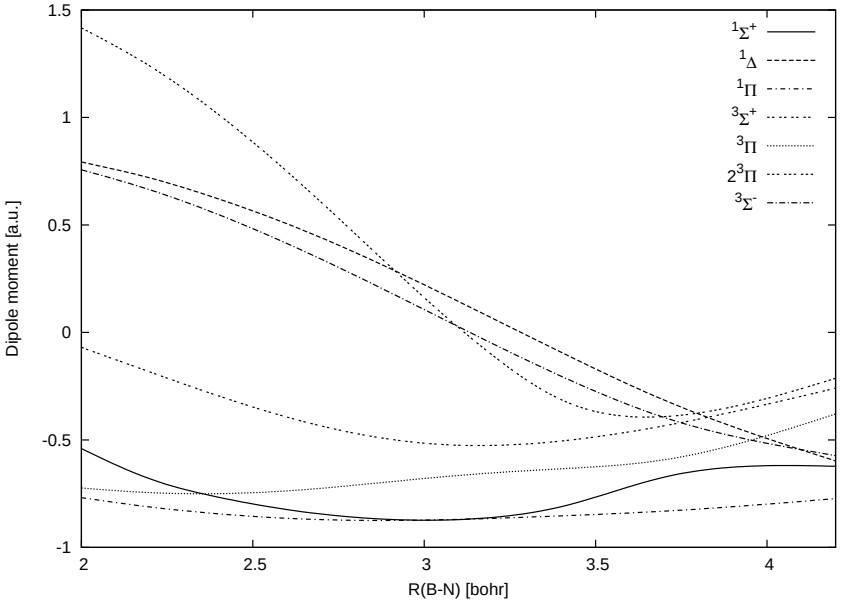

Figure 16: Potential energy curves of the low lying states of AlN at the MRCI+Q level of theory.

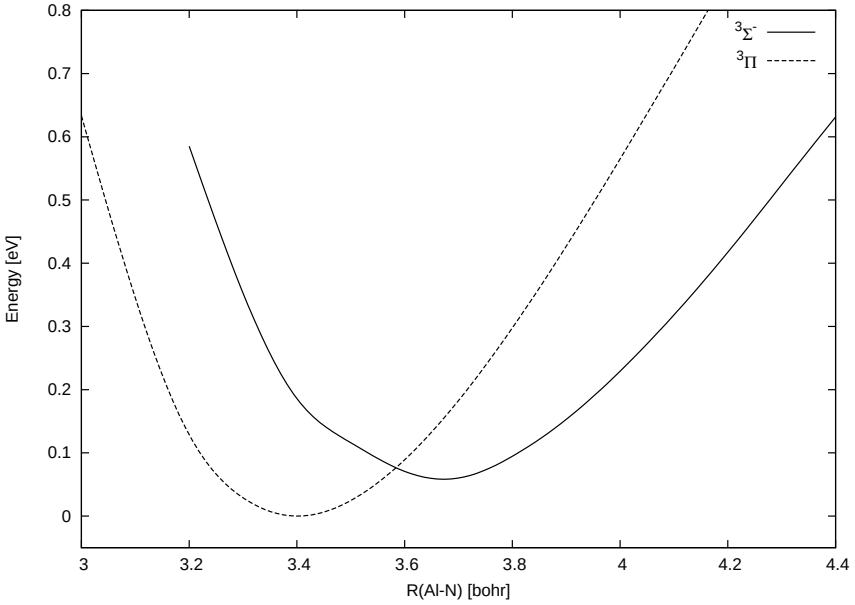

Figure 17: Dipole moments of the low lying states of AlN at the MRCI level of theory.

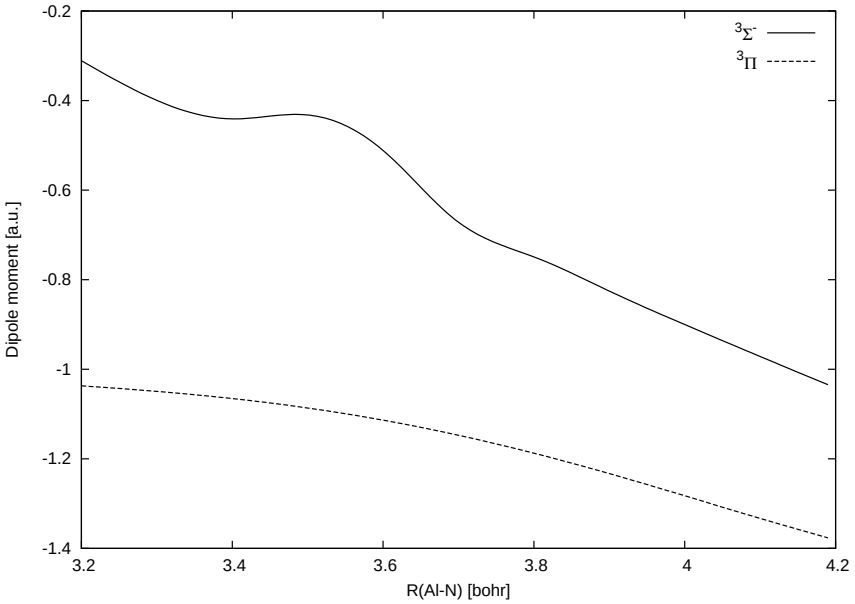

Figure 18: Potential energy curves of the low lying states of AlP at the MRCI+Q level of theory.

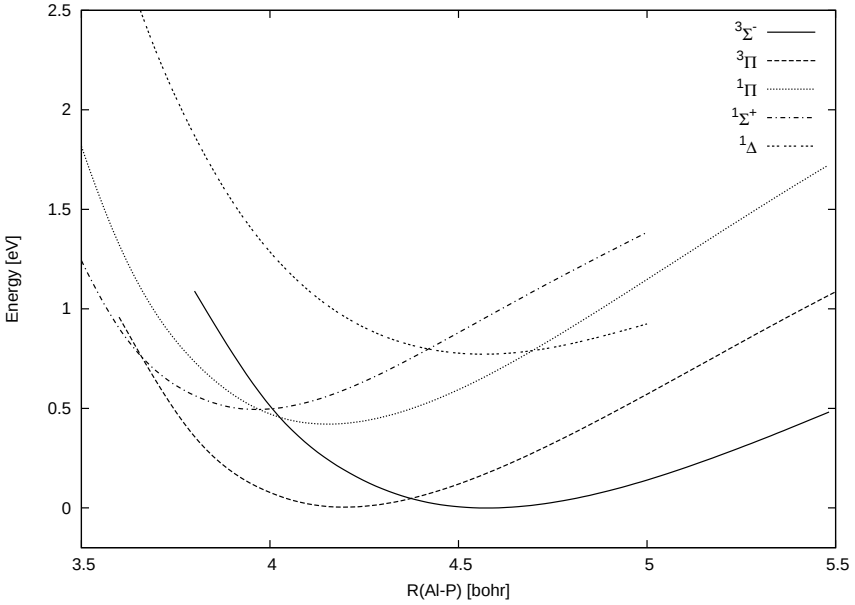

Figure 19: Dipole moments of the low lying states of AlP at the MRCI level of theory.

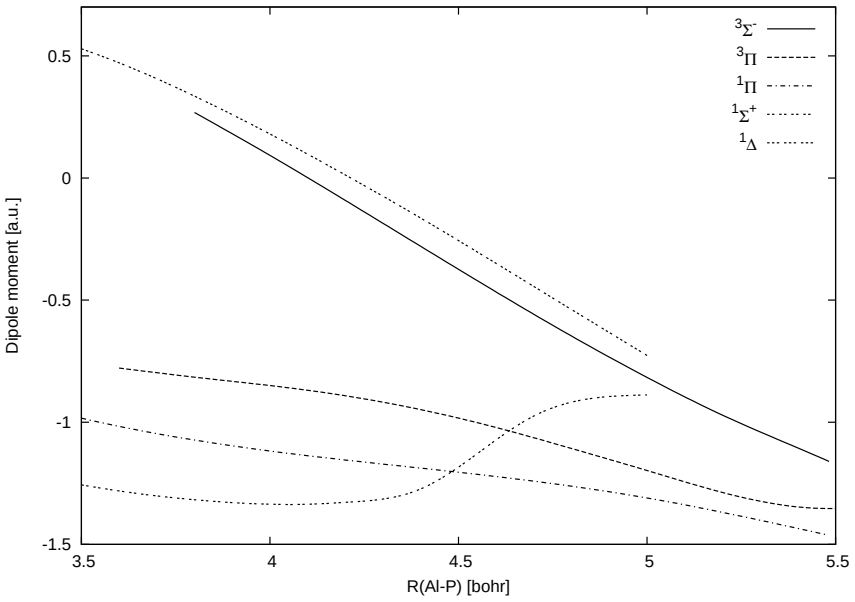

The potential curves of the lowest electronic states of AlN, calculated at the MRCI+Q level, are presented in Figure 16 and the corresponding dipole moments, calculated at the MRCI level, are shown in Figure 17. Figures 18 and 19 show respectively the potential curves (at the MRCI+Q level) and the dipole moments (at the MRCI level) of the five lowest states of AlP. In Tables 8 and 9, we list also the corresponding spectroscopic constants of the these lowest states of AlN and AlP together with the previous available data. The behaviour of their potential curves and of their dipole moments, specially those of the $^1\Sigma^+$ and $^3\Sigma^-$ states, are quite different from the case of BN, due to the large difference of electronegativity and of size between B and Al. It becomes clear that the $^3\Pi$ state and the $^3\Sigma^+$ state are the two lowest ones and separated in energy from the other electronic states. From our calculations, the ground state is the $^3\Pi$ state in AlN, contrary to the $^3\Sigma^-$ state in AlP. As shown in Tables 8 and 9, the energy differences between the $^3\Sigma^-$ state and the $^3\Pi$ state are very small and even negative, which remains yet a controversial problem, even with the AV5Z basis sets, as to know which is lower between these two states. From our results on AlN, the $^3\Sigma^-$ state lies at 471.7 cm^{-1} above the $^3\Pi$ ground state with a difference of the equilibrium distances of 0.27 bohr. The ratio of 1.6 is found between the dipole moments of the $^3\Pi$ and the $^3\Sigma^-$ states. For AlP, the energy difference, the ratio of the dipole moments, and the difference of the equilibrium distances between the two lowest states are found to be 35 cm^{-1}, 2, and 0.378 bohr. Beside the question of the determination of the ground state, these features of the two lowest states imply that AlN and AlP are good candidates for piezoelectric effects. The piezoelectric tensors of AlN in Table 1 support our conclusion on AlN, however the previous DFT calculations [21] performed on the blende structure of AlP are showing indeed that AlP does not present significant piezoelectric properties.

Table 8: Spectroscopic constants of the low lying electronic states of AlN.

State	Method	r_e /bohr	ω_e /cm^{-1}	T_e /cm^{-1}	μ_e /a.u.
$^3\Pi$					
This work[a]	MRCI+Q	3.399	751.1	0	1.08
Langhoff88[b]	MRCI+Q	3.436	738	0	1.019
Gutsev99[c]	CCSD	3.384	756	-20.6	1.037
Gan06[d]	FCI	3.422		0	
Chase98[e]	Exp.	3.376	746.9		
$^3\Sigma^-$					
This work[a]	MRCI+Q	3.673	700.1	471.7	0.68
Langhoff88[b]	MRCI+Q	3.683	587	99	0.650
Gutsev99[c]	CCSD	3.620	628	0	0.632
Gan06[d]	FCI	3.652		38.5	
$^1\Sigma^+$					
This work[a]	MRCI+Q	3.164	953.3	3822.2	1.79
Langhoff88[b]	MRCI+Q	3.202	913	4689	
Gutsev99[c]	CCSD	3.150	985	3359	
Gan06[d]	FCI	3.184		4232.0	
Stull71[f]	Exp.	3.118	930		
$^1\Pi$					
This work[a]	MRCI+Q	3.340	828.6	6059.6	1.59
$^3\Sigma^+$					
This work[a]	MRCI+Q	3.120	990.9	14617.2	1.60

(a): AV5Z basis set. Minimal energy relative to the minimum of the ground state.
(b): Taken from ref. [67] MRCI+Q calculations.
(c): Taken from ref. [68] CCSD(T) calculations.
(d): Taken from ref. [61] Full CI calculations.
(e): Taken from ref. [69] Experimental value.
(f): Taken from ref. [70] Experimental value.

Table 9: Spectroscopic constants of the low lying electronic states of AlP.

State	Method	r_e /bohr	ω_e /cm^{-1}	T_e /cm^{-1}	μ_e /a.u.
AlP					
$^3\Sigma^-$					
This work[a]	MRCI+Q	4.575	370.3	0	0.44
Gan06[b]	FCI	4.596		0	
Boldyrev93[c]	QCISD	4.584	361	0	
Gomez02[d]	Exp.	4.536	379	0	
$^3\Pi$					
This work[a]	MRCI+Q	4.197	467.1	34.8	0.89
Gan06[b]	FCI	4.220		381.2	
Boldyrev93[c]	QCISD	4.214	487	455	
Gomez02[d]	Exp.	4.270	457	943	
$^1\Pi$					
This work[a]	MRCI+Q	4.153	503.7	3399.2	1.15
Gomez02[d]	Exp.		470	4161	
$^1\Sigma^+$					
This work[a]	MRCI+Q	3.965	556.2	3993.3	1.34
Gan06[b]	FCI	3.984		4567.8	
Boldyrev93[c]	QCISD	3.868	670	4687	
Gomez02[h]	Exp.		541	4629	

(a): AV5Z basis set. Minimal energy relative to the minimum of the ground state.
(b): Ref. [61] Full CI calculations.
(c): Ref. [25] QCISD calculations (MP2 results for the ω_e values).
(d): Ref. [26] Anion photoelectron spectroscopy and ZEKE spectroscopy.

5.4.3 Alkaline earth chalcogenides

We discuss below the properties of the lowest electronic states of the MX (M = Be, Mg and X = O, S) compounds as examples for alkaline earth chalcogenides. All electron electronic structure calculations have been performed, using the correlation consistent aug-cc-pVQZ basis sets for the Be, Mg, O, and S atoms [39]. The external four σ and two π orbitals were optimized and the eight valence electrons were correlated in the MCSCF step. Due to the multi configurational character of the $^1\Sigma^+$, $^1\Pi$, and $^3\Pi$ states, the MCSCF calculations have included the following states; one $^1\Sigma^+$, two $^1\Pi$, and two $^3\Pi$ states for BeO, one $^1\Sigma^+$, two $^1\Pi$, and one $^3\Pi$ states for BeS, and two $^1\Sigma^+$, one $^1\Pi$, and one $^3\Pi$ states for MgO and MgS. Taking the MCSCF wavefunction as reference, the subsequent MRCI calculations with the Davidson correction have been performed

in each space and spin symmetries, as well as in the MCSCF step. In the MRCI calculations, all the electrons have been correlated. The size of the calculations in the MRCI step ranges from 0.5 million (for the $^1\Pi$ state of BeO) to 45 million (for the $^3\Pi$ state of MgO) with respect to the number of variational parameters.

Table 10: Spectroscopic constants of the low lying electronic states of the Alkaline earth chalcogenides.

State	Method	r_e /bohr	ω_e /cm^{-1}	$T_e^{(b)}$ /cm^{-1}	μ_e /a.u.
BeO					
$^1\Sigma^+$					
This work$^{(a)}$	MRCI+Q	2.530	1471.7	0	2.56
Buenker07$^{(c)}$	MRD-CI	2.531	1463	0	2.42
Srnec05$^{(d)}$	MRCI	2.538		0	
Gutsev97$^{(e)}$	CCSD(T)	2.517	1491.2		2.46
Fuentealba00$^{(f)}$	DFT	2.492	1512.0		
Huber79$^{(g)}$	Exp.	2.515	1487.3	0	2.26
$^3\Pi$					
This work$^{(a)}$	MRCI+Q	2.784	1161.0	7871	0.51
Buenker07$^{(c)}$	MRD-CI	2.792	1112	8476	0.48
Huber79$^{(g)}$	Exp.			8480$^{(h)}$	
$^1\Pi$					
This work$^{(a)}$	MRCI+Q	2.781	1141.8	8776	0.44
Buenker07$^{(c)}$	MRD-CI	2.786	1135	9992	0.48
Srnec05$^{(d)}$	MRCI			10461$^{(i)}$	
Huber79$^{(g)}$	Exp.	2.765	1144.2	9406	

(a): MRCI+Q level of theory, using the aug-cc-pVQZ basis sets for all atoms.
(b): Absolute energy values calculated at the minimum of the $^1\Sigma^+$ ground state : -89.78089194 a.u. for BeO, -412.63209154 a.u. for BeS, -275.14591579 a.u. for MgO and -597.69675700 a.u. for MgS.
(c): Taken from ref. [71], using the cc-pVTZ basis sets with additional s and p type diffuse functions for Be and O atoms.
(d): Taken from ref. [72], using the cc-pVTZ basis sets for Be, Mg, O, and S.
(e): Taken from ref. [73], using the large atomic natural orbital basis of Widmark-Malmqvist-Roos (WMR) contracted as (14s9p4d3f)/[7s7p4d3f] for Be and O, and as (17s12p5d4f)/[7s7p5d4f] for Mg.
(f): Taken from ref. [74], calculated by the hybride density functional method (B3LYP), using the two-valence electron pseudopotentials for Be and Mg with the (6s6p5d1f)/[5s5p4d1f] basis sets. The O atom was treated at the all-electron level using the 6-331G** basis sets.

State	Method	r_e /bohr	ω_e /cm^{-1}	$T_e^{(b)}$ /cm^{-1}	μ_e /a.u.
MgO					
$^1\Sigma^+$					
This work$^{(a)}$	MRCI+Q	3.309	789.5	0	2.32
Srnec05$^{(d)}$	MRCI	3.348		0	
Gutsev97$^{(e)}$	CCSD(T)	3.288	818.3		2.53
Fuentealba00$^{(f)}$	DFT	3.309	789.0		
Thümmel89$^{(m)}$	MRD-CI	3.377	806	0	
Bauschlicher01$^{(n)}$	ACPF	3.347	760	0	
Huber79$^{(g)}$	Exp.	3.305	785.0	0	
Kim01$^{(o)}$	Exp.		780	0	
Busener87$^{(s)}$	Exp.				2.4
$^3\Pi$					
This work$^{(a)}$	MRCI+Q	3.536	653.5	2134	1.17
Thümmel89$^{(m)}$	MRD-CI	3.605	615	1929	
Bauschlicher01$^{(n)}$	ACPF	3.568	645	1766	
Huber79$^{(g)}$	Exp.	3.401$^{(h)}$	650$^{(h)}$	2400$^{(h)}$	
Kim01$^{(o)}$	Exp.	3.522	600	2510/2520	
Ikeda77$^{(p)}$	Exp.		648	2623	
Mürtz95$^{(q)}$	Exp.	3.532	650	2620	
$^1\Pi$					
This work$^{(a)}$	MRCI+Q	3.525	664.3	3768	1.21
Srnec05$^{(d)}$	MRCI			3054$^{(i)}$	
Thümmel89$^{(m)}$	MRD-CI	3.570	677	2666	
Bauschlicher01$^{(n)}$	ACPF	3.560	654	2621	
Huber79$^{(g)}$	Exp.	3.522	664.4	3563	
Kim01$^{(o)}$	Exp.	3.503	650	3390/3400	

(g): Taken from ref. [24]

(h): This value is still uncertain.

(i): Deduced from the vertical absorption $X^1\Sigma^+$ - $A^1\Pi$.

(j): Taken from ref. [75], using the polarized basis sets (POL) contracted as (10s6p4d)/[5s3p2d] for Be and (13s10p4d)/[7s5p2d] for S.

(k): Calculated at the experimental equilibrium geometry of 3.291 bohr.

(l): Taken from ref. [76], analyzed the spectroscopic data obtained by Cheetham *et al.* [*Trans. Faraday Soc.* **61**, 1308-1316 (1965)], based on the CI calculations with STO basis sets for Be and O.

(m): Taken from ref. [77], calculated at the MRD-CI level using the [7s5p2d] basis sets for Mg and the [4s4p2d] basis sets for O.

(n): Taken from ref. [78], using the cc-pVQZ basis sets for Mg and the aug-cc-pVQZ for O.

State	Method	r_e /bohr	ω_e /cm^{-1}	$T_e^{(b)}$ /cm^{-1}	μ_e /a.u.
BeS					
$^1\Sigma^+$					
This work[a]	MRCI+Q	3.298	998.8	0	2.04
Srnec05[d]	MRCI	3.328		0	
Noga97[j]	CCSD(T)				2.05[k]
Huber79[g]	Exp.	3.291	997.9	0	
$^3\Pi$					
This work[a]	MRCI+Q	3.605	761.5	6769	0.24
Pouilly82[l]	Exp.	3.626	737	7100	
$^1\Pi$					
This work[a]	MRCI+Q	3.610	769.8	7764	0.20
Srnec05[d]	MRCI			9039[i]	
Huber79[g]	Exp.	3.605	762.5	7960	
Pouilly82[l]	Exp.	3.607	762.1	7962	

State	Method	r_e /bohr	ω_e /cm^{-1}	$T_e^{(b)}$ /cm^{-1}	μ_e /a.u.
MgS					
$^1\Sigma^+$					
This work[a]	MRCI+Q	4.064	524.2	0	2.78
Srnec05[d]	MRCI	4.103		0	
Huber79[g]	Exp.	4.049	529		
Walker97[r]	Exp.	4.049			
$^3\Pi$					
This work[a]	MRCI+Q	4.391	427.0	3170	1.16
$^1\Pi$					
This work[a]	MRCI+Q	4.386	449.0	4173	1.18
Srnec05[d]	MRCI			4682[i]	

(o): Taken from ref. [43], vibrationally resolved photoelectron spectra of MgO^- using two different methods.

(p): Taken from ref. [79], photoluminescence spectra.

(q): Taken from ref. [80], observed the $A^1\Pi$-$X^1\Sigma^+$ and $a^3\Pi$-$X^1\Sigma^+$ bands, by the Faraday laser magnetic resonance (LMR) technique.

(r): Taken from ref. [81], microwave Fourier Transform Spectroscopy.

(s): Taken From ref. [82], Stark quantum beat spectroscopy.

Figure 20: Potential energy curves of the low lying states of BeO at the MRCI+Q level of theory.

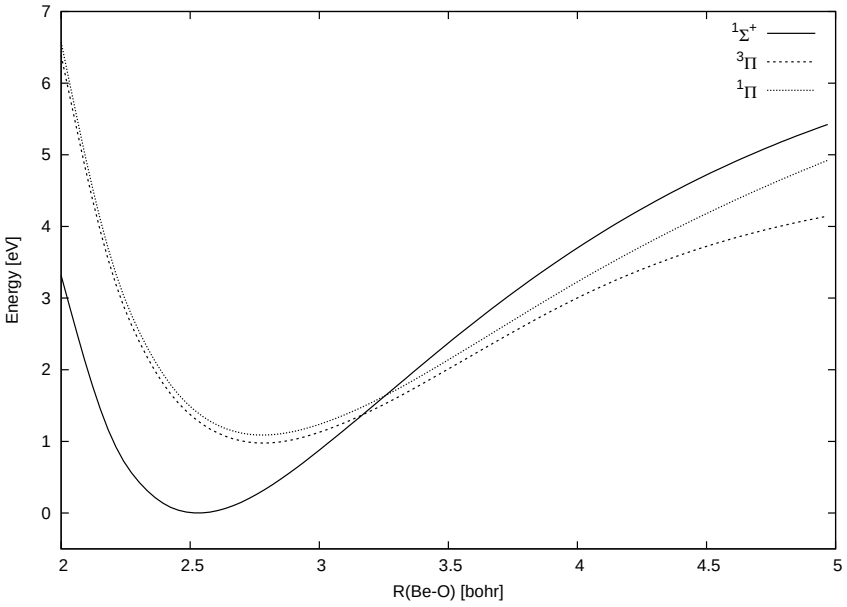

The potential curves and the dipole moments for the three lowest states, calculated at the MRCI+Q level and at the MRCI level respectively, appear quite similar among these alkaline earth chalcogenides, as shown in Figures 20 to 27. The spectroscopic constants obtained from the MRCI+Q level calculations are listed in Table 10 for the three lowest $^1\Sigma^+$, $^1\Pi$, and $^3\Pi$ states. From the figures of the potential curves, the three lowest states of all compounds present the typical tendencies that were explained using a simplified MOs diagram: the ground state is the $^1\Sigma^+$ state followed by the $^3\Pi$ state. The $^1\Pi$ state is the third one in energy lying quite close to the $^3\Pi$ state. The separation in energy is less than 1 eV in the investigated interatomic distances. We can also summarize the common features of the dipole moments as follows: the $^1\Sigma^+$ state has an almost constant value much larger than those of two Π states which are increasing when increasing the interatomic distance. In Table 10, the ratio of the dipole moments between the $^1\Sigma^+$ state and $^3\Pi$ state is shown to be much larger in beryllium compounds than in magnesium compounds. These compounds show in common that the equilibrium distance of the $^1\Sigma^+$ state is slightly shorter by 0.23-0.32 bohr than that of the $^3\Pi$ state. However the energy differences of the $^3\Pi$ state relative to the $^1\Sigma^+$ state are found to be about 2100 cm^{-1} for MgO and 3200 cm^{-1} for MgS, in contrast to the large differences of 7900 cm^{-1} for BeO and of 6800 cm^{-1} for BeS. Considering these data, we can conclude that the magnesium compounds are better candidates for piezoelectric effects than the beryllium compounds, in agreement with the calculated piezoelectric tensors listed in Table 1.

Figure 21: Dipole moments of the low lying states of BeO at the MRCI level of theory.

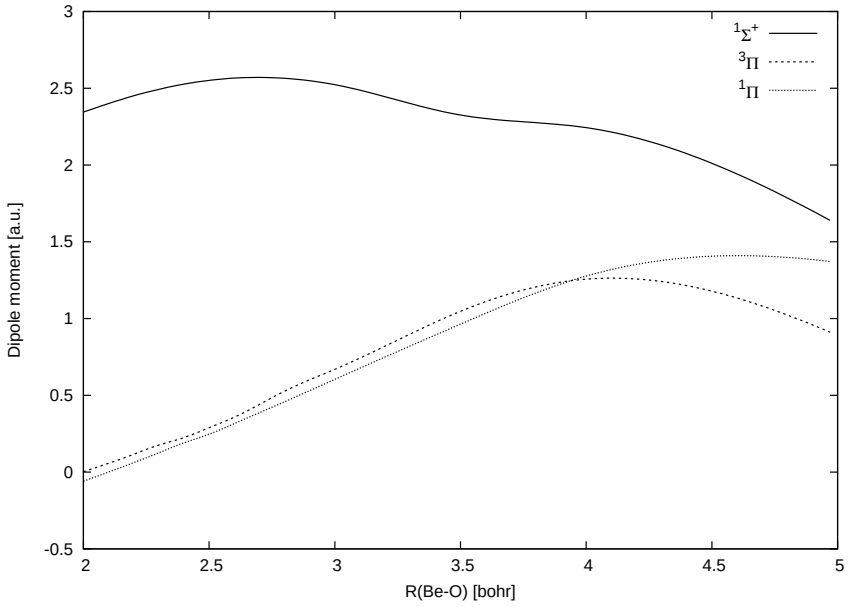

5.5 Conclusions

In this study, we have presented an accurate description of the electronic structure of the low lying states of the diatomic compounds, IIb chalcogenides (M = Zn, Cd, Hg and X = O, S), III-V compounds (M = B, Al and X = N, P), and alkaline earth chalcogenides MX (M = Be, Mg and X = O, S), based on electronic structure calculations at the MRCI+Q level with the appropriate large basis sets. The common characteristics at the diatomic level as precursors for piezoelectric effects have been revealed as follows: the two low lying states are very close in energy with slightly different bonding distances and different charge distributions. These properties lead to a mechanism such that an abrupt change occurs in the electronic structure and in the electric polarization of the molecule under a small geometric distortion with a small variation of energy. Based on these criteria, we have examined what is a good candidate for piezoelectric effects and compared with the existing piezoelectric tensors determined in solid phase.

Figure 22: Potential energy curves of the low lying states of BeS at the MRCI+Q level of theory.

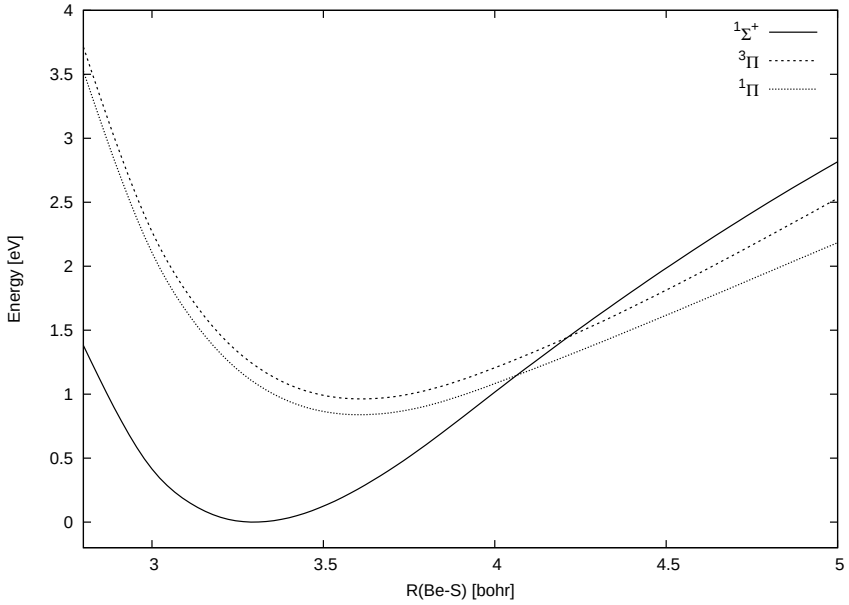

Figure 23: Dipole moments of the low lying states of BeS at the MRCI level of theory.

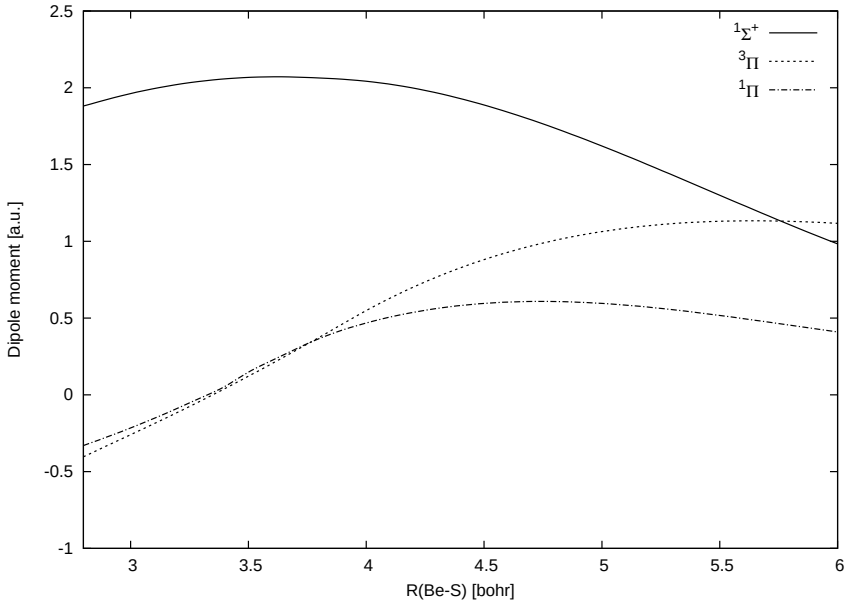

Figure 24: Potential energy curves of the low lying states of MgO at the MRCI+Q level of theory.

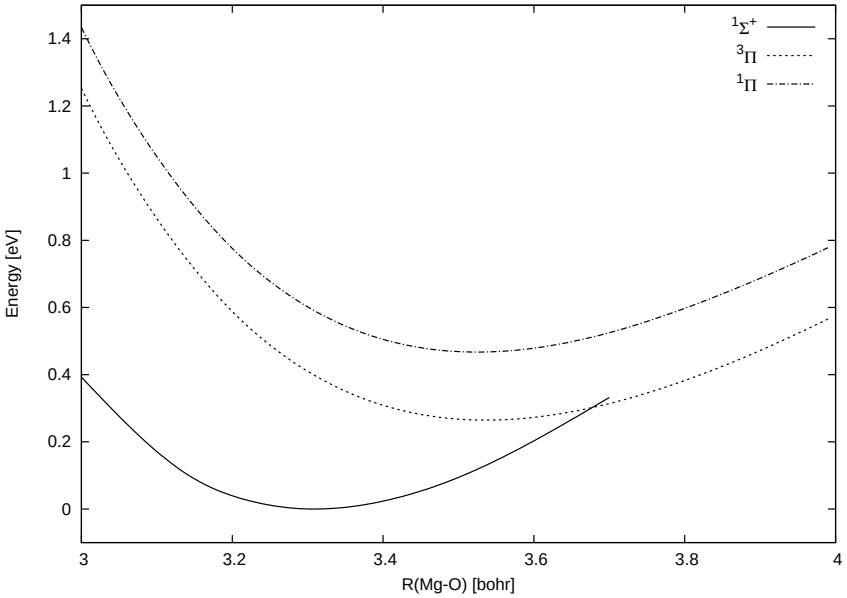

Figure 25: Dipole moments of the low lying states of MgO at the MRCI level of theory.

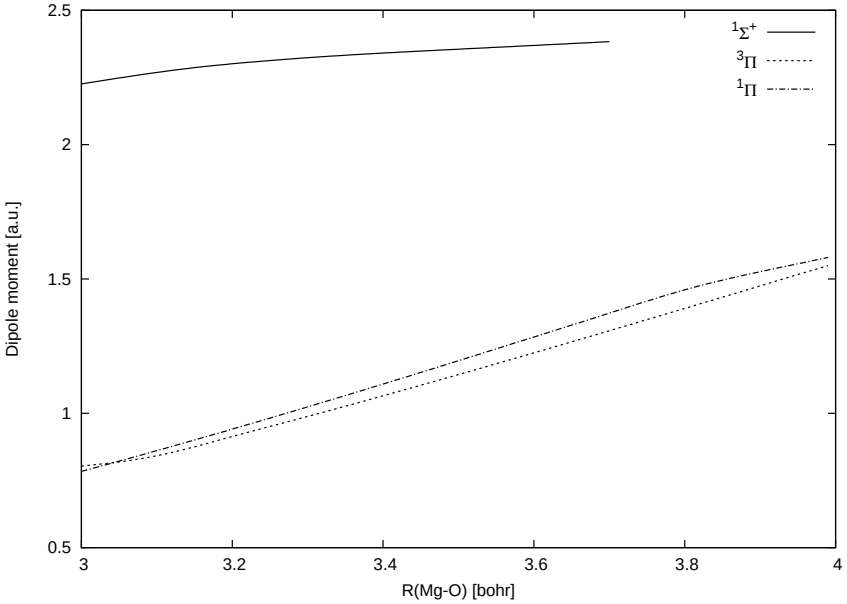

Figure 26: Potential energy curves of the low lying states of MgS at the MRCI+Q level of theory.

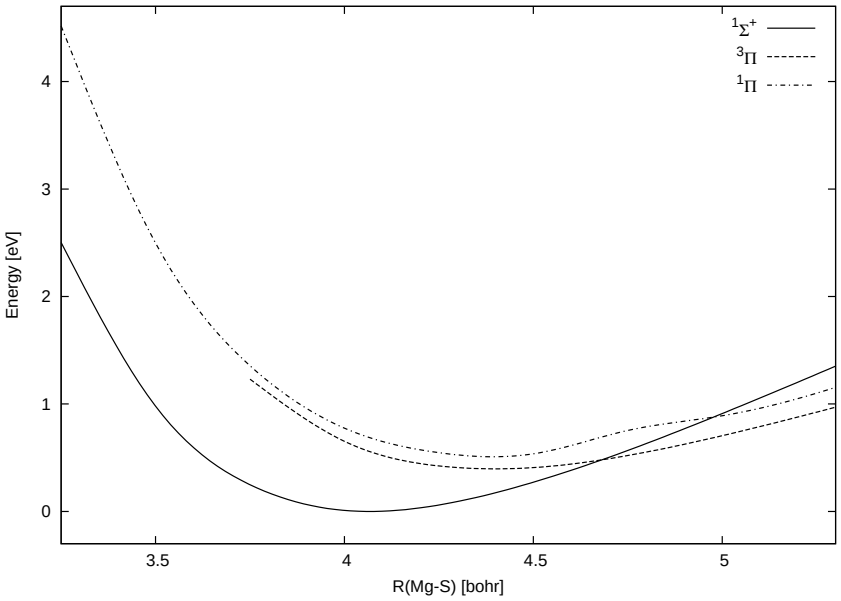

Figure 27: Dipole moments of the low lying states of MgS at the MRCI level of theory.

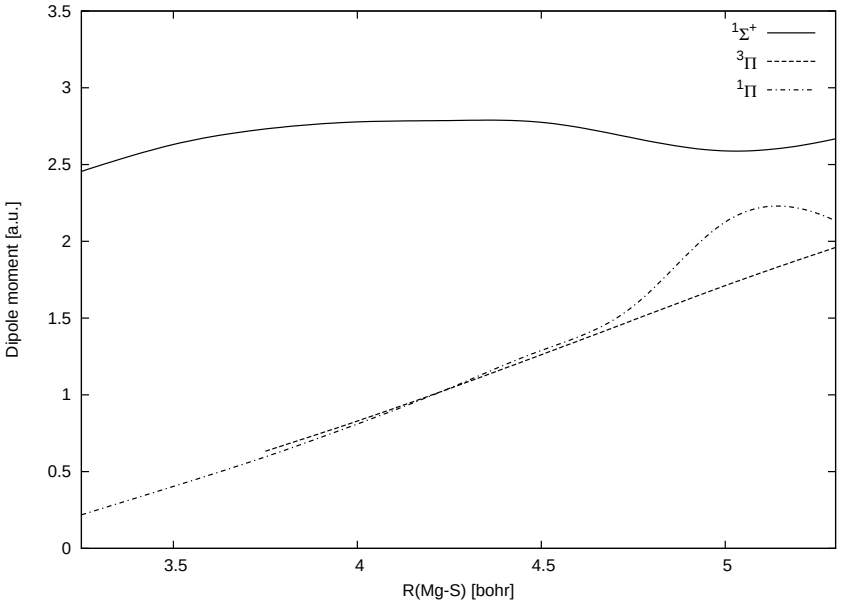

References

[1] J. Nye, *Physical Properties of Crystals: Their representation by Tensors and Matrices*, Oxford University Press, London, 1987.

[2] R. M. Martin, *Phys. Rev. B*, **5**, 1607 (1972).

[3] R. D. King-Smith and D. Vanderbilt, *Phys. Rev. B*, **47**, 1651 (1993).

[4] D. Vanderbilt and R. D. King-Smith, *Phys. Rev. B*, **48**, 4442 (1993).

[5] Y. Noel, C. M. Zicovich-Wilson, B. Civalleri, Ph. D'Arco, and R. Dovesi, *Phys. Rev. B*, **65**, 014111 (2001).

[6] Y. Noel, M. Llunell, R. Orlando, Ph. D'Arco, and R. Dovesi, *Phys. Rev. B*, **66**, 214107 (2002).

[7] Y. D. Herzbach and M. H. Müser, *Comp. Phys. Commun.*, **174**, 17 (2006).

[8] A. Dal Corso, M. Posternak, A. Resta, and A. Baldereschi, *Phys. Rev. B*, **50**, 10715 (1994).

[9] N. A. Hill and U. Waghmare, *Phys. Rev. B*, **62**, 8802 (2000).

[10] M. Catti, Y. Noel, and R. Dovesi, *J. Phys. Chem. Solids*, **64**, 2183 (2003).

[11] X. Wu, D. Vanderbilt, and D. R. Hamann, *Phys. Rev. B*, **72**, 035105 (2005).

[12] H. J. Xiang, J. Yang, J. G. Hou, and Q. Zhu, *Appl. Phys. Lett.*, **89**, 223111 (2006).

[13] F. Bernardini, V. Fiorentini, and D. Vanderbilt, *Phys. Rev. B*, **56**, R10 024 (1997).

[14] P. Gopal and N. A. Spaldin, *J. of Electronic Materials*, **35**, 538 (2006).

[15] O. Madelung, W. von der Osten, and U. Rössler, *Zahlenwerte und Funktionen aus Naturwissenshaften une Technik*, edited by O. Madelung and M. Schultz, Landolt-Börnstein, New Series, Group III, Vol. 22, Pt. a, Springer-Verlag, Berlin, p. 164Vol. 17, Pt. b, pp. 342 and 376; Vol.11, p. 370, 1987.

[16] *Elastic, Piezoelectric, Pyroelectric, Piezooptic, Electrooptik Constants, and Nonlinear Dielectric Susceptibilities of Crystals*, edited by K. H. Hellwege and A. M. Hellwege, Landolt-Börnstein, New Series, Group III, Vol. 11, Springer, Berlin, 1979.

[17] Landolt-Börnstein, in : O. Madelung (Ed.), New Series, Group III : Solid State Physics, Low Frequency Properties of Dielectric Crystals: Elastic Constants, vol. 29a, Springer, Berlin, 1993.

[18] E. E. Tokarev, I. B. Kobyakov, I. P. Kuz'mina, A. N. Lobachev, and G. S. Pado, *Sov. Phys. Solid State*, **17**, 629 (1975).

[19] V. A. Zhdanov and L. A. Brysneva, *Sov. Phys. Crystallog.*, **19**, 368 (1974).

[20] J. G. Gualtieri, J. A. Kosinski, and A. Ballato, *IEEE Trans. Ultrason. Ferroelectr. Freq. Control*, **UFFC-41**, 53 (1994).

[21] S. de Gironcoli, S. Baroni, and R. Resta, *Ferroelectrics*, **111**, 19 (1990).

[22] J. Emsley, *The Elements, Second Edition*, Oxford University Press, 1989.

[23] Ch. E. Moore, *Atomic Energy Levels, Vol. I-II*, Circular of the National Bureau of Standards 467, U.S. Government Printing Office, Washington, DC, 1949.

[24] K. P. Huber and G. Herzberg, *Molecular Spectra and Molecular Structure, Vol. IV, Constants of Diatomic Molecules*, Van Norstrand Reinhold, New York, 1979.

[25] A. I. Boldyrev and J. Simons, *J. Phys. Chem.*, **97**, 6149 (1993).

[26] H. Gomez, T. R. Taylor, Y. Zhao, and D. M. Neumark, *J. Chem. Phys.*, **117**, 8644 (2002).

[27] H.-J. Werner and P. J. Knowles, *J. Chem. Phys.*, **82**, 5053 (1985).

[28] P. J. Knowles and H.-J. Werner, *Chem. Phys. Lett.*, **115**, 259 (1985).

[29] H.-J. Werner and P. J. Knowles, *J. Chem. Phys.*, **89**, 5853 (1988).

[30] P. J. Knowles and H.-J. Werner, *Chem. Phys. Lett.*, **145**, 514 (1988).

[31] S. R. Langhoff and E. R. Davidson, *Int. J. Quantum Chem.*, **8**, 61 (1974).

[32] M. R. A. Blomberg and P. E. M. Siegbahn, *J. Chem. Phys.*, **78**, 5682 (1983).

[33] MOLPRO, version 2006, a package of *ab initio programs*, H.-J. Werner, P. J. Knowles, R. Lindh, F. R. Manby, M. Schtz, and others, see http://www.molpro.net

[34] D. Figgen, G. Rauhut, M. Dolg, and H. Stoll, *Chem. Phys.*, **311**, 227 (2005).

[35] K. A. Peterson, D. Figgen, E. Goll, H. Stoll, and M. Dolg, *J. Chem. Phys.*, **119**, 11113 (2003).

[36] K. A. Peterson and C. Puzzarini, *Theor. Chem. Acc.*, **114**, 283 (2005).

[37] T. H. Dunning Jr., *J. Chem. Phys.*, **90**, 1007 (1989).

[38] R. A. Kendall, T. H. Dunning Jr., and R. J. Harrison, *J. Chem. Phys.*, **96**, 6796 (1992).

[39] D. E. Woon and T. H. Dunning Jr., *J. Chem. Phys.*, **98**, 1358 (1993).

[40] D. E. Woon and T. H. Dunning Jr., *J. Chem. Phys.*, **103**, 4572 (1995).

[41] The NUMEROV method, written by J. Senekowitsch *et al.*, Johan Wolfgang Goethe Universität, Frankfurt-am-Main, Germany, 1988.

[42] K. A. Peterson, B. C. Shepler, and J. M. Singleton, *Mol. Phys.*, **105**, 1139 (2007).

[43] J. H. Kim, X. Li, L.-S. Wang, H. L. de Clercq, C. A. Fancher, O. C. Thomas, and K. H. Bowen, *J. Phys. Chem. A*, **105**, 5709 (2001).

[44] C. A. Fancher, H. L. de Clercq, O. C. Thomas, D. W. Robinson, and K. H. Bowen, *J. Chem. Phys.*, **109**, 8426 (1998).

[45] K. P. Jensen, B. O. Roos, and U. Ryde, *J. Chem. Phys.*, **126**, 14103 (2007).

[46] A. I. Boldyrev and J. Simons, *Mol. Phys.*, **92**, 365 (1997).

[47] O. Kullie, H. Zhang, J. Kolb, and D. Kolb, *J. Chem. Phys.*, **125**, 244303 (2006).

[48] M. Dolg, U. Wedig, H. Stoll, and H. Preuss, *J. Chem. Phys.*, **86**, 2123 (1987).

[49] C. W. Bauschlicher Jr. and H. Partridge, *Chem. Phys. Lett.*, **342**, 441 (2001).

[50] E. G. Bakalbassis, M.-A. D. Stiakaki, A. C. Tsipis, and C. A. Tsipis, *Chem. Phys.*, **205**, 389 (1996).

[51] C. A. Fancher, H. L. de Clercq, O. C. Thomas, D. W. Robinson, and K. H. Bowen, *J. Chem. Phys.*, **109**, 8426 (1998).

[52] S. G. Raptis, M. G. Papadopoulos, and A. J. Sadlej, *J. Chem. Phys.*, **111**, 7904 (1999).

[53] C. Cressiot, M. Guitou, A. O. Mitrushchenkov, and G. Chambaud, *Mol. Phys.*, **105**, 1207 (2007).

[54] T. Helgaker, W. Klopper, H. Koch, and J. Noga, *J. Chem. Phys.*, **106**, 9639 (1997).

[55] A. Halkier, T. Helgaker, P. Jørgensen, W. Klopper, H. Koch, J. Olsen, and A. K. Wilson, *Chem. Phys. Lett.*, **286**, 243 (1998).

[56] R. Linguerri, N. Komiha, R. Oswald, A. Mitrushchenkov, and P. Rosmus, *Chem. Phys.*, **346**, 1 (2008).

[57] P. A. Denis, *Chem. Phys. Lett.*, **395**, 12 (2004).

[58] J. M. L. Martin, T. Lee, G. E. Scuseria, and P. T. Taylor, *J. Chem. Phys.*, **97**, 6549 (1992).

[59] C. W. Bauschlicher Jr. and H. Partridge, *Chem. Phys. Lett.*, **257**, 601 (1996).

[60] K. A. Peterson, *J. Chem. Phys.*, **102**, 263 (1995).

[61] Z. Gan, D. J. Grant, R. J. Harrison, and D. A. Dixon, *J. Chem. Phys.*, **125**, 124311 (2006).

[62] S.-I. Lu, *J. Chem. Phys.*, **123**, 174313 (2005).

[63] M. Lorenz, J. Agreiter, A. M. Smith, and V. E. Bondibey, *J. Chem. Phys.*, **104**, 3143 (1996).

[64] A. Karton and J. M. L. Martin, *J. Chem. Phys.*, **125**, 144313 (2006).

[65] K. R. Asmis, T. R. Traylor, and D. M. Neumark, *Chem. Phys. Lett.*, **295**, 75 (1998).

[66] A. I. Boldyrev, N. Gonzales, and J. Simons, *J. Phys. Chem.*, **98**, 9931 (1994).

[67] S. R. Langhoff, C. W. Bauschlicher Jr., and L. G. M. Pettersson, *J. Chem. Phys.*, **89**, 7354 (1988).

[68] G. L. Gutsev, P. Jena, and R. J. Bartlett, *J. Chem. Phys.*, **110**, 2928 (1999).

[69] M. W. Chase, *J. Phys. Chem. Ref. Data, Monograph 9, NIST-JANAF Thermochemical Tables, fourth ed. ACS, AIP, NSRDS, Gaithersburg*, (1998).

[70] D. R. Stull and H. Prophet, *JANAF Thermochemical Tables, second ed., NSRDS-NBS 37, US Nat. Bur. Std., Washington*, (1971).

[71] R. J. Buenker, H.-P. Liebermann, L. Pichl, M. Tachikawa, and M. Kimura, *J. Chem. Phys.*, **126**, 104305 (2007).

[72] M. Srnec and R. Zahradník, *Chem. Phys. Lett.*, **407**, 283 (2005).

[73] G. L. Gutsev, M. Nooijen, and J. Bartlett, *Chem. Phys. Lett.*, **276**, 13 (1997).

[74] P. Fuentealba and A. Savin, *J. Phys. Chem. A*, **104**, 10882 (2000).

[75] J. Noga and T. Pluta, *Chem. Phys. Lett.*, **264**, 101 (1997).

[76] B. Pouilly, J. M. Robbe, J. Schamps, R. W. Field, and L. Young, *J. Mol. Spectrosc.*, **96**, 1 (1982).

[77] H. Thümmel, R. Klotz, and D. Peyerimhoff, *Chem. Phys.*, **129**, 417 (1989).

[78] C. W. Bauschlicher Jr. and H. Partridge, *Chem. Phys. Lett.*, **342**, 441 (2001).

[79] T. Ikeda, N. B. Wong, D. O. Harris, and R. Field, *J. Mol. Spectrosc.*, **68**, 452 (1977).

[80] P. Mürtz, H. Thümmel, C. Pfelzer, and W. Urban, *Mol. Phys.*, **86**, 513 (1995).

[81] K. A. Walker and M. C. L. Gerry, *J. Mol. Spectrosc.*, **182**, 178 (1997).

[82] H. Büsener, F. Heinrich, and A. Hese, *Chem. Phys.*, **112**, 139 (1987).

6 Theoretical investigation of the HZnF molecule

6.1 Introduction

Zinc is an interesting metal because of its important role in synthetic organic chemistry as well as in biological system. For example, zinc dichloride is reported to be a highly efficient catalyst in the alkylation of ketones [1]. As the second most abundant transition metal in the body, zinc has been related to neurological effects such as Alzheimer's disease [2]. Furthermore, zinc is an important biological trace metal present in many enzymes, including alcohol dehydrogenase, carbonic anhydrase, DNA and RNA polymerase, carboxypeptidase, and thermolysin [3]. On the other hand, a particular interest for the vibrational spectroscopy of the compounds containing Zn is the abundance of the various stable isotopes; the isotopes of Zn are ^{64}Zn(48.6%), ^{66}Zn(27.9%), ^{68}Zn(18.8%), ^{67}Zn(4.1%), and ^{70}Zn(0.6%) [4]. Their isotopomers make a specific signature in the vibrational spectra.

Recently, three experimental and theoretical studies have been reported to investigate the ground state of zinc hydrochloride HZnCl. First, Macrae *et al.* [5] prepared HZnCl in Ar cold matrices and recorded their infrared spectrum, from which they estimated three normal modes of vibration. However, because of the absence of rotational analysis, no data were extracted for the bond lengths. Later, the vibration-rotation emission spectrum of gaseous HZnCl was recorded by Yu *et al.* [6]. Their spectrum appeared to be complicated due to a small value of the rotational constant 2B and the abundant different isotopomers of HZnCl. Their determination of the bond lengths became quite confused because of many uncertainties arising from this spectrum complexity. From the calculations at the RCCSD(T) level including one-electron Douglas-Kroll-Hess relativistic effects, Kerkines *et al.* [7] have obtained reliable values of the bond lengths and the harmonic wavenumbers of the three normal modes.

Motivated by these successful studies, we try to investigate the ground state of HZnF, which has never been studied up to now. Starting with the ZnH and ZnF diatomic molecules, the spectroscopic characteristics of the ground state of HZnF will be revealed, based on highly correlated *ab initio* calculations. In the first section, to confirm our method including relativistic effects by pseudopotentials, we will perform the electronic structure calculations of the low lying states of ZnH and compare our results with the existing data. The low lying states of the ZnH^+ cation, which has been less studied, will be treated using the same ansatz to calculate the ionization energy relative to the ground state of ZnH. This quantity will be involved in the ionic dissociation asymptote of ZnH^+ and F^- in linear geometry.

In the second section, we will present the results from the electronic structure calculations of the low lying states of ZnF, using the pseudopotentials for both Zn and F atoms. This part is contributed not only to validate our method, but also to reveal the properties of the low lying states of ZnF. These informations are necessary to investigate the dissociation asymptotes into H and ZnF. However, there is actually no reliable information on these states, except for the ground state. Based on highly correlated *ab initio* calculations, their electronic structures and the corresponding calculated spectroscopic constants will be discussed. Vibronic transitions can

occur between the ground state and the excited bound states and the corresponding vibrationally resolved absorption spectra will be simulated. Additionally, we will show the results of ZnF^- anion and ZnCl, obtained from the same method as for ZnF, and compare with the existing data.

At the end of this chapter, the study of the ground state of HZnF will be presented. First, we will reveal globally the properties of the low lying states of HZnF from the MCSCF calculations and then will report, at the MRCI+Q level, the determination of the potential energy surface of the ground state, from which the spectroscopic characteristics will be extracted. The effects of the isotopic substitutions of Zn will be shown in term of the harmonic wavenumbers of the normal vibration modes and of the rovibrational levels. To obtain the accurate description of the ground state, it will be required to include into the calculations at the MCSCF level many low lying excited states and then this point will need many efforts to determine how many excited states should de considered. Based on the calculated electronic structures of the low lying states of the concerned diatomic fragments, Table 11 shows, as the preliminary results, the lowest covalent and ionic dissociation asymptotes of HZnF in linear geometry.

Table 11: Lowest covalent and ionic dissociation asymptotes of HZnF with the resulting low lying electronic states in linear geometry.

Dissociation asymptotes	Energies$^{(a)}$ [eV]	Molecular states
HZn + F		
$ZnH(X^2\Sigma^+) + F(^2P_u)$	0	$^{1,3}\Sigma^+$, $^{1,3}\Pi$
$ZnH(A^2\Pi) + F(^2P_u)$	2.888	$^{1,3}\Sigma^+$, $^{1,3}\Pi$, $^{1,3}\Delta$, $^{1,3}\Sigma^-$
$ZnH(B^2\Sigma^+) + F(^2P_u)$	3.470	$^{1,3}\Sigma^+$, $^{1,3}\Pi$
$ZnH^+(X^1\Sigma^+) + F^-(^1S_g)$	4.096	$^1\Sigma^+$
H + ZnF		
$H(^2S_g) + ZnF(X^2\Sigma^+)$	0	$^{1,3}\Sigma^+$
$H(^2S_g) + ZnF(A^2\Pi)$	4.634 (T_v)	$^{1,3}\Pi$
$H(^2S_g) + ZnF(B^2\Sigma^+)$	4.101	$^{1,3}\Sigma^+$
$H(^2S_g) + ZnF(C^2\Pi)$	4.876	$^{1,3}\Pi$
$H(^2S_g) + ZnF(D^2\Sigma^+)$	6.694	$^{1,3}\Sigma^+$
$H(^2S_g) + ZnF(^2\Delta/^2\Sigma^-)$	8.323 (T_v)	$^{1,3}\Delta/^{1,3}\Sigma^-$
$H(^2S_g) + ZnF(^2\Pi)$	9.907 (T_v)	$^{1,3}\Pi$

(a): Taken from our calculations at the MRCI + Q level. T_e values are used for the bound states and T_v vertical values at the equilibrium distance of the ground state for the repulsive states. The Atomic energies are taken from [8] and are averaged over the fine structure levels.

6.2 ZnH diatomic molecule and ZnH^+ cation

6.2.1 Introduction

We have considered the zinc mono-hydride diatomic molecule (ZnH) and its anion (ZnH^+), as the first step in the study of the HZnF triatomic molecule. Since the beginning of the 1920s, many works have been carried out on the $X^2\Sigma^+$ ground state of ZnH and on its low lying excited states. ZnH is also a molecule of astrophysical interest [9, 10]. Wojslaw and Peery identified the spectrum lines corresponding to the $A^2\Pi$(v=0,1) - $X^2\Sigma^+$(v'=0) vibronic transitions of ZnH in the violet spectrum of the cool carbon star 19 Piscium between 398 and 434 nm. Recently Shayesteh *et al.* [11] reported their multi-isotopologue analyses of the ground state from the observed infrared emission spectra. The most recent theoretical work of Kerkines *et al.* [7] indicated that the one electron relativistic effects estimated within the second-order Douglas-Kroll-Hess (DKH) approximation are important to obtain an accurate description of the ground state of ZnH. The DKH approximation bases the idea on reduction of the coupling between the positron and the electron states by the repetitive unitary transformations on the Dirac-Coulomb-Breit Hamiltonian and on its four-component wavefunction. While, in this study of HZnF, we will employ the most recently reported pseudopotentials for Zn with the associated basis set to take the relativistic effects into account. Thus the first purpose of this chapter is to evaluate our following method, compared with the already well known data of ZnH.

It is also necessary to calculate the ionization energy of the $X^2\Sigma^+$ ground state of ZnH to the ground state of ZnH^+, because this quantity is involved in the ionic dissociation asymptote of $HZn^+ + F^-$ in linear geometry. In addition, all existing studies of ZnH^+ are concerned only with the $X^1\Sigma^+$ and the $A^1\Sigma^+$ states. To obtain an accurate description of the low lying electronic states of ZnH^+, calculations will be performed using the same method as for ZnH. This is the second objective in this chapter.

6.2.2 Existing data on ZnH and ZnH^+

All of the previous studies of ZnH and ZnH^+ are listed in Table 12.

(i) Previous studies of ZnH

A nearly complete summary of the experimental studies on ZnH prior to 1975 was compiled by Huber and Herzberg [12]. The ZnH molecule was first observed in the 1920s through its spectra in the visible and near-ultraviolet regions. The most detailed analyses reported by Stenvinkel on the $A^2\Pi$ - $X^2\Sigma^+$ and $B^2\Sigma^+$ - $X^2\Sigma^+$ electronic transitions revealed the harmonic and anharmonic wavenumbers $\omega_e/\omega_e x_e$ = 1607.6/55.14, 1910.2/40.8, and 1020.7/16.5 cm^{-1} respectively for the $X^2\Sigma^+$, $A^2\Pi$, and $B^2\Sigma^+$ states. The equilibrium distances r_e and the energy differences relative to the ground state T_e, were determined in this work as follows: 3.014 bohr for the $X^2\Sigma^+$ ground state, 2.857 bohr/2.886 eV for the $A^2\Pi$ state, and 4.295 bohr/3.420 eV for the $B^2\Sigma^+$ state. The extrapolated dissociation energy D_0 of the ground state was reported by Herzberg and Huber [12] to be 0.85 eV. Another electronic transition $C^2\Sigma^+$ - $X^2\Sigma^+$ was found

by Khan [13] from the absorption spectra in the far-ultraviolet region. For this $C^2\Sigma^+$ state, the following spectroscopic constants were reported: $\omega_e/\omega_e x_e$ = 1824/48 cm^{-1}, r_e = 2.891 bohr, and T_e = 5.094 eV. It was predicted that the $C^2\Sigma^+$ state is predissociated by a quartet state correlated with the H(^2S_g) + Zn(^3P_u) dissociation asymptote. Hyperfine structure was investigated by Knight and Weltner [14], more recently by McKinley *et al.* [15] using matrix-isolation electron spin resonance techniques. They discussed the characters of the Zn(4s), Zn(4p), and H(1s) atomic orbitals in the 8σ molecular orbital of the ground state occupied by the unpaired electron. Urban *et al.* [16] recorded the infrared spectra of several isotopologues of ZnH in the ground state, using a diode laser spectrometer, determining the Dunham parameters [17]. More recently, Shayesteh *et al.* have confirmed the spectroscopic constants $\omega_e/\omega_e x_e$ = 1603.2/50.5 cm^{-1} and r_e = 3.011 bohr for the $X^2\Sigma^+$ ground state deduced from infrared emission spectra.

Chong *et al.* [18, 19] reported the calculated spectroscopic constants for the ground state by the singles-plus-doubles configuration interaction (SDCI) and the coupled pair functional (CPF) method, using the [9s7p4d] and [4s3p] contracted Gaussian basis sets for Zn and H atom respectively. They estimated also the relativistic effects at the SDCI and CPF levels with the larger [9s7p4d3f1g] and [4s3p2d] basis sets, using the first-order perturbation theory to compute the mass-velocity and Darwin contributions. The theoretical study including the ground and excited states was perfomed by Jamorski *et al.* [20] at the CI level. In this study, the relativistic effects were taken into account by the a relativistic effective core potential. The polarization and intrashell correlation effects were treated with a semiempirical core polarization potential. They noted that the $C^2\Sigma^+$ state has two close minima, one of them is found in the same range of distance as the X and A states. More recently, Kerkines *et al.* [7] have reported at the RCCSD(T) level the spectroscopic constants r_e = 3.001 bohr, D_e = 0.919 eV, and μ_e = 0.232 a.u. for the $X^2\Sigma^+$ ground state. They discussed the relativistic effects at the complete basis set (CBS) limit, using the second-order DKH approximation and the corresponding cc-pV(T,Q,5)Z-DKH basis sets. It has been noted in this study that the relativistic effects contribute more than the core-valence effects estimated at the CBS limit using the cc-pwCV(T,Q,5)Z basis sets.

(ii) Previous studies of ZnH^+

So far, three available studies exist for the ZnH^+ cation. The emission spectra of ZnH^+ in the region from 200 to 250 nm was recorded and assigned to the $A^1\Sigma^+$ - $X^1\Sigma^+$ electronic transition by Bengtsson and Grundström [21]. They revealed the spectroscopic constants as follows for the $X^1\Sigma^+$ ground state: $\omega_e/\omega_e x_e$ = 1916/39 cm^{-1}, r_e = 2.863 bohr, and the extrapolated dissociation energy D_0 = 2.5 eV. For the $A^1\Sigma^+$ excited state, they obtained the values $\omega_e/\omega_e x_e$ = 1365/15 cm^{-1}, r_e = 3.243 bohr, and T_e = 5.790 eV. Since this work, no experimental study has been reported. Schilling *et al.* [22] calculated the spectroscopic constants for the ground state, by dissociation-consistent configuration with a generalized valence bond wavefunction. They used the VDZ basis sets for both H and Zn atoms. A little later, Greene *et al.* [23] performed calculations for $X^1\Sigma^+$ ground state, at the MP2 and CCSD(T) levels, using the contracted (9s8p6d2f)/[8s6p5d2f] and (10s2p)/[7s2p] basis sets for Zn and H respectively. At the CCSD(T) level, their calculated values are ω_e = 1878 cm^{-1} and r_e = 2.872 bohr. Beside the ground state,

there is no theoretical work on the excited states of ZnH^+ cation.

Table 12: Spectroscopic constants of the low lying states of ZnH and ZnH^+ cation.

States	Method	r_e [bohr]	$\omega_e/\omega_e x_e$ [cm^{-1}]	D_e [eV]	T_e [eV]	μ_e [a.u.]
ZnH						
$X^2\Sigma^+$						
This work[(a)]	MRCI+Q	2.997	1621.6/53.9(^{64}ZnH) 1621.2/53.8(^{66}ZnH) 1621.0/53.8(^{67}ZnH) 1620.9/53.8(^{68}ZnH)	0.940	0	0.016
Kerkines [7]	RCCSD(T)	3.001		0.919		0.232
Jamorski [20]	CI	3.037	1647	0.82	0	
Chong[(b)]	SDCI	2.958	1775	1.00	0	0.297
	CPF	3.005	1622	1.01	0	0.249
Shayesteh [11]	Exp.	3.011	1603.2/50.5			
Urban [16]	Exp.		1615.7/59.61(^{64}ZnH) 1615.3/59.58(^{66}ZnH) 1615.1/59.57(^{67}ZnH) 1615.0/59.56(^{68}ZnH)			
Stenvinkel [12]	Exp.	3.014	1607.6/55.14		0	
Herzberg [12]	Exp.			0.85[(c)]		
$A^2\Pi$						
This work	MRCI+Q	2.851	1906.5/40.0	2.039	2.888	0.718
Jamorski	CI	2.874	1875	1.98	2.88	
Stenvinkel	Exp.	2.857	1910.2/40.8		2.886	
$B^2\Sigma^+$						
This work	MRCI+Q	4.295	1029.2/16.5	1.440	3.470	-0.025
Jamorski	CI	4.297	1046	1.48	3.35	
Stenvinkel	Exp.	4.295	1020.7/16.5		3.420	
$C^2\Sigma^+$						
Jamorski	CI	2.882	1825	1.56	5.01	
Khan [13]	Exp.	2.891	1824/48		5.094	

States	Method	r_e [bohr]	$\omega_e/\omega_e x_e$ [cm^{-1}]	D_e [eV]	T_e [eV]	μ_e [a.u.]
ZnH^+						
$X^1\Sigma^+$						
This work	MRCI+Q	2.861	1950.6/65.7	2.488	0	
Greene [23]	CCSD(T)	2.872	1878			
Schilling [22]	GVB-DCCI	2.919	1868	2.271		
Bengtsson [21]	Exp.	2.863	1916/39	2.5$^{(c)}$	0	
$A^1\Sigma^+$						
This work	MRCI+Q	3.297	1245.8/35.4	2.583	5.896	
Bengtsson	Exp.	3.243	1365/15		5.790	
$b^3\Pi$						
This work	MRCI+Q	3.306	1205.5/26.0	1.107	7.363	
$B^1\Pi$						
This work	MRCI+Q	3.705	997.2/88.6	0.430	8.107	

(a):Absolute energy values calculated at the minimum of the ground state; -227.01988183 a.u. for ZnH and -226.74448416 a.u. for ZnH^+. The dipole moment is calculated at the MRCI level.
(b):Taken from ref. [18, 19], using the [9s7p4d3f1g] and [4s3p2d] contracted Gaussian basis sets for Zn and H respectively, with included relativistic effects. Only the dipole moments were calculated with the [9s7p4d] and [4s3p] contracted Gaussian basis sets.
(c):Extrapolated D_0 value.

6.2.3 Dissociation asymptotes of ZnH and ZnH^+

The first dissociation asymptote of ZnH comes from a combination of the Zn(^1S_g) and H(^2S_g) ground states, correlating with one $^2\Sigma^+$ molecular state. The lowest dissociation asymptotes depend only on excitation energies of the Zn atom, which are smaller than excitation from the H(1s:^2S_g) ground state to the H(2s:^2S_g) first excited state (10.199 eV) [8]. Thus the second and third lowest dissociation asymptotes lie at 4.038 eV and 5.796 eV above the first one, respectively, corresponding to the excitation energies to the ^3P_u and ^1P_u excited states of Zn (the value is averaged over the fine structure levels for the ^3P_u state) [8]. The Zn(^3P_u) excited and H(^2S_g) ground states lead to the second dissociation asymptote correlating with one $^{2,4}\Sigma^+$ and one $^{2,4}\Pi$ molecular states. The third one involving the Zn(^1P_u) excited and H(^2S_g) ground states results in one $^2\Sigma^+$ and one $^2\Pi$ molecular states. The 4^{th} and 5^{th} asymptotes including the Zn(^3S_g) and Zn(^1S_g) excited states correlate respectively with one $^{2,4}\Sigma^+$ and one $^2\Sigma^+$ molecular states, lying 6.654 and 6.917 eV above the first asymptote. Based on the ionization energy of Zn (9.394 eV) [8] and the electronic affinity of H (0.754 eV) [4], the first ionic asymptote, lying 8.640 eV above the lowest covalent one, correlates with one $^2\Sigma^+$ state. This ionic asymptote is much higher in energy than the others and will not be included in the calculations. The crossing between the covalent and the ionic state in the $^2\Sigma^+$ symmetry occurs at a distance

around 3.155 bohr. The distance of this crossing can be roughly estimated by considering a variation as $-1/R$ for the potential energy of the ionic Zn^+H^- form and a quasi constant energy for the covalent states. According to the position of the asymptotes and considering the simple equation $\Delta E = -1/R_c$, where ΔE represents the energy difference in atomic units between the asymptote of the covalent states and that of the ionic state, we deduce $\Delta E = -0.317$ a.u. (-8.640 eV) and $R_c = 3.155$ bohr. This region should be treated with particular attention.

The lowest dissociation asymptote of ZnH^+ corresponds to the combination of $Zn^+(3d^{10}4s: {}^2S_g)$ and $H({}^2S_g)$ fragments, lying at 9.394 eV above the lowest one of the neutral ZnH, according to the ionization energy of Zn [8] and correlates with one $^{1,3}\Sigma^+$ molecular states. The second asymptote resulting from the $Zn^+(3d^{10}4p:{}^2P_u)$ and $H({}^2S_g)$ states, lies at 6.065 eV (averaged over the fine structure levels) above the first one, corresponding to the excitation energy of the $Zn^+({}^2P_u)$ state [8]. This second asymptote correlates with one $^{1,3}\Sigma^+$ and one $^{1,3}\Pi$ molecular states. Totally six molecular states $^{1,3}\Sigma^+$, $^{1,3}\Pi$, and $^{1,3}\Delta$ are correlated with the third asymptote involving the $Zn^+(3d^9 4s^2: {}^2D_g)$ and $H({}^2S_g)$ states, lying 7.945 eV (averaged over the fine structure levels) above the first asymptote [8].

The lowest dissociation asymptotes of ZnH and ZnH^+ and the low lying electronic molecular states adiabatically correlated with these dissociation asymptotes are presented in Table 13. The calculations performed in this study are concerned with all electronic molecular states correlated with the five lowest asymptotes of ZnH and the three lowest ones of ZnH^+ mentioned above.

Table 13: Lowest dissociation asymptotes of the diatomic ZnH and the ZnH^+ cation and the resulting low lying electronic states.

Dissociation asymptotes	Energies$^{(a)}$[eV]	Molecular states
ZnH		
$Zn({}^1S_g) + H({}^2S_g)$	0	$^2\Sigma^+$
$Zn({}^3P_u) + H({}^2S_g)$	4.038	$^{2,4}\Sigma^+$, $^{2,4}\Pi$
$Zn({}^1P_u) + H({}^2S_g)$	5.796	$^2\Sigma^+$, $^2\Pi$
$Zn({}^3S_g) + H({}^2S_g)$	6.654	$^{2,4}\Sigma^+$
$Zn({}^1S_g) + H({}^2S_g)$	6.917	$^2\Sigma^+$
$Zn^+({}^2S_g) + H^-({}^1S_g)$	8.640	$^2\Sigma^+$
ZnH^+		
$Zn^+({}^2S_g) + H({}^2S_g)$	0	$^{1,3}\Sigma^+$
$Zn^+({}^2P_u) + H({}^2S_g)$	6.065	$^{1,3}\Sigma^+$, $^{1,3}\Pi$
$Zn^+({}^2D_g) + H({}^2S_g)$	7.945	$^{1,3}\Sigma^+$, $^{1,3}\Pi$, $^{1,3}\Delta$

(a): Taken from ref. [8].

6.2.4 Computational details

The core electrons of the zinc atom have been described by atomic pseudopotentials which allow relativistic effects to be taken into account. We employed the most recent energy-consistent ECP10MDF effective core potentials [24], with 10 inner electrons presented by a pseudopotential and the outer electrons explicitly treated using the associated aug-cc-pVQZ basis sets contracted as (14s11p11d3f2g1h)/[6s6p5d3f2g1h] [25]. For the hydrogen atom, the Dunning *et al.* correlation consistent aug-cc-pVQZ basis sets are employed [26].

Molecular structure calculations are performed in the same method with 21 or 20 valence electrons for ZnH or ZnH^+. In the first step, the wave functions of 21 (ZnH) and 20 (ZnH^+) valence electrons are determined by state-averaged Multi-Configuration-Self-Consistent-Field (MCSCF) calculations [27, 28] with 15 active molecular orbitals constructed on the 3s, 3p, 3d, 4s, 4p, and 5s of Zn and 1s of H. Among these 15 orbitals, the 4 inner shells of the 3s and 3p of Zn are optimized but not correlated in this step. Thus the effective active space results in the (3-7)σ, (2-3)π, and 1δ molecular orbitals. The MCSCF wavefunctions are taken as reference for the subsequent internally contracted Multi-Reference-Configuration-Interaction (MRCI) calculations [29,30]. The Davidson correction [31,32], which approximates the contribution of higher excitation terms, has been introduced in the last step of the calculation (MRCI+Q). All electronic structure calculations are performed in the C_{2v} symmetry group, using the MOLPRO program package [33].

6.2.5 Results

(i) Results of ZnH

The state-averaged MCSCF calculations were performed for all doublet and quartet states correlated with the five lowest dissociation asymptotes. The potential curves of all the doublet and quartet states correlated with the three lowest asymptotes and the dipole moments of these doublet states are presented in Figures 28 and 29. Taking the MCSCF wavefunctions as reference, the subsequent MRCI calculations for the electronic states correlated with two lowest asymptotes were performed separately in each space and spin symmetries. Figure 30 shows the potential curves of all the doublet and quartet states calculated at the MRCI level including the Davidson correction. The dipole moment functions of the doublet states, calculated as an expectation value at the MRCI level, are presented in Figure 31. The sign convention is defined such as the positive value corresponds to the Zn^+H^- polarity. Our result confirms that the ground state is found to be a $^2\Sigma^+$ state. In turn, we can assign the $A^2\Pi$ and $B^2\Sigma^+$ to the excited doublet states. These assignments are consistent with the previous studies. The energy difference between the two lowest dissociation asymptotes (3.983 eV) compares well with the experimental value (4.038 eV) shown in Table 13. The $B^2\Sigma^+$ state correlated with the second asymptote presents an avoided crossing with the $C^2\Sigma^+$ state around the interatomic distance of 3 bohr and then their dipole moments interchange. We can see the crossing between the $C^2\Sigma^+$ state and the $^4\Pi$ state correlated with the second asymptote in Figure 28, which confirms the previous experiment [13].

Figure 28: Potential energy curves of the low lying states of ZnH, correlated with the three lowest asymptotes, at the MCSCF level of theory.

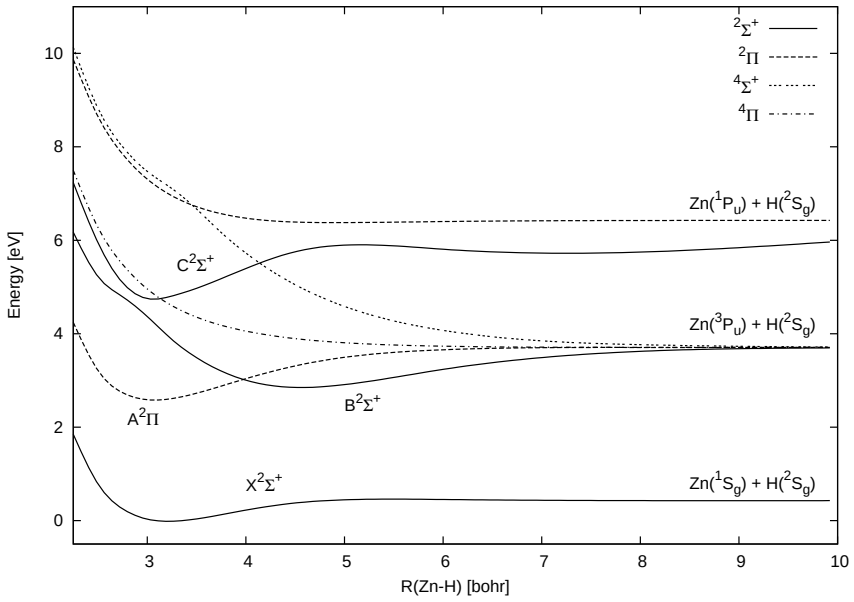

The spectroscopic constants for the $X^2\Sigma^+$, $A^2\Pi$, and $B^2\Sigma^+$ states of ^{64}ZnH are obtained from our potential curves at the MRCI+Q level, using the NUMEROV algorithm [34] and are listed in Table 12. For the $X^2\Sigma^+$ ground state, its spectroscopic constants are deduced as follows: $\omega_e/\omega_e x_e = 1621.6/53.9$ cm^{-1}, $r_e = 2.997$ bohr, and $D_e = 0.940$ eV. These constants are in good agreement with the previous values presented in Table 12. However, our harmonic wavenumber seems to be somehow larger than the experimental values, but closer to them than all previous calculations which overestimated this quantity. The dipole moment of 0.016 a.u. at the equilibrium distance shows a large difference compared with the previous calculations. Ignoring such difference, the dipole moment of quasi-zero value in the bonding region indicates the covalent character of the ground state as depicted in Figure 31. Tezcan *et al.* [35] determined the Fermi-contact constant b_F of the H atom in ZnH, from their far-infrared rotational spectra of the $X^2\Sigma^+$ ground state. Comparing this obtained b_F parameter with that in the free H atom, they reported that the character of the H(1s) atomic orbital in the 8σ molecular orbital containing the unpaired electron is about 35%. McKinley *et al.* [15] measured the magnetic parameters of ^{67}ZnH, using matrix-isolation electronic spin resonance spectroscopy. Also by the free atom comparison method, they analyzed that the 8σ molecular orbital consists of about 30% of the Zn(4s) character and 50% of the Zn(4p$_z$) character. Based on our state-averaged MCSCF calculations, the dominant configuration of the ground state at its equilibrium distance is $1\sigma^2 2\sigma^2 3\sigma^2 1\pi^4 4\sigma^2 5\sigma^2 2\pi^4 3\pi^4 6\sigma^2 1\delta^4 7\sigma^2 8\sigma^1$ (in which $1\sigma^2 2\sigma^2 3\sigma^2 1\pi^4$ is replaced by the pseudopotentials for Zn) with the coefficient of 0.957, in which the 8σ molecular orbital is found to be anti-bonding and has roughly contributions of 51%, 11%, and 38%, respectively, from the Zn(4s), Zn(4p$_z$), and H(1s) atomic orbitals. Thus, our result is in a better agreement with the

Figure 29: Dipole moment functions of the doublet states of ZnH, correlated with the three lowest asymptotes, at the MCSCF level of theory.

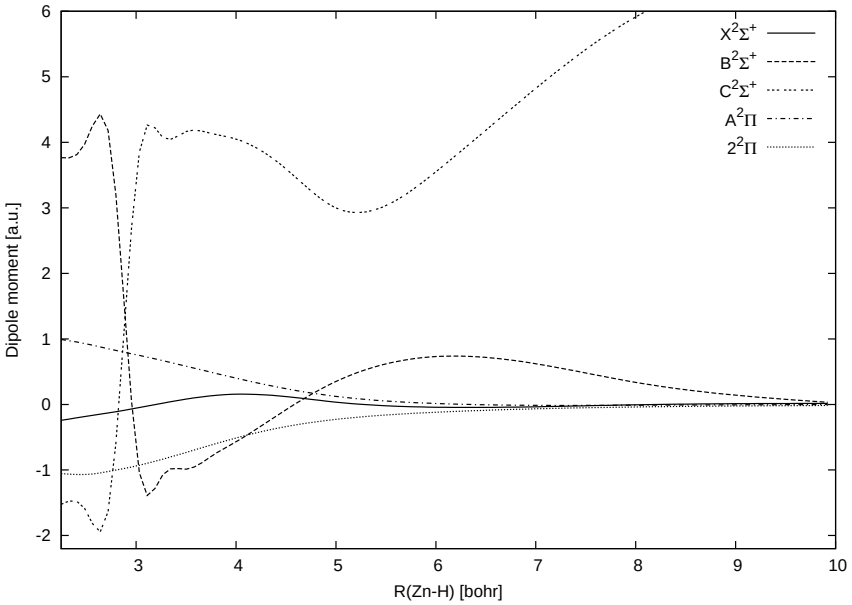

Figure 30: Potential energy curves of the low lying states of ZnH, correlated with the two lowest asymptotes, at the MRCI+Q level of theory.

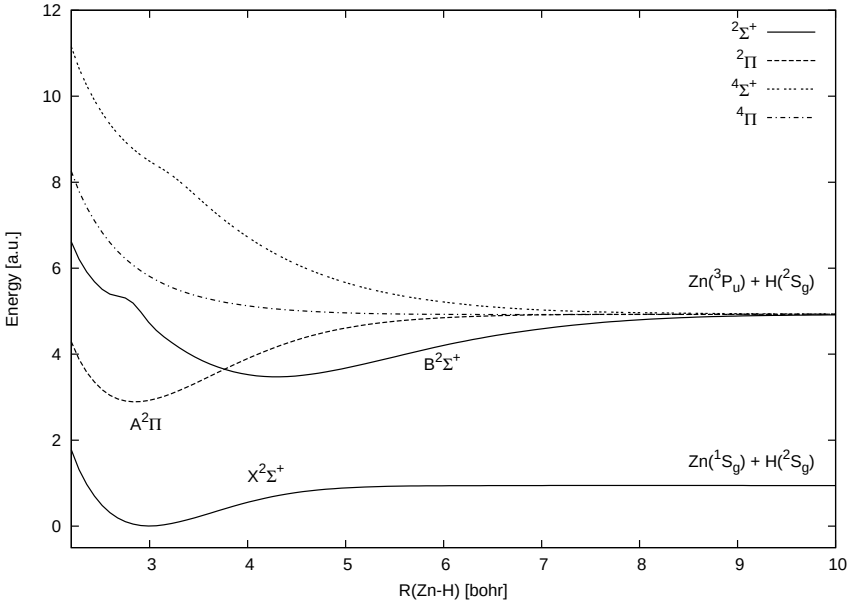

Figure 31: Dipole moment functions of the doublet states of ZnH, correlated with the two lowest asymptotes, at the MRCI level of theory.

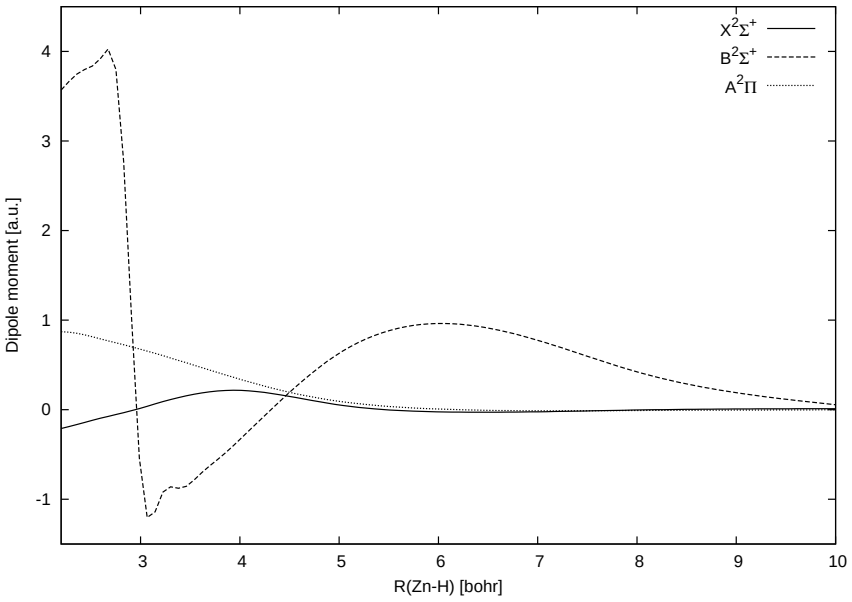

previous experimental analysis by Tezcan *et al.* than with that of McKinley *et al.*.

The $A^2\Pi$ state, correlated with the second dissociation asymptote, has the following values $\omega_e/\omega_e x_e = 1906.5/40.0$ cm^{-1}, $r_e = 2.851$ bohr, $T_e = 2.888$ eV, and $D_e = 2.039$ eV which compare quite well with those reported by the previous studies. This state has a partially ionic bond according to the positive dipole moment in the molecular region, and becomes rapidly covalent at distances longer than 5 bohr. With the long equilibrium distance of 4.295 bohr, the $B^2\Sigma^+$ state has a flat minimum. For this state, the following spectroscopic values are determined: $\omega_e/\omega_e x_e = 1029.2/16.5$ cm^{-1}, $T_e = 3.470$ eV, and $D_e = 1.440$ eV, in excellent agreement with the previous studies. A drastical change of the dipole moment of the $B^2\Sigma^+$ state around 3 bohr indicates an avoided crossing with a higher $^2\Sigma^+$ state. The $B^2\Sigma^+$ has also a partially ionic bonding in the molecular region, according to its dipole moment with the maximum around 6 bohr.

(ii) Results of ZnH^+

For ZnH^+ cation, the state-averaged MCSCF calculations with 20 valence electrons were performed for all singlet and triplet states correlated with the three lowest dissociation asymptotes. Taking the MCSCF wavefunctions as reference, the subsequent MRCI calculations were carried out for all molecular states correlated with the two lowest asymptotes, separately in each space and spin symmetries. Figure 32 shows the potential curves of all singlet and triplet states calculated at the MRCI+Q level. The ground state of ZnH^+ is found to be a $^1\Sigma^+$ state, with the main

Figure 32: Potential energy curves of the low lying states of ZnH^+ at the MRCI+Q level of theory.

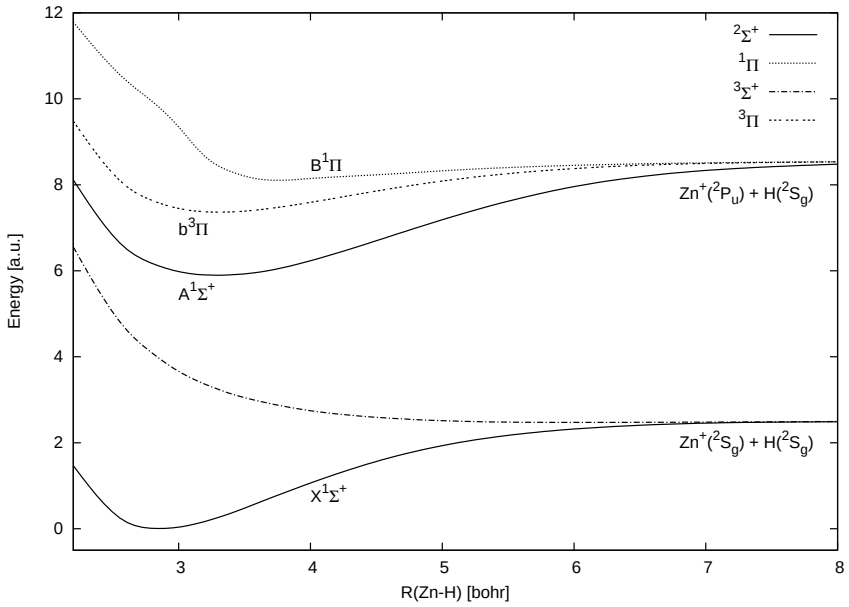

configuration $(...)4\sigma^2 5\sigma^2 2\pi^4 3\pi^4 6\sigma^2 1\delta^4 7\sigma^2$ at the equilibrium geometry which is consistent with the lowest one-electron ionization from the main configuration $(...)4\sigma^2 5\sigma^2 2\pi^4 3\pi^4 6\sigma^2 1\delta^4 7\sigma^2 8\sigma^1$ of the $X^2\Sigma^+$ ground state of ZnH. In turn, we can assign the $A^1\Sigma^+$ and $B^1\Pi$ to the excited singlet states and $a^3\Sigma^+$ and $b^3\Pi$ to the excited triplet states. The energy difference between the first and second dissociation asymptotes (6.031 eV) compares well with the experimental value (6.065 eV) listed in Table 13. The spectroscopic constants for the $X^1\Sigma^+$, $A^1\Sigma^+$, $B^1\Pi$, and $b^3\Pi$ states are obtained from our potential curves at the MRCI+Q level, using the NUMEROV algorithm [34] and are added in Table 12.

Our calculated harmonic and anharmonic wavenumbers of the $X^1\Sigma^+$ state are somehow larger by about 30 cm^{-1} than those reported by Bengtsson and Grundström [21], even though the equilibrium distance and the dissociation energy are in good agreement. However these discrepancies are much smaller, compared with the other theoretical works. From the state-averaged MCSCF calculations, the $7\sigma^2$ orbital in the main configuration $(...)3\pi^4 6\sigma^2 1\delta^4 7\sigma^2$ for the ground state at its equilibrium distance with a coefficient of 0.967, is constructed on 50% of both Zn(4s) and H(1s) atomic orbitals with minor contributions from Zn(3d) and Zn(4p). The ionization energy from the $X^2\Sigma^+$ of ZnH to the $X^1\Sigma^+$ of ZnH^+ is calculated to be 7.494 eV, using the D_e values at the MRCI+Q level. The ionization energy of 7.514 eV calculated with the D_0 values compares reasonably with that obtained from the experimental data (7.744 eV). Table 12 lists also the spectroscopic constants for the other bound states. Compared with the measurement by Bengtsson and Grundström, there remain again the large discrepancies on the values of $\omega_e/\omega_e x_e$ for the $A^1\Sigma^+$ state. Because of no available data on the other bound states,

we can estimate only a quality of the same order as for the $X^1\Sigma^+$ and $A^1\Sigma^+$ states.

6.2.6 Conclusions

To evaluate our method to treat the HZnF molecule, we first performed the electronic structure calculations on the ZnH molecule at the MRCI level including the Davidson correction. Using the energy-consistent pseudopotentials for Zn with the associated aug-cc-pVQZ basis sets, we have obtained an accurate description for the low lying states, and our results compared well with the previous studies. Using the same method, we have studied the low lying states of ZnH^+, revealing unknown excited states. Finally the ionization energy from the $X^2\Sigma^+$ of ZnH to the $X^1\Sigma^+$ of ZnH^+ has been determined to be 7.494 eV, using the D_e values at the MRCI+Q level, which will allow us to calculate the position in energy of the ionic dissociation asymptote of $HZn^+ + F^-$ in linear geometry.

6.3 ZnF and ZnCl diatomic molecules

6.3.1 Introduction

Before starting the part of the HZnF triatomic molecules, we will make a consideration about the zinc monofluoride and zinc monochloride to validate our method in this study and to elucidate the properties of the low lying electronic states of these systems. Even though the ground states $X^2\Sigma^+$ of ZnF and ZnCl have been studied recently both theoretically and experimentally, it is necessary to obtain an accurate description of the lower excited states of these diatomic molecules, in order to advance towards the triatomic part. Additionally we are interested in comparison of the properties of the low lying states between ZnF and ZnCl.

ZnF and ZnCl are ionic molecules belonging to the family of monohaloides of the $3d$-transition metals, which have been recently investigated by spectroscopic methods to understand the characteristics of their chemical bonds. The equilibrium distances in the ground states of $3d$-transition metal (from Sc to Zn) monochlorides and monofluorides have been reported by experimental studies [36–56]. The trend in bond distances are similar for these two series, however, there are subtle differences, particularly in going from copper to zinc. Comparing with the case of CuF and CuCl, the bond distance of ZnF increases by 0.8%, while by 3.8% for ZnCl. This difference can be due to the variation in ionic character of the zinc species. As listed in Table 14, a particular interest for the vibrational spectroscopy of ZnF and ZnCl is the abundance of the various stable isotopes of these elements; the isotopes of Zn are ^{64}Zn (48.6%), ^{66}Zn (27.9%), ^{68}Zn (18.8%), ^{67}Zn (4.1%), and ^{70}Zn (0.6%). These of Cl are ^{35}Cl (75.8%) and ^{37}Cl (24.2%) [4]. These isotopologues make a specific signature in the vibrational spectra.

Even though ZnF and ZnCl can be easily produced by the exothermic reactions of zinc vapor with F_2 or Cl_2 gas [49, 55] (for example: $\Delta E = 1.55$ eV for ZnF), these systems have not been much studied. The previous experimental data for ZnF and ZnCl until 1979 are summarized by Huber and Herzberg [12], indicating that there were a few reliable informations on the low lying states at that time, especially few information on the low lying excited states of ZnF. Motivated to obtain an accurate description of the low lying electronic states of ZnF and ZnCl, we have performed highly correlated *ab initio* calculations. Using effective core pseudopotentials and aug-cc-pVQZ basis sets for Zn, F, and Cl atoms, the potential energy curves, the dipole moments functions, and the transition dipole moments have been calculated at the MRCI level including the Davidson correction. The obtained spectroscopic constants and properties of electronic structures of the low lying states have been compared with the previous theoretical and experimental works. Based on the transition dipole moments between relevant electronic states, the vibronic transitions from the v = 0 level of the ground state $X^2\Sigma^+$ to the bound states of interest have been evaluated and their vibrationally resolved absorption spectra have been simulated for the abundant isotopologues of ZnF.

Table 14: Abundances and masses of the isotopologues of ZnCl.

Isotopes/Isotopologues	Abundances [%]	Atomic/Molecular Masses
^{35}Cl	75.8	34.97
^{37}Cl	24.2	36.97
^{64}Zn	48.6	63.93
^{66}Zn	27.9	65.93
^{67}Zn	4.1	66.93
^{68}Zn	18.8	67.92
^{70}Zn	0.6	69.93
^{64}Zn^{35}Cl	36.8	98.90
^{66}Zn^{35}Cl	21.1	100.90
^{68}Zn^{35}Cl	14.3	102.89
^{64}Zn^{37}Cl	11.8	100.86
^{66}Zn^{37}Cl	6.8	102.90
^{68}Zn^{37}Cl	4.5	104.89
^{67}Zn^{35}Cl	3.1	101.90
^{67}Zn^{37}Cl	1.0	103.90
^{70}Zn^{35}Cl	0.5	104.90
^{70}Zn^{37}Cl	0.1	106.90

6.3.2 Theoretical and experimental previous studies

(i) Studies on the low lying states of ZnF

All results of the previous studies mentioned below are presented in Table 15.

The first measurement on the ZnF system was reported by Rochester and Olsson in 1939, from an absorption spectrum in the ultraviolet domain [57]. Their measured harmonic $\omega_e = 628$ cm^{-1} and anharmonic wavenumbers $\omega_e x_e = 3.5$ cm^{-1} had not been confirmed before the work of Moravec *et al.* [58], who reported the values $\omega_e/\omega_e x_e = 620/2$ cm^{-1}, from their 4.66 eV photoelectron spectroscopy of the ZnF^- anion. More recently, Flory *et al.* recorded the pure rotational spectrum of the ground state of ZnF, from which they deduced an equilibrium distance $R_e = 3.341$ bohr, a dissociation energy $D_e = 3.123$ eV, and harmonic and anharmonic wavenumbers of the abundant isotopologues $\omega_e/\omega_e x_e = 631/4.0$, 629/3.9, and 627/3.9 cm^{-1}, respectively for ^{64}ZnF, ^{66}ZnF, and ^{68}ZnF [55]. Concerned with the excited states, Moravec *et al.* mentioned that the $A^2\Pi$ state must lie at more than 2.69 eV above the ground state $X^2\Sigma^+$ [58], estimating isoelectronic neutral states with the configuration $(9\sigma^2 4\pi^4 10\sigma^2)$ in the $X^1\Sigma^+$ lowest anion state. Supposing that the second order spin-orbit coupling in the ground state primarily arises from interactions with the $A^2\Pi$ state, Flory *et al.* predicted that the $A^2\Pi$ state should be at 2.53 eV above the $X^2\Sigma^+$ state. Rochester and Olsson reported that the $C^2\Pi$ state lies at 4.586 eV (for $\Omega = 1/2$) and 4.632 eV (for $\Omega = 3/2$) with an harmonic wavenumber ω_e of about 599 cm^{-1} from their early work, indicating that predissociated levels were found between 36000 and 39000

cm^{-1} [57].

In the last decade, several theoretical studies, based on various approaches, have been reported focusing on the ground state of ZnF. The first calculation was conducted by Bowmaker and Schwerdtfeger in 1990 [59], at the SDCI level of theory with the size-consistency correction (SDCISC), using the pseudopotentials for Zn with the associated (8s7p6d)/[6s5p3d] basis sets with an additional diffuse (1s1p1d) set. Their obtained spectroscopic constants were $R_e = 3.371$ bohr, $\omega_e = 601$ cm^{-1}, and $D_e = 2.028$ eV. A few years later, Kaupp and von Schnering obtained $R_e = 3.390$ bohr, using again the quasi-relativistic 20 valence electron pseudopotentials of Zn at the MP2 level of theory [60]. Using the density functional theory (DFT) approach, Liao *et al.* [61] reported $R_e = 3.364$ bohr and $\omega_e = 609$ cm^{-1}, later Belanzoni *et al.* [62] obtained $R_e =$ 3.399 bohr.

The more extensive studies have been performed by Boldyrev and Simons [63] and Harrison *et al.* [64]. The former study calculated $R_e = 3.388$ bohr, $\omega_e = 593$ cm^{-1}, $D_e = 2.931$ eV, and the dipole moment at the equilibrium distance $\mu_e = 1.275$ a.u. for the ground state at the QCISD(T) level, using the 6-331++G(d,f) basis sets. They reported also the van der Waals $A^2\Pi$ state correlated with the first dissociation asymptote with the spectroscopic constants as follows: $R_e = 8.520$ bohr, $\omega_e = 13$ cm^{-1}, $T_e = 2.928$ eV, and $\mu_e = 0.015$ a.u.. The latter study calculated extensively the ZnF, ZnF^+ cation and ZnF^- anion system to compare the bonding characteristics with the CaF, CaF^+ cation and CaF^- anion system at the RCCSD(T) level, using the Dunning aug-cc-pVQZ basis sets contracted as (13s7p4d3f)/[6s5p4d3f] without the g functions for F [65], and the (20s15p9d6f4g) primitive set with an ANO contraction to [7s6p4d3f2g] for Zn [66]. They reported $R_e = 3.354$ bohr, $\omega_e = 633$ cm^{-1}, $D_0 = 3.16$ eV, and μ_e $= 1.227$ a.u. for the ground state and $R_e = 3.320$ bohr, $\omega_e = 659$ cm^{-1}, $D_0 = 2.59$ eV, $T_0 = 4.63$ eV and $\mu_e = 1.500$ a.u. for the $^2\Pi$ excited state which seems to be correlated with the second dissociation asymptote. Even though Harrison *et al.* studied globally this system, it remains the question whether the RCCSD(T) method could correctly describe the electronic states of an ionic molecule. The validity of the method taken by Harrison *et al.* should be discussed later, comparing with our calculations.

Table 15: Spectroscopic constants and dipole moments of the low lying states of ZnF and for the electronic ground state of ZnF^-.

States	Method	R_e [bohr]	$\omega_e/\omega_e x_e$ [cm^{-1}]	D_e [eV]	T_e [eV]	μ_e [a.u.]
			ZnF			
$X^2\Sigma^+$						
This work[(a)]	MRCI+Q	3.337	638.6/3.2(^{64}ZnF) 636.4/3.2(^{66}ZnF) 634.3/3.2(^{68}ZnF)	3.030	0	0.939
Harrison [64]	RCCSD(T)	3.354	633	3.16 (D_0)	0	1.227
Belanzoni[(b)]	DFT	3.399				
Boldyrev[(c)]	QCISD(T)	3.388	593	2.931	0	1.275
Liao[(d)]	DFT	3.364	609			
Kaupp[(e)]	MP2	3.390				
Bowmaker [59]	SDCISC	3.371	601	2.028		
Flory [55]	Exp.	3.341	631/4.0(^{64}ZnF) 629/3.9(^{66}ZnF) 627/3.9(^{68}ZnF)	3.123	0	
Moravec [58]	Exp.		620/2		0	
Rochester [57]	Exp.		628/3.5		0	
$A^2\Pi$						
This work[(a)]	MRCI+Q				4.634	0.997
Harrison	RCCSD(T)	3.320	659	2.59 (D_0)	4.63 (T_0)	1.50
Boldyrev[(c)]	QCISD(T)	8.520	13		2.928	0.015
Moravec	Exp.				>2.69 (T_v)	
Flory	Exp.				2.53 (T_v)	
$B^2\Sigma^+$						
This work[(a)]	MRCI+Q	4.901	327.7/2.7	2.875	4.101	0.607
$C^2\Pi$						
This work[(a)]	MRCI+Q	3.516	935.3/17.2	2.129	4.876	1.066
Rochester	Exp.		599		4.586(Ω=1/2) 4.632(Ω=3/2)	
$D^2\Sigma^+$						
This work[(a)]	MRCI+Q	3.325	705.1/12.0	0.310	6.694	1.299

States	Method	R_e [bohr]	$\omega_e/\omega_e x_e$ [cm^{-1}]	D_e [eV]	T_e [eV]	μ_e [a.u.]
			ZnF^-			
$X^1\Sigma^+$						
This work$^{(a)}$	MRCI+Q	3.638	413.3/4.4	1.531	-1.829	
Harrison	RCCSD(T)	3.615	425	1.60 (D_0)	-1.929 (T_0)	
Moravec	Exp.	+0.283$^{(f)}$	420		-1.974	

(a): Absolute energy value calculated at the minimum of the $X^2\Sigma^+$ ground state:-250.63266307 a.u.. For the $A^2\Pi$ state, T_e is the vertical excitation energy at the equilibrium geometry of the $X^2\Sigma^+$ ground state. The dipole moments are calculated at the MRCI level, at the equilibrium geometry of each bound state and at the equilibrium geometry of the ground state for the repulsive state.
(b): Taken from ref. [62], calculated by the density functional approach using the zero order regular approximated (ZORA) method.
(c): Taken from ref. [63], calculated T_e value at the QCISD(T)/6-311++G(2d,2f) level, using the equilibrium geometry optimized at the QCISD/6-311++G(d,f) level.
(d): Taken from ref. [61], calculated by the local density functional method with atomic-centered STO basis sets.
(e): Taken from ref. [60], calculated at the MP2 level, with the quasi-relativistic 20 valence electron pseudopotentials for Zn. They used the segmented (8s7p6d)/[6s5p3d] valence basis sets, associated with the pseudopotentials for Zn, and the segmented (5s5p1d)/[3s3p1d] valence basis sets for F.
(f): Shift from R_e for the $X^2\Sigma^+$ state of ZnF.

(ii) Studies on the low lying states of ZnCl

All results of the previous studies mentioned below are presented in Table 16.

All of the early experimental studies done until 1975 were summarized by Huber and Herzberg [12]. Walter and Barratt reported the absorption spectra of ZnCl with ten heads between 290 and 300 nm [67]. A little later, Cornell recorded the vibrationally resolved emission spectra in the wavelength region from 207.4 to 298 nm [68]. Their spectrum around 295 nm was assigned to the $C^2\Pi$ - $X^2\Sigma^+$ transition, determining the spectroscopic constants $\omega_e/\omega_e x_e$ for the $X^2\Sigma^+$ and $C^2\Pi$ states and T_e for the $C^2\Pi$ excited state. Herzberg assigned subsequently the spectrum around 207.4 nm obtained by Cornell to the $E^2\Sigma^+$ - $X^2\Sigma^+$ transition, deriving the values $\omega_e/\omega_e x_e$ = 345.4/5.0 cm^{-1} and T_e = 5.974 eV for the $E^2\Sigma^+$ state. Givan and Lowenschuss measured the fundamental vibrational frequency of 385 cm^{-1} for the $X^2\Sigma^+$ ground state, using matrix-isolation Raman spectroscopy [69]. The dissociation energy D_0 of the ground state was reported to be 2.37 ± 0.08 eV by Hildenbrand *et al.* [70], monitoring the gaseous isomolecular reaction Zn + $ZnCl_2$ = 2ZnCl by magnetic deflect ion mass spectrometer system. More recently the rotational spectrum of the ground state was recorded by Tenenbaum *et al.*, from which they obtained the following constants: the equilibrium distance R_e = 4.025 bohr, $\omega_e/\omega_e x_e$ =

392.1/1.7 cm^{-1} for the most abundant isotopologue $^{64}Zn^{35}Cl$, and $D_0 = 2.73$ eV [56]. Concerning the other excited states, Herzberg and Huber listed in their summary the $B^2\Sigma^+$ state lying at 3.387 eV above the ground state with the values $\omega_e/\omega_e x_e = 185.0/0.5$ cm^{-1}. Sureshkumar *et al.* reported the $A^2\Pi$ state which lies at about 2.23 eV above the ground state [71].

Table 16: Spectroscopic constants and dipole moments of the low lying states of ZnCl.

States	Method	R_e [bohr]	$\omega_e/\omega_e x_e$ [cm^{-1}]	D_e [eV]	T_e [eV]	μ_e [a.u.]
ZnCl						
$X^2\Sigma^+$						
This work[(a)]	MRCI+Q	4.043	395.2/0.1		0	1.043
Kerkines [7]	RCCSD(T)	4.010		2.146		1.106
Boldyrev[(b)]	QCISD(T)	4.074	386	2.027	0	1.095
Bowmaker [59]	SDCISC	4.099		1.805		
Tenenbaum [56]	Exp.	4.025	392.1/1.7 ($^{64}Zn^{35}Cl$)	2.73 (D_0)		
Cornell [68]	Exp.		390.5/1.5		0	
Givan[(c)]	Exp.		385			
Hildenbrand [70]	Exp.			2.37(D_0)		
$A^2\Pi$						
This work[(a)]	MRCI+Q				4.155	-0.629
Boldyrev[(b)]	QCISD(T)	8.853	14		2.019	0.031
Sureshkumar [71]	Exp.				about 2.23	
$B^2\Sigma^+$						
This work[(a)]	MRCI+Q	5.917	186.5/0.3		3.479	1.390
Herzberg [12]	Exp.		185.0/0.5		3.387	
$C^2\Pi$						
This work[(a)]	MRCI+Q	4.087	662.8/47.9		4.392	0.708
Cornell	Exp.		384.0/1.1		4.165(Ω=1/2)	
			381.8/1.0		4.213(Ω=3/2)	
$D^2\Sigma^+$						
This work[(a)]	MRCI+Q				6.623	2.855
$E^2\Sigma^+$						
Cornell	Exp.		345.4/5.0		5.974	
$3^2\Pi$						
This work[(a)]	MRCI+Q	3.837	520.5/12.8		7.319	4.919

(a): Absolute energy value calculated at the minimum of the $X^2\Sigma^+$ ground state:-241.41013660 a.u.. For the repulsive states, T_e is the vertical excitation energy at the equilibrium geometry of the $X^2\Sigma^+$ ground state. The dipole moments are calculated at the MRCI level, at the equilibrium geometry of each bound state and at the equilibrium geometry of the ground state for the repulsive states. The most abundant isopotologue $^{64}Zn^{35}Cl$ is used to deduce $\omega_e/\omega_e x_e$.
(b): Taken from ref. [63], calculated T_e value at the QCISD(T)/6-311++G(2d,2f) level, using

the equilibrium geometry optimized at the QCISD/6-311++G(d,f) level.
(c): Value of the fundamental vibrational frequency.

Only three theoretical studies have been carried out in the last decade. Bowmaker and Schwerdtfeger [59] studied the ground state of ZnCl at the CISDSC level, using the pseudopotentials for Zn with the associated basis set contracted as (9s8p7d)/[7s6p4d]. They obtained spectroscopic constants as $R_e = 4.099$ bohr and $D_e = 1.805$ eV. The second theoretical work was performed by Boldyrev and Simons at the QCISD level using the 6-331++G(d,f) basis set, obtaining the following values for the $X^2\Sigma^+$ ground state: $R_e = 4.074$ bohr, $\omega_e = 386$ cm^{-1}, $D_e = 2.027$ eV, and the dipole moment $\mu_e = 1.095$ a.u. at the equilibrium geometry [63]. They reported also the van der Waals $A^2\Pi$ state correlated with the first dissociation asymptote with the spectroscopic constants as follows: $R_e = 8.853$ bohr, $\omega_e = 14$ cm^{-1}, $T_e = 2.019$ eV, and $\mu_e = 0.031$ a.u.. More recently, Kerkines *et al.* reported the values $R_e = 4.010$ bohr, $D_e = 2.146$ eV, and $\mu_e = 1.106$ a.u. for the ground state at the RCCSD(T) level [7]. They took the one-electron relativistic effects into account, using the second-order Douglas-Kroll-Hess (DKH) approximation.

6.3.3 Nature of the low lying electronic states

In order to identify the electronic states which play a role in the molecular region, we have first examined the situation close to the lowest dissociation limits. As shown in Table 17, the lowest covalent dissociation asymptotes of ZnF and ZnCl are determined only by the excited states of the zinc atom, because their excitation energies are smaller than the value of 12.701 and 8.979 eV for the ^4P_g - ^2P_u fine structure averaged excitation energy of F and Cl, respectively.

The lowest dissociation asymptote comes from a combination of the ^1S_g ground state of Zn and the ^2P_u ground state of F/Cl, correlating with the $^2\Sigma^+$ and $^2\Pi$ molecular states. The second asymptote corresponds to a combination of the first excited ^3P_u state of Zn and the ^2P_u ground state of F/Cl. This second asymptote correlates with two $^{2,4}\Sigma^+$, one $^{2,4}\Sigma^-$, two $^{2,4}\Pi$ and one $^{2,4}\Delta$, thus a total of 12 molecular states. The energy separation between the first and the second asymptotes equals to 4.038 eV, averaged excitation energy of the experimental fine structure levels ($J = 0, 1, 2$) of the ^3P_u state of Zn [8]. The excited ^1P_u state of Zn and the ^2P_u ground state of F/Cl lead to the third homolytic dissociation asymptote lying 5.796 eV above the first one. The lowest asymptotes involving the first excited state ^4P_g of F and Cl lie at 12.701 and 8.979 eV, respectively (averaged over the fine structure levels for the ^2P_u and ^4P_g states) above the first asymptote of this series and will not be considered.

The atomic energy levels of Cl are lower than these of F, thus other covalent asymptotes should be discussed and the resulting molecular states should be included in calculations to obtain an accurate description of the ZnCl system, taking into account the interactions between them. The combinations of the Cl(^2P_u) ground state with the ^3S_g, ^1S_g, and ^3P_u excited states of Zn result in the three following asymptotes, lying at 6.654, 6.917, and 7.598 eV above the first dissociation asymptote respectively. These three asymptotes correlate with totally 10 doublet

and 8 quartet molecular states.

The first ionic asymptotes of ZnF and ZnCl correspond to the combinations of $Zn^+(^2S_g)$ and $[F/Cl]^-(^1S_g)$ fragments. According to the experimental ionization energy of Zn (9.394 eV) [8] and the electronic affinity of F/Cl (3.398/3.616 eV) [4], the first ionic asymptotes are found to be the fourth asymptote of ZnF and to be the third one of ZnCl, lying at 5.994 and 5.778 eV respectively above the first covalent asymptote. With these ionic asymptotes is correlated only a $^2\Sigma^+$ state which can interact with the lower states of the same symmetry. The distance R_c (or zone) of crossing between the low lying covalent states and this ionic state can be roughly estimated by considering a variation as $-1/R$ for the potential energy of the ionic $Zn^+[F/Cl]^-$ form and a quasi constant energy for the covalent states. According to the position of the asymptotes and considering the simple equation $\Delta E = -1/R_c$, where ΔE represents the energy difference in atomic units between the asymptote of the covalent state and that of the ionic state, we deduce $\Delta E = -0.220$ a.u. (-5.994 eV) and $R_c = 4.545$ bohr for ZnF and -0.212 a.u. (-5.788 eV) and 4.717 bohr for ZnCl, for the crossing of the ionic state with the lowest $^2\Sigma^+$ state correlated with the first asymptote. These regions should be treated with particular attention.

The lowest covalent and ionic dissociation asymptotes of the diatomic ZnF and ZnCl and the low lying electronic states adiabatically correlated with these dissociation asymptotes are presented in Table 17. The calculations performed in the present study are concerned with all the electronic states correlated with the two lowest asymptotes for ZnF and with the six lowest covalent and one ionic asymptotes for ZnCl.

Table 17: Lowest covalent and ionic dissociation asymptotes of the diatomic ZnF and ZnCl with the resulting low lying electronic states.

Dissociation asymptotes	Energies$^{(a)}$ [eV]	Molecular states
$Zn(^1S_g) + F/Cl(^2P_u)$	0	$^2\Sigma^+$, $^2\Pi$
$Zn(^3P_u) + F/Cl(^2P_u)$	4.038	$^{2,4}\Sigma^+(2)$, $^{2,4}\Sigma^-$, $^{2,4}\Pi(2)$, $^{2,4}\Delta$
$Zn^+(^2S_g) + Cl^-(^1S_g)$	5.788	$^2\Sigma^+$
$Zn(^1P_u) + F/Cl(^2P_u)$	5.796	$^2\Sigma^+(2)$, $^2\Sigma^-$, $^2\Pi(2)$, $^2\Delta$
$Zn^+(^2S_g) + F^-(^1S_g)$	5.994	$^2\Sigma^+$
$Zn(^3S_g) + Cl(^2P_u)$	6.654	$^{2,4}\Sigma^+$, $^{2,4}\Pi$
$Zn(^1S_g) + Cl(^2P_u)$	6.917	$^2\Sigma^+$, $^2\Pi$
$Zn(^3P_u) + Cl(^2P_u)$	7.598	$^{2,4}\Sigma^+(2)$, $^{2,4}\Sigma^-$, $^{2,4}\Pi(2)$, $^{2,4}\Delta$
$Zn(^1S_g) + F/Cl(^4P_g)$	12.701/8.979	$^4\Sigma^-$, $^4\Pi$

(a) Experimental atomic energy averaged over the fine structure levels, taken from ref [8].

6.3.4 Computational details

(i) Pseudopotentials and Basis sets

The core electrons of the Zn, F, and Cl atoms have been described by atomic pseudopotentials which allow relativistic effects to be taken into account. For Zn, we employed the most recent energy-consistent ECP10MDF effective core potentials [24], with 10 electrons represented by a pseudopotential and the 20 outer electrons explicitly treated via the associated aug-cc-pVQZ basis sets contracted as (14s11p11d3f2g1h)/[6s6p5d3f2g1h] [25]. The energy-consistent ECP2MWB and ECP10MWB effective core potentials are used, respectively for F and Cl, with 2 and 10 core electrons represented by a pseudopotential [72]. The outer 7 electrons of F and Cl are explicit in the calculations, using the associated (4s5p)/[2s3p] basis sets [72] augmented with the 4d, 3f, and 2g primitives taken from the Dunning *et al.* correlation consistent aug-cc-pVQZ basis sets [26,65]. Such ansatz allows to treat both diatomic systems in a very similar way.

(ii) Molecular structure calculations

The wavefunctions of the 27 valence electrons of ZnF are determined by state-averaged Multi-Configuration Self-Consistent-Field (MCSCF) calculations [27, 28] with 18 active molecular orbitals constructed on the 3s, 3p, 3d, 4s, and 4p of Zn, and 2s, 2p, and 3s of F. For the case of ZnCl, the MCSCF calculations for 27 valence electrons have been performed with 21 active molecular orbitals constructed on the 3-5s, 3-5p, and 3d of Zn and 3s and 3p of Cl. Among these 18 or 21 orbitals, the 10 inner shells, including the 3d orbitals of Zn and the 2s orbital of F or 3s of Cl are optimized but not correlated in this step. The effective active space consists thus in the (5-8)σ and (3-4)π orbitals for ZnF and in the (5-9)σ and (3-5)π orbitals for ZnCl. The MCSCF wavefunctions are taken as reference for the subsequent internally contracted Multi-Reference-Configuration-Interaction (MRCI) calculations [29, 30]. The Davidson correction [31, 32], which approximates the contribution of higher excitation terms, has been introduced in the last step of the calculation (MRCI+Q). All electronic structure calculations are performed in the C_{2v} symmetry group, using the MOLPRO program package [33].

6.3.5 Electronic structure of ZnF

(i) Potential energy curves

Starting with the state-averaged MCSCF calculations including all the states correlated with the two lowest dissociation asymptotes, the subsequent MRCI calculations are performed separately in each space and spin symmetries. The energy difference between the two lowest asymptotes is calculated to be 3.958 eV, in good agreement with the experimental value of 4.038 eV (see Table 17). Figures 33 and 35 present the potential energy curves of the doublet and quartet states of ZnF obtained from calculations at the MRCI level including the Davidson correction. Figure 33 shows that the electronic ground state of ZnF is the $X^2\Sigma^+$ state with the equilibrium geometry calculated close to R = 3.3 bohr. This state is correlated with the first asymptote and presents an interaction with a higher $^2\Sigma^+$ state in the region close to 5 bohr, which is the crossing region

with the first ionic state, as discussed in the previous section. Our RCCSD(T) calculation for the $X^2\Sigma^+$ ground state, using the same pseudopotentials and basis sets, is shown in Figure 34, thus it should be noted that the RCCSD(T) method can not describe accurately this interaction and is adapted only in the vicinity of the equilibrium distance of the ground state. Both the $B^2\Sigma^+$ and the $D^2\Sigma^+$ states are correlated with the second asymptote : the $B^2\Sigma^+$ state presents a deep minimum around R = 5.0 bohr, resulting from the interaction with the $X^2\Sigma^+$ state, the $D^2\Sigma^+$ state has a shallow minimum around R = 3.3 bohr.

In Figure 33 one can see that the $A^2\Pi$ and $C^2\Pi$ states, correlated with the first and second asymptotes respectively, form an avoided crossing around R = 3.5 bohr. The $A^2\Pi$ state is not bound but has a shoulder in the region of the avoided crossing. The minimum of the potential energy of the $C^2\Pi$ state is located at the avoided crossing with the $A^2\Pi$ state. This situation has not been discussed by Harrison *et al.* [64], who found only one excited $^2\Pi$ state correlated with the second asymptote with an equilibrium geometry close to the local minimum of the $A^2\Pi$ state using the RCCSD(T) method. As demonstrated in Figure 34, this *ab initio* method could not be adapted for the electronic calculations of these excited crossing states.

All the other doublet and all the quartet states correlated with the second asymptote are found to be repulsive, as shown in Figures 33 and 35.

Figure 33: Potential energy curves of the doublet states of ZnF at the MRCI+Q level of theory.

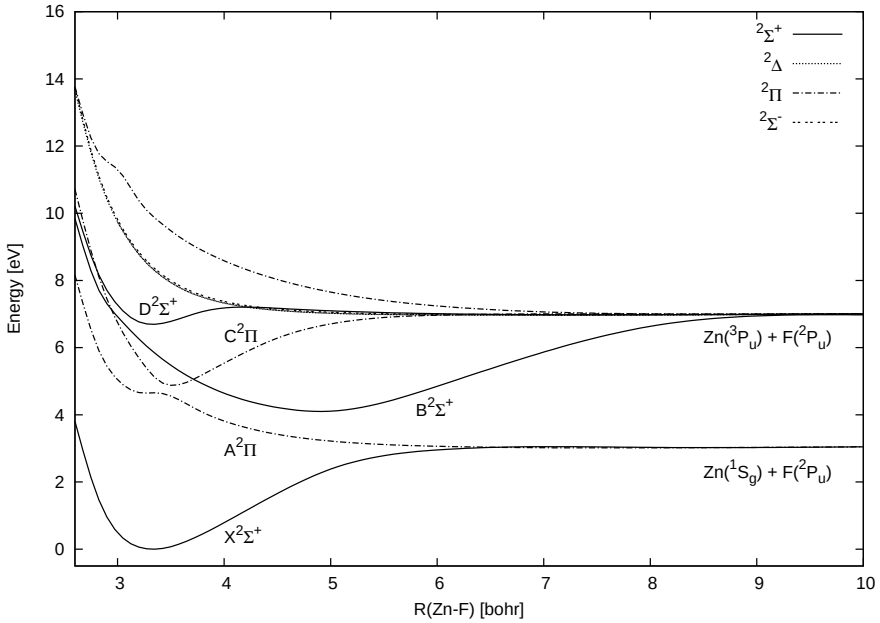

(ii) Electronic wavefunctions

In this section, we discuss the electronic wavefunctions of the low lying states of ZnF, based on the state-averaged MCSCF calculations. The (1-4)σ, 1δ, and (1-2)π molecular orbitals are almost identical to atomic orbitals and are fully occupied in all the examined configurations. The external (5-8)σ and (3-4)π orbitals are roughly constructed as follows : the 5σ orbital is a bonding combination of the 4s of Zn and the 2p$_z$ of F, while the 6σ orbital corresponds to the antibonding combination of the same atomic orbitals. The 5σ has a dominant contribution from the 2p$_z$ of F; in contrast, the 4s of Zn contributes mainly to the 6σ, as already mentioned in previous studies [55,62], even though the small contribution from other atomic orbitals is found here slightly different as a result of our state-averaged procedure. The 7σ orbital is more diffuse and almost identical to the 4p$_z$ of Zn with a small contribution from the 3s of F. The 8σ orbital is equivalent to the 3s of F. The 3π and 4π orbitals are identical to the 2p$_x$,2p$_y$ of F and to the 4p$_x$,4p$_y$ of Zn respectively.

In Table 18, we give the dominant configurations and their coefficients in the low lying electronic states at the MCSCF level of theory. For the bound states, we refer to the equilibrium geometry of the state, and for the repulsive states the data are given at the equilibrium geometry of the $X^2\Sigma^+$ ground state. At long distance, the dominant configuration of the $X^2\Sigma^+$ ground state is $(1\sigma^2 2\sigma^2 3\sigma^2 4\sigma^2 1\delta^4 1\pi^4 2\pi^4)5\sigma^1 6\sigma^2 3\pi^4$ corresponding to a covalent ZnF situation. For interatomic distances between 2.6 and 4.0 bohr the dominant configuration of the $X^2\Sigma^+$ ground state is $(....)5\sigma^2 6\sigma^1 3\pi^4$, corresponding to a charge transfer from Zn to F and that of the $B^2\Sigma^+$ state becomes $(....)5\sigma^1 6\sigma^2 3\pi^4$ as a result of the avoided crossing occurring close to

Figure 34: Potential energy curves of the lowest $^2\Sigma^+$ and $^2\Pi$ states of ZnF at the RCCSD(T) level of theory. The potential curves of the $X^2\Sigma^+$, $A^2\Pi$, and $C^2\Pi$ states from the MRCI+Q calculations are also presented for comparison.

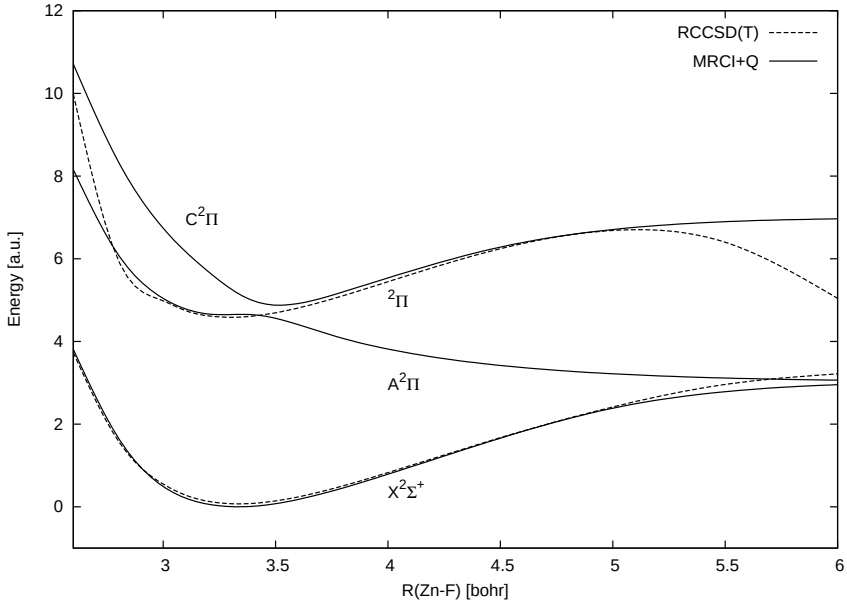

Figure 35: Potential energy curves of the quartet states of ZnF at the MRCI+Q level of theory.

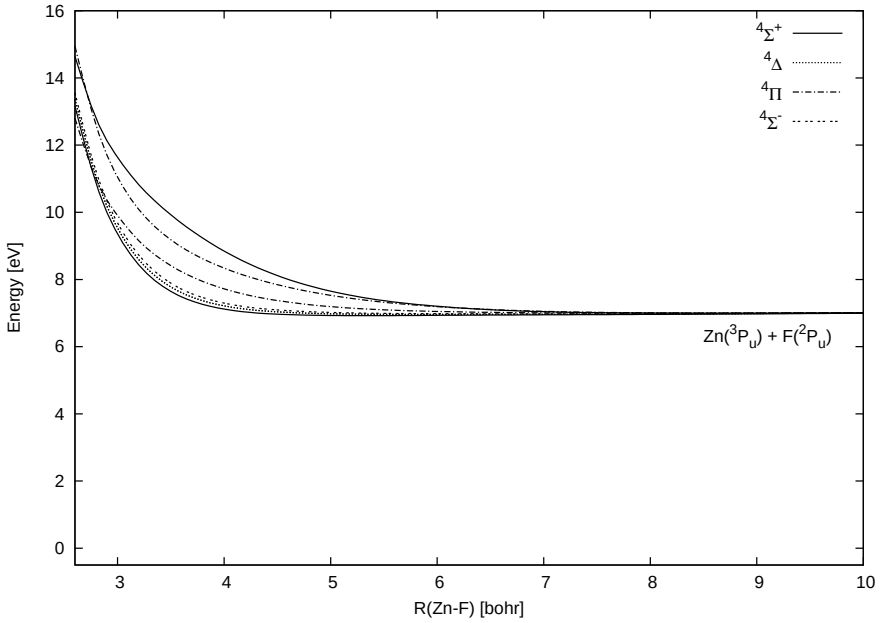

R = 5.0 bohr. At larger distance the dominant configuration of the $B^2\Sigma^+$ state is again the ionic one $(....)5\sigma^2 6\sigma^1 3\pi^4$ with a coefficient of 0.543 at R= 5.0 bohr and of 0.605 at R = 6.0 bohr. At its equilibrium geometry the $D^2\Sigma^+$ state has the leading configuration $(....)5\sigma^2 7\sigma^1 3\pi^4$, which stays dominant until R = 4.0 bohr. This configuration is associated with a charge transfer from Zn to F. For interatomic distances shorter than 3.0 bohr the $D^2\Sigma^+$ state takes the leading configuration $(....)5\sigma^1 6\sigma^2 3\pi^4$ from the $B^2\Sigma^+$ state as a result of an avoided crossing occurring close to $R = 3.0$ bohr.

At long distances, the main configuration contributing to the $A^2\Pi$ state is $(....)5\sigma^2 6\sigma^2 3\pi^3$, while the $C^2\Pi$ state is dominated by $(....)5\sigma^2 3\pi^4 4\pi^1$. These configurations correspond qualitatively to $Zn(3d^{10}4s^2)$ + $F(2s^2 2p^5)$ for the $A^2\Pi$ state and $Zn^+(3d^{10}4p^1)$ + $F^-(2s^2 2p^6)$ for the $C^2\Pi$ state. Because of an avoided crossing between these states near 3.5 bohr, as seen in Figure 33, the dominant configurations of these two states are interchanged at distances below 3.4 bohr.

The main configuration of the $X^1\Sigma^+$ state of the ZnF^- molecular anion is $(....)5\sigma^2 6\sigma^2 3\pi^4$ at its equilibrium geometry. In the photoelectron spectroscopy experiments performed by Moravec *et al.* [58] the accessible states of the ZnF species are preferentially those which correspond to the elimination of one electron from this configuration. The preceding analysis shows that the $X^2\Sigma^+$, the $A^2\Pi$ and the $B^2\Sigma^+$ should be accessible in photoelectron spectroscopy experiments, provided that the photons posses a sufficient energy to reach these states. Unfortunately, the photon energy employed in the experiments of Moravec *et al.* [58] was only sufficient to reach the $X^2\Sigma^+$ state.

Table 18: Dominant configurations of the low lying electronic states of ZnF at the MCSCF level of theory.

States	Configurations[(a)]	Coefficients
$X^2\Sigma^+$	$(....)5\sigma^2 6\sigma^1 3\pi^4$	0.909
$A^2\Pi$	$(....)5\sigma^2 6\sigma^2 3\pi^3$	0.908
$B^2\Sigma^+$	$(....)5\sigma^1 6\sigma^2 3\pi^4$	0.731
$C^2\Pi$	$(....)5\sigma^2 3\pi^4 4\pi^1$	0.857
$D^2\Sigma^+$	$(....)5\sigma^2 7\sigma^1 3\pi^4$	0.782

(a): The molecular orbitals in parentheses are fully occupied and correspond to:
$1\sigma^2 2\sigma^2 3\sigma^2 4\sigma^2 1\delta^4 1\pi^4 2\pi^4$.

(iii) Dipole moment functions

Figures 36 and 37 show the dipole moments of the $^2\Sigma^+$ and $^2\Pi$ states, respectively, as a function of the interatomic distance R. Table 15 presents the dipole moments at the equilibrium geometries of the bound states and at the equilibrium geometry of the $X^2\Sigma^+$ ground state for the repulsive states. These dipole moments are calculated as an expectation value at the MRCI

level separately in each space and spin symmetries. The sign convention is defined such as the positive value corresponds to the Zn^+F^- polarity. The dipole moments are used here to discuss the polarity of the states and the interactions between them. The transition dipole functions calculated as an expectation value, in the next section, will be used to discuss the intensity of the electronic transitions between the bound doublet states.

Based on an averaged slope of the dipole moment function of the $X^2\Sigma^+$ ground state in the bonding region, between 3 and 4 bohr, one can estimate the charge separation to be $0.56e$, corresponding to a partially ionic bond $Zn^{\delta+}F^{\delta-}$. This result confirms the conclusion of Flory *et al.* [55], from their analysis of the electron density at the Zn and F nuclei, that the ground state is partially ionic and confirms also the previous calculations of Harrison *et al.* [64] who found, at the RCCSD(T) level, a partial charge of $+0.72e$ and $-0.72e$ for Zn and F respectively. For an interatomic distance R close to 4.5 bohr the dipole moment of this state presents the maximum and then decreases to zero for interatomic distances longer than 6.0 bohr, corresponding to the covalent dissociation limit.

The dipole moment of the $B^2\Sigma^+$ state is almost equal to zero at interatomic distances larger than 10.0 bohr, corresponding to the covalent structure: the $B^2\Sigma^+$ has an ionic structure of Zn^+F^- type between 10.0 and 6.0 bohr, with the maximum of the dipole moment function around R = 6.0 bohr. At this distance the $B^2\Sigma^+$ starts to interact with the $X^2\Sigma^+$ ground state and the ionic character is transferred to the ground state in the region of the avoided crossing which spreads over 1.5 bohr, as shown in Figure 36. The polarity of the $X^2\Sigma^+$ and the $B^2\Sigma^+$ states results from the charge transfer appearing in the configuration $(....)5\sigma^2 6\sigma^1 3\pi^4$.

For $R > 6.0$ bohr, the $D^2\Sigma^+$ state is covalent according to the quasi zero value of the dipole moment. In the bonding region, the dipole moment of this state is positive, corresponding to a $Zn^{\delta+}F^{\delta-}$ polarity.

The sharp avoided crossing between the $A^2\Pi$ and $C^2\Pi$ states that is seen in Figure 37 near 3.4 bohr leads to a drastic change in the dipole moment of the two states, as the electronic character of the state changes dramatically near this interatomic distance. At interatomic distances longer than 3.6 bohr, the dipole moment of the $C^2\Pi$ state is positive with the maximum value around $R = 3.8$ bohr due to an ionic structure of $Zn^{\delta+}F^{\delta-}$ type, in agreement with the charge transfer associated to the configuration $(....)5\sigma^2 3\pi^4 4\pi^1$. The third $^2\Pi$ state is covalent at large interatomic distances ($R > 7$ bohr) and presents a dipole moment function which is close to zero. In the region between 3 and 7 bohr, this state has an ionic structure of Zn^-F^+ type, according to the negative value of the dipole moment.

(iv) Spectroscopic constants for the four lowest bound states

The potential energy curves calculated at the MRCI+Q level have been used to derive the spectroscopic constants of the electronic states of ZnF via the NUMEROV algorithm [34]. The calculated data on ZnF are presented in Table 15 together with the spectroscopic constants

Figure 36: Dipole moment functions of the $^2\Sigma^+$ states of ZnF at the MRCI level of theory.

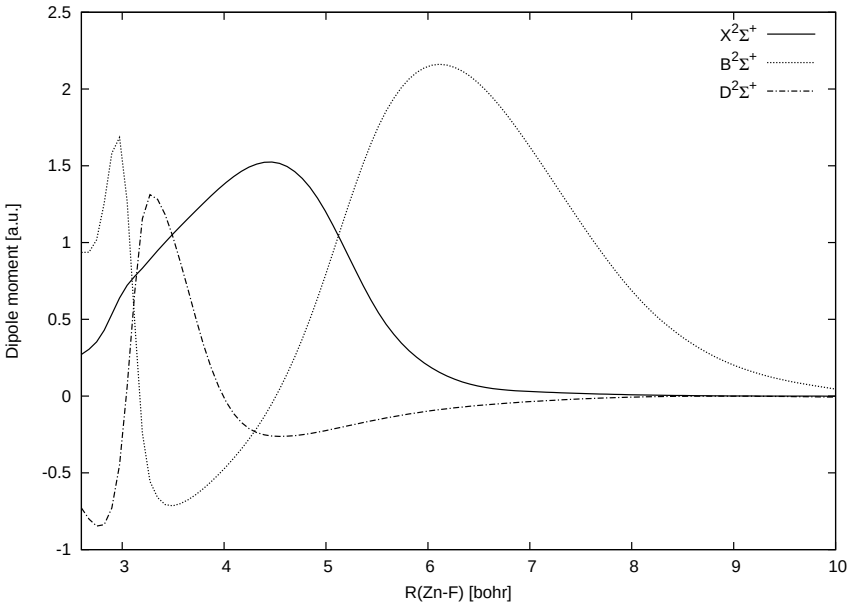

Figure 37: Dipole moment functions of the $^2\Pi$ states of ZnF at the MRCI level of theory.

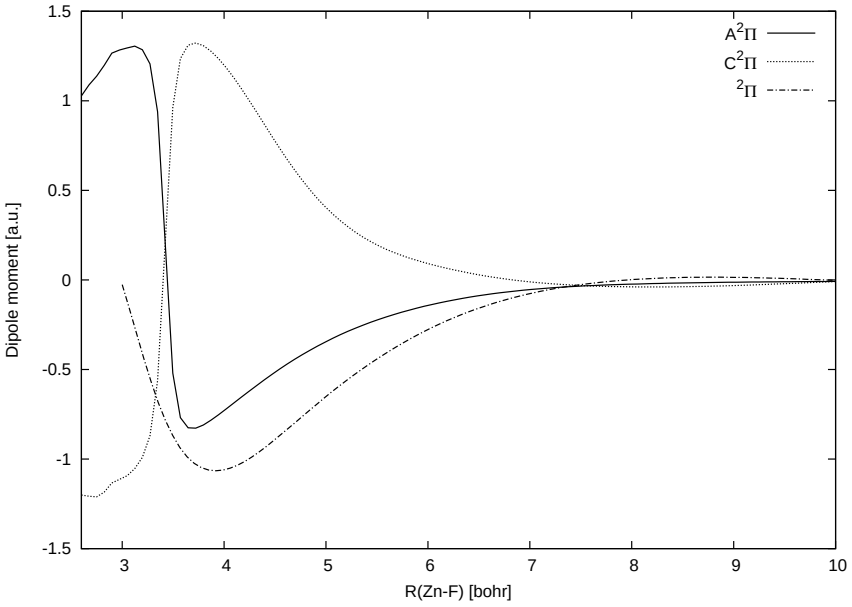

of the $X^1\Sigma^+$ of the ZnF^- molecular anion. The equilibrium bond distance R_e of the ground state $X^2\Sigma^+$ is determined to be 3.337 bohr, quite close to the most recent experimental value R_e = 3.341 bohr by Flory *et al.* [55] and to the theoretical value R_e = 3.354 bohr by Harrison *et al.* [64] calculated at the RCCSD(T) level of theory. For the harmonic vibrational (ω_e) and anharmonic vibrational wavenumbers ($\omega_e x_e$) of the ground state for the main isotopologue $^{64}Zn^{19}F$, we obtain 638.6 cm^{-1} and 3.2 cm^{-1} respectively. Our harmonic vibrational wavenumber is slightly larger (6-8 cm^{-1}) than the previous values [55,64]. We report also in Table 15 the wavenumbers (ω_e and $\omega_e x_e$) of the $X^2\Sigma^+$ state for the other isotopologues $^{66}Zn^{19}F$ and $^{68}Zn^{19}F$. The dissociation energy D_e of the $X^2\Sigma^+$ ground state obtained with our MRCI+Q potential is equal to 3.030 eV, smaller by about 0.1 eV than the values determined by Harrison *et al.* (D_0 = 3.16 eV) and by Flory *et al.* (D_e = 3.123 eV), but higher by about 0.1 eV than the value of 2.931 eV calculated by Boldyrev and Simons [63]. For the $B^2\Sigma^+$ and $D^2\Sigma^+$ states, there is no known data to compare with and we believe that the accuracy on these quantities is of the same quality as for the $X^2\Sigma^+$ state.

The spectroscopic constants of the first excited $^2\Pi$ states (A and C) have also been given in Table 15. At the QCISD(T) level, Boldyrevand Simons [63] predicted a van der Waals $A^2\Pi$ state with a minimum at 8.520 bohr. However, we have found this state purely dissociative for the large ZnF bond lengths. The $C^2\Pi$ state lies at 4.876 eV (T_e) above the ground state with $\omega_e/\omega_e x_e$ = 935.3/17.2 cm^{-1}. These numbers can hardly be compared to the calculated values of Harrison *et al.* [64] (R_e = 3.320 bohr, ω_e = 659 cm^{-1}, D_0 = 2.59 eV and T_0 = 4.63 eV) since they found only one $^2\Pi$ state instead of two. Also, the simple spin-orbit perturbation model of Flory *et al.* [55] that predicted the $A^2\Pi$ state at 2.53 eV above the $X^2\Sigma^+$ state was related to the presence of an isolated first excited $^2\Pi$ state and cannot be valid. However, the only experimental work which has probed the 4.6 eV region is the study of Rochester and Olsson [57] that confirms a complicated situation since they found predissociated levels between 36000 and 39000 cm^{-1} (region of the avoided crossing between both $^2\Pi$ states). The assignments of the experimental UV bands stay problematic. From photoelectron spectroscopy experiments, Moravec *et al.* affirm that there is no absorbing electronic state below 2.69 eV above the $X^2\Sigma^+$ state.

The spectroscopic constants related to the electronic ground state $X^1\Sigma^+$ of ZnF^- are also presented in Table 15 and are compared with the experimental data of Moravec *et al.* [58] and with the calculated data of Harrison *et al.* [64]. The electronic affinity is calculated at 1.829 eV and equals to 1.843 eV with the zero energy point correction which compares well with the experimental value of 1.974 eV of Moravec *et al.* [58] and of 1.929 eV of Harrison *et al.* [64]. These authors found that the equilibrium bond length of the ionic state must be shifted by +0.283 bohr from the R_e of the neutral $X^2\Sigma^+$ state. Our calculated shift is 0.301 bohr. The agreement for the harmonic wavenumbers is within 7 cm^{-1}. If we use the experimental data in Table 15 and the experimental electronic affinity of F (3.398 eV) [4], we can estimate an experimental value of 1.660 eV for D_0 and of 1.686 eV for D_e which is close to the calculated D_e of 1.531 eV.

(v) Vibronic transitions between the $X^2\Sigma^+$ state and the lowest bound states

Figure 38: $B^2\Sigma^+(v) \leftarrow X^2\Sigma^+(v')$ absorption spectra for the three most abundant isotopologues of ZnF.

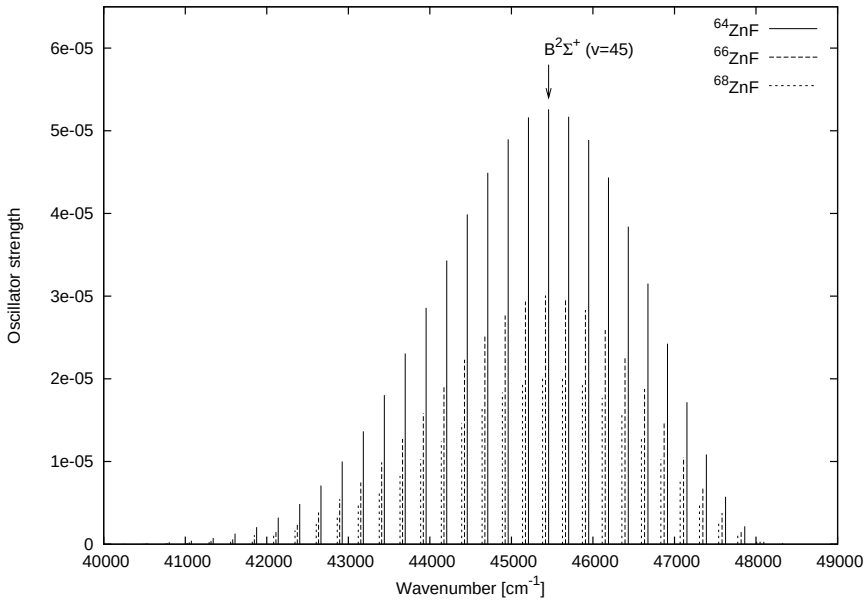

Vibronic transitions can occur between the $X^2\Sigma^+$ and the excited $^2\Sigma^+$ and $^2\Pi$ bound states and the intensity of the lines depends on the magnitude of the transition dipole moments between the two states of interest. At the equilibrium geometry of the $X^2\Sigma^+$ ground state, these values are calculated to be 0.1506 a.u., 1.2931 a.u., and 0.9540 a.u. for the $B^2\Sigma^+$ state, the $C^2\Pi$ state, and the $D^2\Sigma^+$ state, respectively, at the MRCI level of theory. Consequently the transitions to the $C^2\Pi$ and $D^2\Sigma^+$ states are expected to be more intense than to the $B^2\Sigma^+$ state. In the case of the most abundant isotopologue ^{64}ZnF, due to the energy difference $T_0 = 32920$ cm^{-1} (4.082 eV) for the $B^2\Sigma^+$ state and $T_0 = 39471$ cm^{-1} (4.894 eV) for the $C^2\Pi$ state, these transitions can be observed in the UV domain.

The vibrationally resolved absorption spectra to the $B^2\Sigma^+$ and $C^2\Pi$ states, for the three most abundant isotopologues ^{64}ZnF, ^{66}ZnF, and ^{68}ZnF, have been simulated, using the NUMEROV algorithm [34] at $T = 0$ K and they are presented in Figure 38 for the B-X transition and in Figure 39 for the C-X one. One can see the long progression in the B-X spectrum, due to a large difference of the equilibrium distances of both states, in contrast, the transition to the C state is almost vertical and only a few vibrational levels of the $C^2\Pi$ excited electronic state are reached. We assume that the C-X bands associated with transition energies larger than 39000 cm^{-1} could be only slightly disturbed by the avoided crossing between the $A^2\Pi$ and $C^2\Pi$ states lying approximately at 36500 cm^{-1} from the equilibrium of the $X^2\Sigma^+$ state. Only the $D^2\Sigma^+(v = 0)$ level is populated by the X-D absorption with an oscillator strength of 0.193115 and a transition energy of 54022 cm^{-1} for ^{64}ZnF.

Figure 39: $C^2\Pi(v) \leftarrow X^2\Sigma^+(v')$ absorption spectra for the three most abundant isotopologues of ZnF.

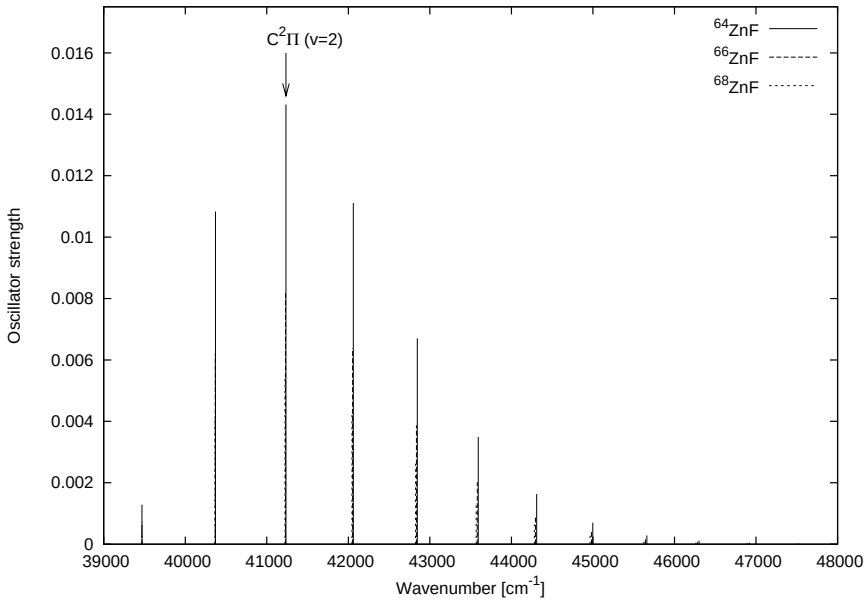

6.3.6 Electronic structure of ZnCl

Potential energy curves calculated at the MRCI level including the Davidson correction are shown in Figures 40 and 41, respectively for the doublet and quartet states which are correlated adiabatically with the two lowest asymptotes. Figure 42 presents the dipole moments at the MRCI level, of the the $^2\Pi$ states. The MRCI calculations have been performed, separately in each space and spin symmetries, taking as reference the MCSCF wavefunctions with the coefficients larger than 0.01 to reduce the size of calculations. At the MCSCF level, calculations have been performed for the molecular states correlated with the seven lowest asymptotes, separately in each space and spin symmetries. This procedure which has not been applied to the case of ZnF, is necessary to obtain the accurate descriptions of the low lying states of ZnCl, due to the dissociation asymptotes of ZnCl lower than those of ZnF. Because the underlying RHF calculations have not been converged, we have to discard the calculations at the MCSCF and the MRCI levels at distances longer than 6.5 bohr. Using the NUMEROV algorithm [34], the calculated spectroscopic constants are listed in Table 16 for the doublet states of interest.

Observing the potential curves of the low lying states, we can find their behaviors similar to those of ZnF. From Figure 40, the $^2\Sigma^+$ state correlated adiabatically with the lowest asymptote is the ground state and the lower A, B, and C states have the same trends of appearances as in the case of ZnF, while the higher excited states $D^2\Sigma^+$ and third $^2\Pi$ show the following differences: the former has the bound structure around the equilibrium distance of the ground state in ZnF and is repulsive with a small shoulder in ZnCl. In contrast, the latter is repulsive in ZnF and has the bound structure with the equilibrium distance of 3.837 bohr in ZnCl. This

fact may be due to the difference of the molecular states included in the MCSCF calculations. Our obtained spectroscopic data of the $X^2\Sigma^+$ and the $B^2\Sigma^+$ show excellent agreement with the previous values. The $E^2\Sigma^+$ state was reported by Cornell [68] with the values $\omega_e/\omega_e x_e = 345.4/5.0$ cm^{-1} and $T_e = 5.974$ eV. In contrast, the higher excited $D^2\Sigma^+$ state is found to be repulsive in our results.

Compared with the previous studies, the most obvious difference appears in the descriptions of the $A^2\Pi$ and $C^2\Pi$ states. An avoided crossing occurs between these states at the interatomic distance around 4 bohr, where their dipole moments interchange drastically behaviors shown in Figure 42. As in the case of ZnF, this avoided crossing determines the minimum of the $C^2\Pi$ state correlated adiabatically with the second dissociation asymptote, while the $A^2\Pi$ state is correlated with the first one. Compared with the previous experimental values measured by Cornell [68], our obtained harmonic and anharmonic wavenumbers of the $C^2\Pi$ state show obviously large differences, in contrast, the energy difference relative to the ground state is in reasonable agreement. About the $C^2\Pi$ state, there is no other comparative data. Boldyrev and Simons [63] reported, from their QCISD(T) calculations, that the $A^2\Pi$ state is a van der Waals state correlated with the lowest asymptote owning the following constants: $R_e = 8.835$ bohr, $\omega_e = 14$ cm^{-1}, and $T_e = 2.019$ eV. Sureshkumar *et al.* [71] recorded the vibrationally resolved emission spectra at the wavelengths from 510 to 655 nm. They assigned their spectra to the $A^2\Pi$ - $X^2\Sigma^+$ transition and revealed the energy difference of about 2.23 eV between these two states. However our calculations at the MRCI+Q level show that the $A^2\Pi$ state is globally repulsive and lies much higher than 2.23 eV in the molecular region. We can comment that the accurate descriptions of both the $A^2\Pi$ and the $C^2\Pi$ states in the vicinity of their avoided crossing remain yet difficult.

6.3.7 Conclusions

The potential energy curves and the dipole moment functions of the low lying electronic states of ZnF and ZnCl and of the electronic ground state of ZnF^- are calculated at the MRCI+Q level of theory. As presented in Figure 33 and 35, only four low lying electronic states of ZnF are bound: the $X^2\Sigma^+$, $B^2\Sigma^+$, $C^2\Pi$ and $D^2\Sigma^+$ states. The spectroscopic constants of these bound states are obtained, many of them for the first time and vibronic transitions from the electronic ground state $X^2\Sigma^+$ towards these three excited states can be observed in the UV domain. All the low lying quartet states are found to be repulsive. For the low lying states of ZnCl, we have obtained the similar results to those of ZnF. The potential energy of the ZnF^- molecular anion has been determined in the vicinity of its equilibrium geometry and the electronic affinity of ZnF has been calculated in agreement with the photoelectron spectroscopy experiments. Compared with the previous theoretical study using the RCCSD(T) method, we conclude that it is necessary to treat these molecules by the multi-configurational method, in order to take into account the interactions between the states. In both cases of ZnF and ZnCl, our results of the $A^2\Pi$ and $C^2\Pi$ states show discrepancies from the previous works. For the disagreement of the $C^2\Pi$ state, it should be discussed in term of the rovibronic levels, including the spin-orbit interactions between $A^2\Pi$ and $C^2\Pi$ states. About the difference of the description of the $A^2\Pi$ state between our study

Figure 40: Potential energy curves of the doublet states of ZnCl at the MRCI+Q level of theory.

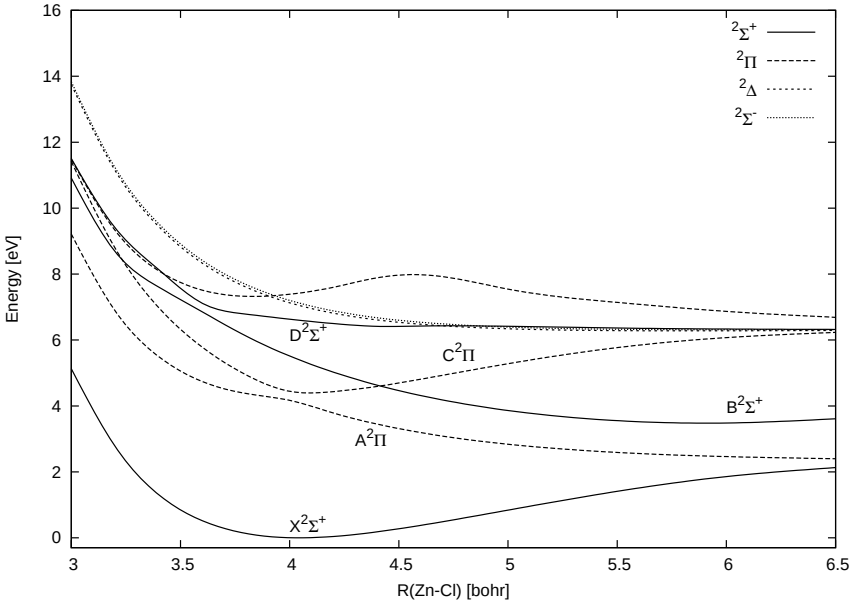

Figure 41: Potential energy curves of the quartet states of ZnCl at the MRCI+Q level of theory.

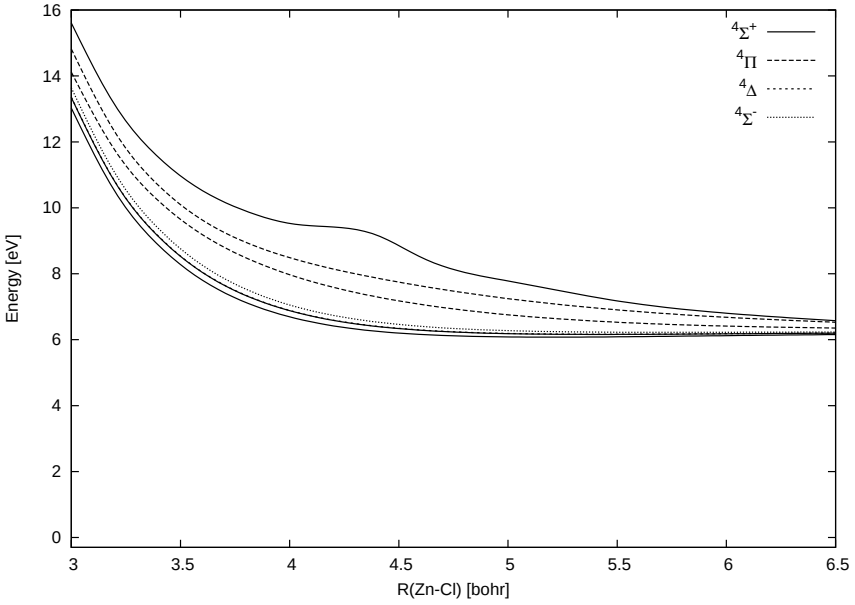

Figure 42: Dipole moment functions of the $^2\Pi$ states of ZnCl at the MRCI level of theory.

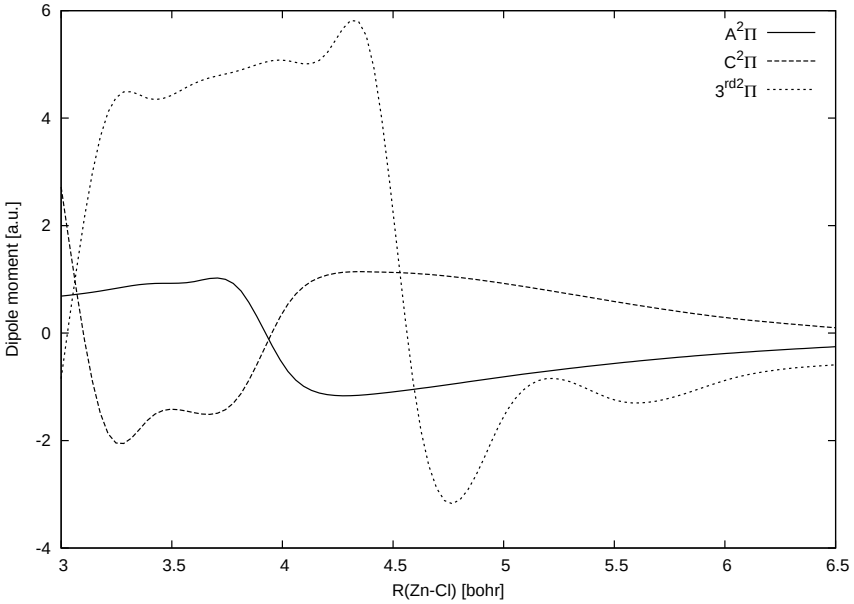

and the previous ones, we note that the method employed by Boldyrev and Simons [63] tends to predict a van der Waals state for the low lying states of the zinc diatomic compounds.

6.4 Study of the ground state of HZnF

6.4.1 Introduction

From the information on the structures of the ZnH and ZnF diatomic fragments, we can turn towards the HZnF triatomic molecule, focusing on its ground state. This study is motivated by previous experimental and theoretical work on the zinc hydrochloride HZnCl, revealing the electronic structure and spectroscopic data of the $^1\Sigma^+$ ground state.

Recently, Macrae *et al.* [5] prepared HZnCl, HCdCl, and HHgCl in Ar cold matrixes and recorded their infrared spectra, from which it turned out that these molecules are linear in their ground state. They observed three normal modes of vibration at 1952.3 cm^{-1} for the Zn-H stretching mode ν_1, at 449.6 cm^{-1} for the bending mode ν_2, and at about 420 cm^{-1} for the Zn-Cl stretching mode ν_3, with assignments pointed out by isotopic substitution and density functional theory (DFT) calculations.

On the other hand, Yu *et al.* [6] have recorded the vibration-rotation emission spectrum for the four most abundant isotopomers in gaz phase. They have observed a very dense emission infrared spectrum around 1966 cm^{-1}, corresponding to the Zn-H stretching mode (ν_1). This density of the spectrum was due to the small value of the rotational constant 2B (circa 0.3 cm^{-1}) and various natural isotopomers of HZnCl. The complex spectrum was fitted using the simple energy level expression (6.1) where the bending mode ν_2 and the Zn-Cl stretching mode ν_3 and the J assignments were made with the help of DFT(B3LYP) calculations. They have obtained the (1, 0, 0) energies of the four most abundant isotopomers (1966.87 cm^{-1} for $H^{64}Zn^{35}Cl$) and the (2, 0, 0) energies of $H^{64}Zn^{35}Cl$.

$$E = G(v_1, v_2, v_3) + B(v_1, v_2, v_3)J(J+1) - D(v_1, v_2, v_3)[J(J+1)]^2 \qquad (6.1)$$

The determination of the bond lengths between H and Zn (R_{HZn}) and between Zn and F (R_{ZnCl}) was rather controversial, especially for the former one. Using the moment of inertia equation applied to the six pairwise combinations of isotopomers, they have calculated the value of R_{HZn} ranging from 3.016 to 3.381 bohr, in contrast the obtained value for R_{ZnCl} ranges more consistently from 3.929 to 3.946 bohr. With the help of the Kraitchman's equation for linear molecule [73], they have obtained the value of 3.937 bohr for R_{ZnCl}. Substituting this value (3.937 bohr) into the moment of inertia equation and into the center of mass equation, the value of 3.221 and 3.322 bohr are derived respectively for the bond length of R_{ZnH} of the main isotopomer $H^{64}Zn^{35}Cl$.

To determine the equilibrium structure and the spectroscopic constant, Kerkines *et al.* [7] have performed the calculations for the ground state at the RCCSD(T) level, as well as for the ones of ZnH and ZnCl. Their calculations involved 20 valence electrons (Zn:$3d^{10}4s^2$, Cl:$3s^23p^5$, and H:$1s^1$) using the correlation consistent polarized cc-pV(T,Q,5)Z basis sets for H, Cl, and Zn. The effects of the $3s^23p^6$ and $2s^22p^6$ electron cores of Zn and Cl, respectively, were included using the weighted core cc-pwCVTZ basis sets. They have estimated one-electron relativistic effects within the second-order DKH approximation and the associated cc-pV(T,Q,5)Z-DKH

basis sets. After the elimination of basis set superposition errors (BSSE) with the counterpoise technique, finally, the CBS limit approach was applied using the following formula:

$$P_n = P_\infty + Ae^{-(n-1)} + Be^{-(n-1)^2} \qquad (6.2)$$

Within this approach, they have reported the equilibrium geometries of $R_{HZn} = 2.833$ and $R_{ZnCl} = 3.929$ bohr, with the contribution of the relativistic effect reducing the bond lengths by 0.025-0.032 bohr and that of the core electrons contracting quite slightly by 0.002-0.008 bohr. The harmonic wavenumbers ω_1 (H-Zn stretching mode), ω_2 (bending mode), and ω_3 (Zn-Cl stretching mode) were reported, based on the calculations at the RCCSD(T)/cc-pVTZ level. Their results for the most abundant isotopomer $H^{64}Zn^{35}Cl$ (ω_1 = 2008.2, ω_2 = 421.2, and ω_3 = 431.7 cm^{-1}) are successfully in good agreement with these values obtained from the previous experimental studies.

Motivated by these previous works, we will try to study the ground state of the zinc hydrofluoride HZnF, replacing F by Cl. There is no experimental and theoretical studies about this compound up to the present. Thus we have examined the descriptions of ZnF and ZnH and obtained the more information about them in the last chapters and we have listed the previous works in detail for comparison between HZnF and HZnCl. To complete this comparison, we have performed the calculations of the low lying states of ZnCl, using the same ansatz as for ZnH and ZnF.

6.4.2 Dissociation asymptotes

In order to clarify the electronic states in the molecular region, we start with the situation close to the lowest dissociation limits to both HZn + F and H + ZnF in linear geometry. The low lying dissociation asymptotes in linear geometry and the molecular states correlated with them are listed in Table 11.

(i) Dissociation asymptote into HZn and F

The lowest dissociation asymptote into HZn + F in linear geometry corresponds to a combination between the $^2\Sigma^+$ ground state of HZn and the ^2P_u ground state of F, leading to one $^{1,3}\Sigma^+$ and one $^{1,3}\Pi$ molecular states. In the next, one $^{1,3}\Sigma^+$, one $^{1,3}\Sigma^-$, one $^{1,3}\Pi$, and one $^{1,3}\Delta$ molecular states are correlated with the asymptote HZn($A^2\Pi$) excited state and F(^2P_u) ground state. This second one lies at 2.888 eV (from our calculations) above the lowest one. The third asymptote HZn($B^2\Sigma^+$) + F(^2P_u), lying at 3.470 eV above the first one, correlates with one $^{1,3}\Sigma^+$ and one $^{1,3}\Pi$ states. The dissociation asymptote due to the ^4P_g first excited state of F lies 12.701 eV above the first one and is not taken into account in this study [8]. As revealed in the previous chapter, the $^1\Sigma^+$ ground state of ZnH^+ lies at 7.494 eV above the ground state of ZnH and the experimental electronic affinity of F [4] is 3.398 eV. Thus the first ionic dissociation asymptote lies at 4.096 eV above the lowest covalent one, correlating with one $^1\Sigma^+$ molecular state.

(ii) Dissociation asymptote into H and ZnF

The lowest dissociation asymptote into H and ZnF in linear geometry comes from the ground states $^2\Sigma^+$ and ^2S_g, correlating with one $^{1,3}\Sigma^+$ state. Since the hydrogen has the ^2S_g ground state, the resulting HZnF has the same representation in $C_{\infty v}$ symmetry group as the parent ZnF with the singlet or triplet spin multiplicities. Thus, the other lowest asymptotes (from the second to the seventh) correspond to a combination of the ground state of H with two $^2\Sigma^+$, three $^2\Pi$, one $^2\Delta$, and one $^2\Sigma^-$ states of ZnF and correlate with two $^{1,3}\Sigma^+$, three $^{1,3}\Pi$, one $^{1,3}\Delta$, and one $^{1,3}\Sigma^-$ molecular states. Using the T_e values for the bound states and the T_v values for the repulsive states of ZnF, from our calculations, we list energy differences of these asymptote related to the lowest one in Table 11. To include in the calculations the same number of the molecular states of HZnF in both paths of dissociation, we should include in the calculations one more $^1\Sigma^+$ molecular state correlated adiabatically with the asymptote resulting from the ground state of H and a $^2\Sigma^+$ state of ZnF, which results from the Zn(^1P_u) and F(^2P_u) states.

6.4.3 Computational details

Keeping the same ansatz as the calculations of the diatomic molecules, the 10 core electrons of Zn and the 2 core electrons of F were represented respectively by the ECP10MDF [24] and the ECP2MWB [72] pseudopotentials. The 20 outer electrons of Zn were explicitly treated via the associated aug-cc-pVQZ basis sets contracted as (14s14p11d3f2g1h)/[6s6p5d3f2g1h] [25] and the 7 outer electrons of F using the associated (4s5p)/[2s3p] basis sets [72] augmented with the 4d, 3f, and 2g primitives taken from the Dunning *et al.* correlation consistent aug-cc-pVQZ basis sets [26, 65]. For the hydrogen atom, the Dunning *et al.* correlation consistent aug-cc-pVQZ basis sets was employed [26].

The electronic structure calculations for the four $^1\Sigma^+$, three $^1\Pi$, one $^1\Delta$, and one $^1\Sigma^-$ molecular states have been performed at the MCSCF level with 28 valence electrons [27, 28]. The 19 active molecular orbitals were constructed on the 3s, 3p, 3d, 4s, and 4p of Zn, 2s, 2p, and 3s of F, and 1s of H. Among these 19 orbitals, the 10 inner shells including the 3d orbital of Zn and the 2s orbital of F were optimized but not correlated. The effective active space consists thus in the (5-9)σ and (3-4)π orbitals in C_{2v} symmetry group. Taking the MCSCF wavefunction as reference, the subsequent internally contracted MRCI calculations [29, 30] have been performed for only the ground state, including the Davidson correction [31, 32]. All electronic structure calculations have been realized in C_{2v} or C_s symmetry groups using the MOLPRO program package [33].

6.4.4 Results

According to the potential curves and the dipole moments of the low lying states of both ZnH and ZnF, these states show the interactions among them. Specially, around the equilibrium distances of the ground state of both ZnH and ZnF, we find the obvious avoided crossing. Even though we focus this study on the ground state of HZnF, it is necessary to include many excited

states in the calculation at the MCSCF level, for taking into account such interactions which may affect the description of the HZnF ground state.

(i) Ground and low lying excited states at the MCSCF level

We discuss first qualitatively the electronic structures of the ground and low lying excited states, based on the MCSCF calculations. The potential curves in linear geometry with variation of the distance R_{ZnF} between Zn and F are presented in Figure 43, in which the distance R_{HZn} between Zn and H is fixed at the calculated equilibrium distance 2.997 bohr of the ZnH($X^2\Sigma^+$) state. Figure 44 shows the potential curves in linear geometry in function of R_{HZn} with R_{ZnF} fixed at the calculated equilibrium geometry of 3.337 bohr for the ZnF($X^2\Sigma^+$). The calculations have been performed in C_{2v} symmetry group.

From both Figures 43 and 44, clearly HZnF has the $^1\Sigma^+$ ground state, with the equilibrium bond length of 3.344 bohr for R_{ZnF} and of 2.942 bohr for R_{HZn}. In both linear cuts, the ground state is quite separated in energy from the low lying excited states. The bond energy for the F + ZnH dissociation is larger than that for the other dissociation. The principle configuration of the ground state in the vicinity of the equilibrium bond lengths is found to be $(1\sigma)^2(2\sigma)^2(3\sigma)^2(4\sigma)^2(1\pi)^4(1\delta)^4(2\pi)^4(5\sigma)^2(6\sigma)^2$, with increase of energy. Figure 43 shows the remaining characters of ZnF in the HZnF compound. For example, the second $^1\Sigma^+$ state has the wide minimum around $R_{ZnF} = 5.0$ bohr quite similar to the minimum structure of the $B^2\Sigma^+$ states of ZnF. The avoided crossing between the $A^2\Pi$ and the $C^2\Pi$ states in ZnF appears in HZnF, as found the avoided crossing between the first and second $^1\Pi$ states. In contrast, the effects of addition of F into ZnH are less clear in Figure 44. The wide minimum of the second $^1\Sigma^+$ state of HZnF may be due to the $B^2\Sigma^+$ state of ZnH. The dissociation asymptotes into H + ZnF lie qualitatively well, compared to the energetical order of the lowest states in ZnF at the interatomic distance of 3.337 bohr.

The variation of the potential curves in function of the bending angle θ from 180 to 240° are depicted in Figure 45 for the low lying states of HZnF, calculated at the MCSCF level in C_s symmetry group. The distance between Zn and H is fixed at $R_{ZnH} = 2.942$ bohr and the other at $R_{ZnF} = 3.344$ bohr. Again the ground state $^1\Sigma^+$ is found to be linear and isolated in energy in the region of these bending angles. The higher excited states have the minimum in linear geometry, contrary, the potential energies of the lower excited states decrease with increase of the bending angle. This behavior is likely to arise from the avoided crossings between two $^1A'$ states occurring at 200 and 230° and that between two ^1A" states around 200°.

Figure 43: Potential energy curves (in function of R_{ZnF}) of the ground and low lying excited states of HZnF at the MCSCF level of theory, in linear geometry.

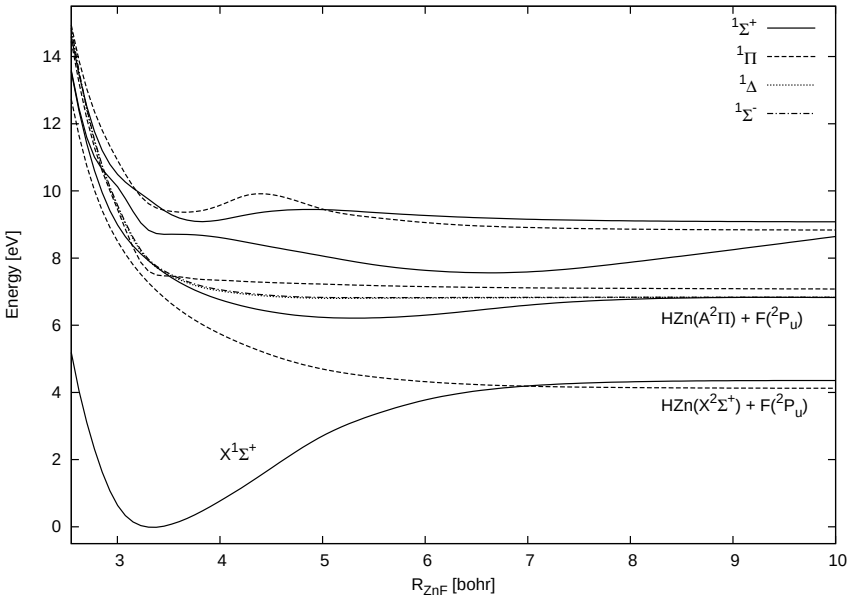

Figure 44: Potential energy curves (in function of R_{ZnH}) of the ground and low lying excited states of HZnF at the MCSCF level of theory, in linear geometry.

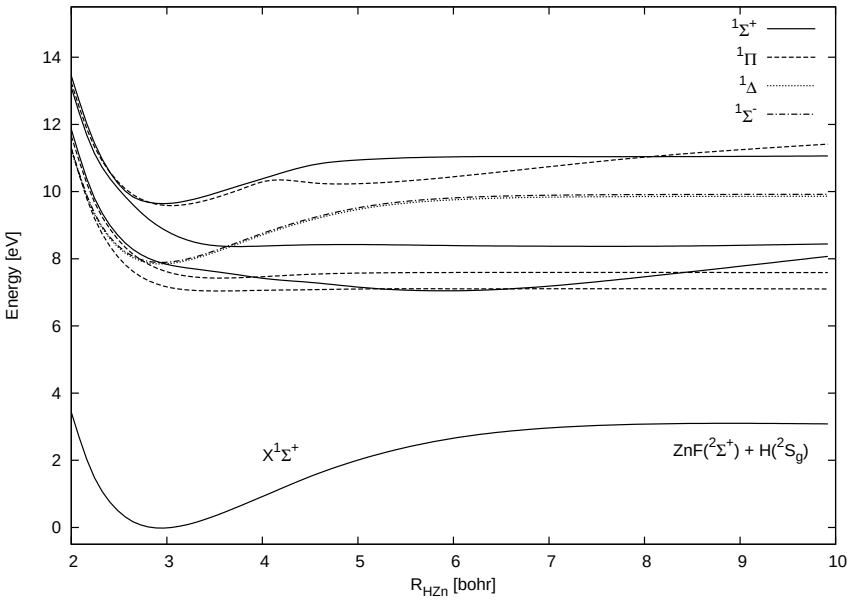

Figure 45: Potential energy curves (in function of the bending angle θ) of the ground and low lying excited states of HZnF at the MCSCF level of theory.

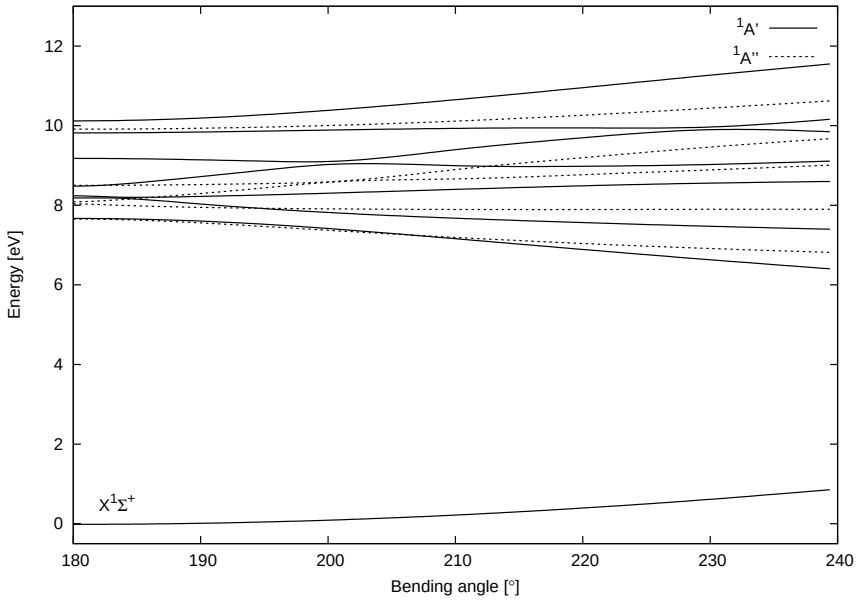

(ii) Potential energy surface of the ground state

The determination of the potential energy surface (PES) of the $^1\Sigma^+$ ground state of HZnF has been performed from the calculations at the MRCI level including the Davidson correction for only the ground state, taking the preceding MCSCF wavefunction as reference. The calculations have been carried out in C_s symmetry group at 31 points (19 linear and 12 non linear), with variations of R_{ZnH}, R_{ZnF}, and the bending angle θ, corresponding to the energy increases less than about 10000 cm^{-1} from the equilibrium energy. These variables included in the PES range from 2.31 to 3.56 bohr, from 2.89 to 3.89 bohr, and from 180 to 220°, respectively for R_{ZnH}, R_{ZnF}, and θ.

The resulting energy values were fitted by the following polynomial expansion up to the fourth order of the displacements of these three internal coordinates, using the SURFIT program [74].

$$V(\Delta R_{ZnH}, \Delta R_{ZnF}, \Delta\theta) = \sum_{i,j,k} (\Delta R_{ZnH})^i (\Delta R_{ZnF})^j (\Delta\theta)^k \qquad (6.3)$$

$$\Delta R_{ZnH} = R_{ZnH} - R^{eq}_{ZnH}$$

$$\Delta R_{ZnF} = R_{ZnF} - R^{eq}_{ZnF}$$

$$\Delta\theta = \theta - \pi$$

where $0 \leq i, j, k \leq 4$ and $0 \leq i + j + k \leq 4$. k should take even values to observe the symmetry of the bending coordinate. The equilibrium geometry where the first derivatives of the PES

are equal to zero was taken as reference. 22 expansion coefficients C_{ijk} optimized by a least square-fitting with the root mean square of 1.37 cm^{-1} are listed in Table 19 with the reference geometry R^{eq}_{ZnH} and R^{eq}_{ZnF}.

At this equilibrium geometry, the dipole moment is calculated at the MRCI level, using the center of mass of the molecule as the coordinate origin. Compared our results with the previous data on the HZnCl and on the concerned diatomic compounds presented in Table 20, the contraction of the bonding lengths in equilibrium geometry appears quite similar between HZnF and HZnCl. R_{ZnF} of the ground state (3.269 bohr) is shorter by 2% than that of the $X^2\Sigma^+$ state (3.337 bohr) in ZnF and this contraction ratio is same between HZnCl and ZnCl in the study of Kerkines et al. [7]. About comparison of contraction of the H-Zn bond length between HZnF and HZnCl, our calculated R_{ZnH} has 93.4% of the equilibrium distance of ZnH and the ratio of 94.4% is found for HZnCl from the calculations by Kerkines et al. [7].

Using the SURFIT code, we have calculated, from the PES derivatives at the minimum, the harmonic wavenumbers of three normal modes ω_1, ω_2, and ω_3 for all natural isotopomers of HZnF and they are listed in Table 21 with the ones of the main HZnCl isotopomers reported in the previous works. Decomposition of the stretching Q_1 and Q_3 normal modes into the displacements of internal coordinates ΔR_{ZnH} and ΔR_{ZnF} are shown in Table 22 and it appears that the Q_1 and Q_3 normal modes are almost localized respectively on the stretching of the ZnH and ZnF bonds. The harmonic wavenumber ω_1 of the ZnH stretching mode has almost similar value between HZnF and HZnCl. With substitution of the various isotopes of Zn, ω_3 is more affected from 696.28 for $H^{64}ZnF$ to 689.63 cm^{-1} for $H^{70}ZnF$, while ω_1 and ω_2 are almost constant. The similar trend was found for the isotopic replacement of Zn in the study of HZnCl reported by Kerkines *et al.* [7].

Table 19: Polynomial expansion coefficients C_{ijk} (a.u.) of the PES of the ground state $^1\Sigma^+$, with its equilibrium geometries and the equilibrium dipole moment calculated at the MRCI level.

Coefficients		Coefficients	
C_{000}	-251.26947415	C_{102}	-0.01285483
C_{100}	0.00000000	C_{012}	-0.01764748
C_{010}	0.00000000	C_{400}	0.03220686
C_{200}	0.08187298	C_{310}	0.00074914
C_{110}	-0.00403714	C_{220}	0.00204196
C_{020}	0.13505205	C_{130}	0.00065378
C_{002}	0.03209212	C_{040}	0.08045024
C_{300}	-0.06947624	C_{202}	0.00620243
C_{210}	-0.00032669	C_{112}	0.01017617
C_{120}	0.00050788	C_{022}	0.01280744
C_{030}	-0.14281362	C_{004}	-0.00240091
R^{eq}_{ZnH}	2.802 (bohr)	R^{eq}_{ZnF}	3.269 (bohr)
μ_e	0.775 (a.u.)		

(a): Taken from ref [7].
(b): Taken from ref [6].
(c): Taken from ref [55].
(d): Taken from ref [56].
(e): Taken from ref [11].

Table 20: Comparison of the structure constants of the ground states of HZnF($^1\Sigma^+$), HZnCl($^1\Sigma^+$), ZnF($^2\Sigma^+$), ZnCl($^2\Sigma^+$), and ZnH($^2\Sigma^+$).

Quantities	This study	Kerkines[a]	Yu[b]	Flory[c]	Tenenbaum[d]	Shayesteh[e]
Method	MRCI+Q	RCCSD(T)	Exp.	Exp.	Exp.	Exp.
ZnH:R_e(bohr)	2.999	3.001				3.010
ZnH:μ_e(a.u.)	0.016	0.232				
ZnF:R_e(bohr)	3.337			3.341		
ZnCl:R_e(bohr)	4.043	4.010			4.025	
ZnF:μ_e(a.u.)	0.939					
ZnCl:μ_e(a.u.)	1.043	1.106				
R^{eq}_{ZnH} (bohr)	2.802	2.833	3.016 to 3.381			
R^{eq}_{ZnF} (bohr)	3.269					
R^{eq}_{ZnCl} (bohr)		3.929	3.938			
μ_e (a.u.)	0.775	0.700				

(a): Taken from ref [7]. Calculated at the RCCSD(T)/cc-pVTZ level of theory.
(b): Taken from ref [6]. Vibration-rotation emission spectrum of gaseous HZnCl.
(c): Taken from ref [5]. Matrix-isolated infrared spectrum.

(iii) Rovibrational levels of the ground state

For the linear triatomic molecule, there is no rigid rotation around the molecular axes (fixed to the z axis). Thus the projection of the total angular moment on the z axis $\hat{J}_z$ has a contribution only from the z component of the vibrational angular moment, whose quantum number l can be related to the quantum number of the bending vibrational mode v_2 as follows; $l = \pm v_2$, $\pm(v_2-2)$, ..., ± 2, 0 (for even value of v_2) or $\pm v_2$, $\pm(v_2-2)$, ..., ± 1 (for odd value of v_2). In the case of the $^1\Sigma^+$ ground state of HZnF, according to the zero quantum numbers of the projection of the electronic and spin angular momenta, the rovibrational levels are characterized by the quantum number K = $|l|$ = 0, 1, 2, and 3.

Using the RVIB3 program [75] with the previously fitted PES, the vibrational levels of the ground state $^1\Sigma^+$ have been computed up to 3000 cm^{-1} for the main isotopomer H^{64}ZnF. The 13 harmonic oscillator wavefunctions for the each stretching mode and the 70 associated Legendre polynomials for the bending mode were involved in the contraction scheme. The primitive set of integration points comprised 14 and 94 points for the stretching and the bending modes, respectively. These rovibrational levels are shown in Table 23. The fundamental frequencies are given as ν_1 = 2000.847 cm^{-1} (for J, K = 0), ν_2 = 474.471 cm^{-1} (for J, K = 1) and ν_3 = 684.828 cm^{-1} (for J, K = 0). Compared with the ν_1 values of HZnCl obtained from the previous experiments [5,6], this value is slightly smaller by about 40 cm^{-1}. From the split of 3.895 cm^{-1} between the J = 0 and J =1 in the zero vibrational level, the rotational constant 2B$_0$ of 3.895 cm^{-1} is much larger than that of HZnCl (about 0.3 cm^{-1}). Compared with the perturbatively

Table 21: Harmonic wavenumbers ω_1, ω_2, and ω_3 for all natural isotopomers of HZnF and the main isotopomers of HZnCl.

	Method	Isotopomers	ω_1 cm^{-1}	ω_2 cm^{-1}	ω_3 cm^{-1}
HZnF					
This work	MRCI+Q	$H^{64}ZnF$	2089.80	484.14	696.28
		$H^{66}ZnF$	2089.25	483.77	693.94
		$H^{67}ZnF$	2088.99	483.60	692.82
		$H^{68}ZnF$	2088.74	483.43	691.73
		$H^{70}ZnF$	2088.26	483.10	689.63
HZnCl					
Kerkines[a]	RCCSD(T)	$H^{64}Zn^{35}Cl$	2008.2	421.2	431.7
		$H^{66}Zn^{35}Cl$	2007.7	420.9	429.4
		$H^{68}Zn^{35}Cl$	2007.2	420.6	427.3
Yu[b]	Exp.	$H^{64}Zn^{35}Cl$	2036.8		
Macrae[c]	Exp.	$H^{64}Zn^{35}Cl$	2023.1	458.8	424.7
		$H^{66}Zn^{35}Cl$			422.6
		$H^{68}Zn^{35}Cl$			420.5

Table 22: Decomposion of the stretching normal modes Q_1 and Q_3 into the displacements of internal coordinates ΔR_{ZnH} and ΔR_{ZnF} for the most abundant isotopomer $H^{64}ZnF$.

Normal modes	ΔR_{ZnH}	Δ_{ZnF}
Q_1	0.9984	-0.0564
Q_3	0.0193	0.9998

calculated anharmonic constants $\chi_{11} = 46.10$ cm^{-1}, $\chi_{22} = 1.00$ cm^{-1}, and $\chi_{33} = 11.61$ cm^{-1}, Table 23 shows consistently the largest anharmonicity in the ZnH stretching mode than the others. However, from the experiment reported by Yu *al.* [6], the anharmonicity in the ZnH stretching mode of HZnCl appears much smaller than that of HZnF.

Table 23: Rovibrational levels (cm^{-1}) of the ground state $^1\Sigma^+$ for the main isotopomer $H^{64}ZnF$.

(v_1,v_2,v_3)	J=0,K=0	J=1,K=0	J=1,K=1	J=2,K=0	J=2,K=1	J=2,K=2
(0,0,0)	$0^{(a)}$	3.895		11.684		
(0,1,0)			474.471		482.257	
(0,0,1)	684.828	688.722		696.507		
(0,2,0)	938.595	942.488		950.271		946.879
(0,1,1)			1157.842		1165.625	
(0,0,2)	1360.813	1364.704		1372.486		
(0,3,0)			1404.570		1412.352	
(0,2,1)	1620.495	1624.386		1632.167		1628.807
(0,1,2)			1832.453		1840.232	
(0,4,0)	1860.239	1864.130		1871.911		1868.501
(1,0,0)	2000.847	2004.639		2012.221		
(0,0,3)	2029.508	2033.415		2041.228		
(0,3,1)			2084.996		2092.775	
(0,2,2)	2293.747	2297.637		2305.414		2302.082
(0,5,0)			2317.775		2325.557	
(1,1,0)			2465.523		2473.103	
(0,1,3)			2502.368		2510.216	
(0,4,1)	2539.160	2543.050		2550.829		2547.453
(1,0,1)	2686.406	2690.236		2697.894		
(0,0,4)	2690.370	2694.270		2702.071		
(0,3,2)			2756.966		2764.744	
(0,6,0)	2765.042	2768.934		2776.717		2773.286
(1,2,0)	2920.120	2923.909		2931.487		2928.249
(0,2,3)	2966.583	2970.525		2978.409		2974.853
(0,5,1)			2995.200			3002.979

(a):The zero rovibrational level at 1853.397 cm^{-1}.

6.4.5 Conclusions

In this chapter we have presented the study of HZnF, focusing on its ground state. Taking in account the interactions between the molecular states of ZnH and ZnF, we have carefully included, in the MCSCF calculations, the low lying states of HZnF owning the interactions between them. Taking the MRCI wavefunctions as referece, we have detremined, from the MRCI+Q calculations, the potential energy surface of the $^1\Sigma^+$ ground state, from which we have estimated the various spectroscopic constants. Then these data have been compared with the previous values of HZnCl. If the vibration-rotation spectrum of HZnF in gaz phase is measured, we estimate that it will become less complex than that of HZnCl, due to the larger rotational constant B.

References

[1] M. Hatano, S. Suzuki, and K. Ishihara, *J. Am. Chem. Soc.*, **128**, 9998 (2006).

[2] M. P. Cuajungco and K. Y. Faget, *Brain Res. Rev.*, **41**, 44 (2003).

[3] H. Sigel, *Metal Ions in Biological Systems, Vol. 15, Zinc and Its Role in Biology and Nutrition*, Marcel Dekker, New York, 1983.

[4] J. Emsley, *The Elements, Second Edition*, Oxford University Press, 1989.

[5] V. A. Macrae, J. C. Green, T. M. Greene, and A. J. Downs, *J. Phys. Chem. A*, **108**, 9500 (2004).

[6] S. Yu, A. Shayesteh, D. Fu, and P. F. Bernath, *J. Phys. Chem. A*, **109**, 4092 (2005).

[7] I. S. K. Kerkines, A. Mavridis, and P. A. Karipidis, *J. Phys. Chem. A*, **110**, 10899 (2006).

[8] Ch. E. Moore, *Atomic Energy Levels, Vol. I-II*, Circular of the National Bureau of Standards 467, U.S. Government Printing Office, Washington, DC, 1949.

[9] B. F. Peery Jr., *Publ. Astron. Soc. Japan*, **31**, 461 (1979).

[10] R. S. Wojslaw and B. F. Peery Jr., *Astrophys. J. Suppl. Ser.*, **31**, 75 (1976).

[11] A. Shayesteh, R. J. Le Roy, T. D. Varberg, and P. F. Bernath, *J. Mol. Spectrosc.*, **237**, 87 (2006).

[12] K. P. Huber and G. Herzberg, *Molecular Spectra and Molecular Structure, Vol. IV, Constants of Diatomic Molecules*, Van Norstrand Reinhold, New York, 1979.

[13] M. S. Khan, *Proc. Phys. Soc.*, **80**, 599 (1962).

[14] L. B. Knight, Jr. and W. Weltner, Jr., *J. Chem. Phys.*, **55**, 2061 (1971).

[15] A. J. McKinley, E. Karakyriakos, L. B. Knigth, Jr., R. Babb, and A. Williams, *J. Phys. Chem. A*, **104**, 3528 (2000).

[16] R.-D. Urban, U. Magg, H. Brik, and H. Jones, *J. Chem. Phys.*, **92**, 14 (1990).

[17] J. L. Dunham, *Phys. Rev.*, **41**, 721 (1932).

[18] D. P. Chong and S. R. Langhoff, *J. Chem. Phys.*, **84**, 5606 (1986).

[19] D. P. Chong, S. R. Langhoff, Ch. W. Bauschlicher, Jr., S. P. Walch, and H. Partridge, *J. Chem. Phys.*, **85**, 2850 (1986).

[20] Ch. Jamorski, A. Dargelos, Ch. Teichteil, and J. P. Daudey, *J. Chem. Phys.*, **100**, 917 (1994).

[21] E. Bengtsson and B. Grundström, *Z. für Physik*, **57**, 1 (1929).

[22] J. B. Schilling, W. A. Goddar III, and J. L. Beauchamp, *J. Am. Chem. Soc.* **108**, 582 (1986).

[23] T. M. Greene, W. Brown, L. Andrews, A. J. Downs, G. V. Chertihin, N. Runeberg, and P. Pyykkö, *J. Phys. Chem.*, **99**, 7925 (1995).

[24] D. Figgen, G. Rauhut, M. Dolg, and H. Stoll, *Chem. Phys.*, **311**, 227 (2005).

[25] K. A. Peterson and C. Puzzarini, *Theor. Chem. Acc.*, **114**, 283 (2005).

[26] T. H. Dunning, Jr., *J. Chem. Phys.* **90**, 1007 (1989).

[27] H.-J. Werner and P. J. Knowles, *J. Chem. Phys.*, **82**, 5053 (1985).

[28] P. J. Knowles and H.-J. Werner, *Chem. Phys. Lett.*, **115**, 259 (1985).

[29] H.-J. Werner and P. J. Knowles, *J. Chem. Phys.*, **89**, 5853 (1988).

[30] P. J. Knowles and H.-J. Werner, *Chem. Phys. Lett.*, **145**, 514 (1988).

[31] S. R. Langhoff and E. R. Davidson, *Int. J. Quantum Chem.*, **8**, 61 (1974).

[32] M. R. A. Blomberg and P. E. M. Siegbahn, *J. Chem. Phys.*, **78**, 5682 (1983).

[33] MOLPRO, version 2006, a package of *ab initio programs*, H.-J. Werner, P. J. Knowles, R. Lindh, F. R. Manby, M. Schtz, and others, see http://www.molpro.net

[34] The NUMEROV method, written by J. Senekowitsch *et al.*, Johan Wolfgang Goethe Universität, Frankfurt-am-Main, Germany, 1988.

[35] F. A. Tezcan, T. D. Varberg, F. Stroh, and K. M. Evenson, *J. Mol. Spectrosc.*, **185**, 290 (1997).

[36] M. A. Lebeaultdorget, C. Effantin, A. Bernard, J. Dincan, J. Chevaleyre, and E. A. Shenyavskaya, *J. Mol. Spectrosc.*, **163**, 276 (1994).

[37] W. Lin, S. A. Beaton, C. J. Evans, and M. C. L. Gerry, *J. Mol. Spectros.*, **199**, 275 (2000).

[38] R. S. Ram and P. F. Bernath, *J. Mol. Spectros.*, **231**, 165 (2005).

[39] R. S. Ram and P. F. Bernath, *J. Mol. Spectros.*, **186**, 113 (1997).

[40] R. S. Ram, P. F. Bernath, and S. P. Davis, *J. Chem. Phys.*, **116**, 7035 (2002).

[41] R. S. Ram, J. Liévin, P. F. Bernath, and S. P. Davis, *J. Mol. Spectros.*, **217**, 186 (2003).

[42] O. Launila, *J. Mol. Spectros.*, **169**, 373 (1995).

[43] R. Koivisto, O. Launila, B. Schimmelpfenning, B. Simard, and U. Wahlgren, *J. Chem. Phys.*, **114**, 8855 (2001).

[44] P. M. Sheridan and L. M. Ziurys, *Chem. Phys. Lett.*, **380**, 632 (2003).

[45] D. T. Halfen and L. M. Ziurys, *J. Chem. Phys.*, **112**, 054309 (2005).

[46] M. D. Allen and L. M. Ziurys, *J. Chem. Phys.*, **106**, 3494 (1997).

[47] J. Lei and P. F. Dagdigian, *J. Mol. Spectrosc.*, **203**, 345 (2000).

[48] R. S. Ram, P. F. Bernath, and S. P. Davis, *J. Mol. Spectrosc.*, **173**, 158 (1995).

[49] M. A. Flory, D. T. Halfen, and L. M. Ziurys, *J. Chem. Phys.*, **121**, 8385 (2004).

[50] M. Benomier, A. van Groenendael, B. Pinchemel, T. Hirao, and P. F. Bernath, *J. Mol. Spectrosc.*, **233**, 244 (2005).

[51] W. Zou and W. Liu, *J. Chem. Phys.*, **124**, 154312 (2006).

[52] T. Hirao, C. Dufour, B. Pinchemel, T. Hirao, and P. F. Bernath, *J. Mol. Spectrosc.*, **202**, 53 (2000).

[53] F. Ahmed, R. F. Barrow, A. H. Chojnicki, C. Dufour, and J. Schamps, *J. Phys. B: At. Mol. Phys.*, **15**, 3801 (1982).

[54] T. Parekunnel, L. C. O'Brien, T. L. Kellerman, T. Hirao, M. Elhanine, and P. F. Bernath, *J. Mol. Spectrosc.*, **206**, 27 (2001).

[55] M. A. Flory, S. K. McLamarrah, and L. M. Ziurys, *J. Chem. Phys.*, **125**, 194304 (2006).

[56] E. D. Tenenbaum, M. A. Flory, R. L. Pulliam, and L. M. Ziurys, *J. Mol. Spectrosc.*, **244**, 153 (2007).

[57] G. D. Rochester and E. Olsson, *Z. für Physik*, **114**, 495 (1939).

[58] V. D. Moravec, S. A. Klopcic, B. Chatterjee, and C. C. Jarrold, *Chem. Phys. Lett.*, **341**, 313 (2001).

[59] G. A. Bowmaker and P. Schwerdtfeger, *J. Mol. Struct.: THEOCHEM*, **205**, 295 (1990).

[60] M. Kaupp and H. G. von Schnering, *Inorg. Chem.*, **33**, 4179 (1994).

[61] M. Liao, Q. Zhang, and W. H. E. Schwarz, *Inorg. Chem.*, **34**, 5597 (1995).

[62] P. Belanzoni, E. van Lenthe, and E. J. Baerends, *J. Chem. Phys.*, **114**, 4421 (2001).

[63] A. I. Boldyrev and J. Simons, *Mol. Phys.*, **92**, 365 (1997).

[64] J. F. Harrison, R. W. Field, and C. C. Jarrold, *J. ACS Symp. Ser.*, **828**, 328 (2002).

[65] R. A. Kendall, T. H. Dunning Jr., and R. J. Harrison, *J. Chem. Phys.*, **96**, 6769 (1992).

[66] C. Heineman, W. Koch, and H. Partridge, *Chem. Phys. Lett.*, **286**, 131 (1998).

[67] J. M. Walter and S. Barratt, *Proc. Roy. Soc.*, **122**, 201 (1929).

[68] S. D. Cornell, *Phys. Rev.*, **54**, 341 (1938).

[69] A. Givan and A. Lowenschuss, *J. Mol. Struct.*, **78**, 299 (1982).

[70] D. L. Hildenbrand, K. H. Lau, and J. W. Roos, *J. Chem. Phys.*, **111**, 1337 (1999).

[71] M. B. Sureshkumar, S. Sharma, A. B. Darji, P. M. Shah, and N. R. Shah, *Opt. Pura Apl.*, **27**, 198 (1994).

[72] A. Bergner, M. Dolg, W. Kuechle, H. Stoll, and H. Preuss, *Mol. Phys.*, **80**, 1431 (1993).

[73] W. Gordy and R. L. Cook, *Microwave Molecular Spectra*, Interscience Publishers, 1970.

[74] The SURFIT method, written by J. Senekowitsch *et al.*, Ph. D. thesis, Johan Wolfgang Goethe Universität, Frankfurt-am-Main, Germany, 1988.

[75] S. Carter, N. C. Handy, C. Puzzarini, R. Tarroni, and P. Palmieri, *Mol. Phys.*, **98**, 1697 (2000).

Conclusions

Despite recent developments in theory and methodology, it remains difficult to obtain an accurate description of the electronic structure of compounds containing heavy atoms and close lying electronic states. The existence of *d* shells introduces complexity in these systems and metallic compounds with elements of the transition block exhibit such characteristics as several accessible ionic forms and large relativistic effects which have been recognized to play an important role, consequently various relativistic approaches have been developed to include these effects during the last decades. In this study, we have employed the pseudopotentials method which allows the implicit introduction of relativistic effects and we have used large basis sets to have enough flexibility to describe the variations of the polarity properties with the geometry. Several metallic compounds have been the subject of the present study.

The diatomic compounds, MX, treated in the first application exhibit this complexity. To take into account the interactions between the close lying electronic states, we have used a multiconfigurational approach throughout this study, atomic pseudopotentials to represent the core electrons of the metals and large basis sets. In the first application, we have elucidated the common characteristics of the low lying electronic states of a large family of diatomic compounds which can be considered as precursors for piezoelectric effects in the solid phase. Based on highly correlated *ab initio* calculations, we have shown that the diatomic compounds involving a metal of Group IIa, IIb, or III and a non-metal of Group V or VI, with their eight valence electrons, have all in common very close lying lowest electronic states with different spin, symmetry, polarity and geometric properties. We could correlate these properties of the diatomics to piezoelectric characteristics of the ionic solids, MX, formed with such pairs of atoms. We could also infer which of these pairs present the largest piezoelectric effects in the solid phase. In previous theoretical studies of piezoelectric effects, the bulk level has been explored and our study could clarify the molecular process between the partners which can be responsible for the effect in the solid phase. Further extensions of this study are, on one hand the analysis of the electronic and polarity properties of larger molecular systems, as for example the dimers $(MX)_2$ and on the other hand the calculation of the piezoelectric tensor for nanowires of the same pairs, particularly ZnO and AlN.

In the second part of this work, we have reported the study on the HZnF molecule and the associated diatomic fragments, ZnH and ZnF. Their electronic structure and the spectroscopic constants have been reported in this study, based on calculations at the MRCI level including the Davidson correction, with pseudopotentials and large basis sets. The calculated spectroscopic data compare well with known previous data. A better knowledge of these molecules has been given, particularly an appropriate description of the low lying excited states of ZnF which were not or poorly described in previous studies. It has been necessary to include the spin-orbit interactions between the $A^2\Pi$ and the $C^2\Pi$ states in order to obtain what we guess is an appropriate description of these states in contradiction with previous interpretations. For the ZnH^+ cation it was not possible to obtain a very accurate description of the properties, certainly because of the Zn pseudopotential, which was designed for the neutral species and not especially for the $Zn^+(3d^94s^2)$ ion [24]. An accurate description of the ground state of HZnF could be obtained by

the inclusion in the MCSCF step of much more low lying excited states than inferred in previous analysis. This point was essential in the present study and required many efforts. The Potential Energy Surface, PES, has been used to calculate the rovibrational spectrum of this molecule.

Both applications have led to publications.

The first one in:
(1) "Specific electronic properties of metallic molecules MX, correlated to piezoelectric properties of solids MX", G. Chambaud, M. Guitou, and S. Hayashi, *Chemical Physics*, **352**, 147, (2008).

For the second application, new results on the ZnF fragments have been published and the complete study of the triatomic will lead to another publication:
(2) "*Ab initio* study of the low lying electronic states of ZnF and ZnF^-", S. Hayashi, C. Léonard, and G. Chambaud, *The Journal of Chemical Physics*, **129**, 044313, (2008).